Doctoral Thesis

New Progression of Study on Organo-Modified Single-Walled Carbon Nanotubes

(有機修飾単層カーボンナノチューブの研究の新展開)

-Interfacial monolayer formation and uniformly dispersible polymer-based nanocomposite -

Graduate School of Science and Engineering

Saitama University

Ahmed A. Almarasy

August 2022

<< Contents >>

1. General Introduction

1-1. Surface modification of single-walled carbon nanotube

Eliminating fossil fuels, which generate abundant greenhouse gas CO_2 via combustion, is a shared mission for modern scientists [1]. The use of nanocarbon materials [2] such as fullerenes [3], carbon nanotubes (CNTs) [4], graphene [5], and nanodiamonds [6] to reduce CO_2 emissions has been warranted for a long time. Fullerenes and graphene have become leading materials, for which researchers were awarded the Nobel Prize in Chemistry and Physics pertaining to their discovery [7] and research on its physical properties [8] in 1996 and 2010, respectively. Fullerenes are important materials for anti-HIV drugs, active oxygen / radical-removing beauty essences, semiconductor materials, lubricants, etc. Graphene has already become an important material for applications of semiconductor device such as field effect transistors, and / or transparent conductive films. By the way, the price of CNT itself is high because the growth efficiency of conventional CNT is low and the discharge, heating, reaction, and gas flow times are long. Therefore, CNTs address the problem of high raw material costs via the recent development of the super-growth chemical vapor deposition (CVD) method [9]. In addition, the conventional arc discharge method has also been improved and developed, and it is becoming easier to obtain CNTs [10]. In particular, single-walled CNTs (SWCNTs) produced via the super-growth CVD method (sgC-SWCNTs) have a small length distribution and have reduced impurities [11].

However, concerns about the persistence of CNTs in the human body and health hazards from cancer [12] cannot be overlooked. CNT, which has high rigidity like asbestos, is highly toxic to mesothelial cells and may develop mesothelioma. It is necessary to investigate the danger of CNT dust being introduced into the human body and the concern that CNTs may stick to the lungs like asbestos [13]. In addition, when using CNTs as a material, there is a problem that it shows extremely remarkable aggregation characteristics. [14]. Despite their excellent mechanical properties [15] and electrical conductivity [16], as well as CNTs/SWCNTs possessing the highest thermal conductivity of solid materials [17], the remarkable bundle-like aggregation properties of CNTs [18] in organic solvents [19] and organic (polymer) materials [20] significantly reduces the performance of materials containing CNTs. At present, cellulose nanofibers (CNFs) [21] with similar shapes to SWCNTs have attracted attention because of their biodegradable characteristics [22]. Like montmorillonite [23] and sepiolite [24], CNFs and SWCNTs have a large aspect ratio [25] and their physical properties are expected to be improved by controlling the orientation of corresponding fillers.

One technique that might be able to overcome various obstacles to the application of CNTs at once is the chemical modification of organic molecular chains on the outermost surface [26]. Inorganic nanoparticles covered with organic chains can be dispersed in organic solvents [27], and uniform nanoparticles can be obtained even in organic polymer materials [28]. The van der Waals interaction between the organic chains creates a wax-like state in which dusting

is suppressed, and the modification at only 1 to 2 nm of the outermost layer makes handling much easier. Previously, nanoclay [29], zirconia [30], zinc oxide nanodisks [31], magnetic nanoparticles [32], and nanodiamonds [33] have been made dispersible in organic solvents and polymers by surface organo-modification. As a result, research on how the Langmuir monolayers [34] and Langmuir-Blodgett (LB) films [35–37] of nanoparticles spread from dispersion media and on polymer-based nanocomposites [38, 39] has been actively conducted. Since the organo-modified inorganic nanoparticles indicates amphipathic properties, they become a material for forming Langmuir monolayers on the water surface, and the LB film technology enables precise layering of nanoparticles. SWCNTs have also been modified using organic molecular chains via hydrophilization technology that employs mixed acid treatment [40]. Desorbable long-chain fatty acid modification alone successfully formed a monolayer film of SWCNTs when they were precipitated as a solid at the air-water interface [41]. The non-desorbable long-chain phosphonic acid modification method is expected to improve the function of modified-materials by controlling the particle arrangement in LB films [42], nanocomposite preparation with crystalline polymers [43], and drawing orientation [44].

1-2. Interaction between single-walled carbon nanotubes and biomolecules

In present times, a novel virus is threatening human life and health [45]. Contemporary techniques adsorb and immobilize viruses [46], enzymes [47], proteins [48], and so on, on solid substrates, suppressing their growth and kill them. However, studies are being conducted to adsorb biomolecules specifically [49]/non-specifically [50] on a template used as a platform and utilize their functions [51].

CNTs [4,52] are expected to be platforms for biomolecule adsorption [53], although there are concerns about their persistence to remain in the human body [54] and their cancerous nature [55]. There are many examples of interaction analysis between biomolecules and adsorbents using surface plasmon resonance (SPR/Biacore) [56-58], and it is important for the development of new biosensors and/or bioelements that they can maintain the activity of biomolecules adsorbed on the substrate [59]. It is known that to maintain activity, adsorbed biomolecules need to maintain their delicate three-dimensional structures [60], while biomolecular organization that is too densely integrated cannot maintain activity [61]. In other words, it is desirable to develop a method that can maintain functionality of biomolecules even under harsher conditions than in solution by maintaining their three-dimensional structures and controlling their adsorption density.

The use of a template for a monolayer on the water surface, Langmuir monolayer [34, 35, 37] of a SWCNT [66, 67] with a regular surface is a promising candidate, which has a

single-layer coaxial tubular six-ring carbon network. Organo-modification [68] of the surface is considered necessary for efficient introduction onto the water surface. So far, studies have been conducted on SWCNT Langmuir monolayers modified by long-chain fatty acids [41] and non-desorbable long-chain phosphonic acids [43]. Organo-modified SWCNTs can be dispersed not only in organic solvents but also in organic polymers [42], and orientation control using this technique [44] has been studied. Biomolecule adsorption/immobilization technology [69], which utilizes the air/water interface, has the potential to control adsorption density by adjusting surface pressure. In addition, studies have been conducted to selectively adsorb A·T base pairs of DNA molecules derived from salmon testes from the subphase on the water surface of comb polymers having a diamide-triazine group [70].

Research has also been conducted on adsorbing and immobilizing various biomolecules from the subphase on Langmuir monolayers of nano-clay with a surface modified by organic molecular chains [71]. In addition, studies have also been conducted to electrostatically adsorb biomolecules from the subphase onto a single-particle layer of organo-modified magnetic nanoparticles [72]. On the other hand, adsorbed biomolecules have the ability to spontaneously adsorb on the air/water interface; therefore, caution is required in immobilization experiments [73]. The advantages of adsorption/immobilization of biomolecules using a monolayer on the water surface of charged organo-inorganic nanoparticles, differences from other methods, and novelty, are corresponded to the simple and effective attainment of arrangement of

biomolecules at the same plane. For example, there is a means of introducing a reactive substituent on the surface of a magnetic bead, introducing it into a solution, interacting with biomolecules, and then recovering it with a magnet [74]. At first glance, this method is full of ideas, but the introduction of substituents requires many organic chemical steps and labor, and adsorbed molecules are also recovered in an extremely random state. As with the antigen-antibody reaction, the introduction of functional groups that induce adsorption interactions is laborious and costly, and adsorption by mere van der Waals force is not efficient. Adsorption to the monolayer of charged inorganic nanoparticles utilizes the charge of field molecules, which are mostly amphoteric electrolytes, the arrangement of biomolecule is homogeneous in Å/sub-nm size, and biomolecules can be immobilized on large-area surfaces. Therefore, this process is quite simple and the range of utilization as a material is wide.

1-3. Polymer-based nanocomposite in which single-walled carbon nanotubes are uniformly dispersed

The organo-modification [75] of functional inorganic nanoparticle surfaces [76] allows the inorganic particles to be dispersed not only in solvents as if they were dissolved [77], but also in organic polymers (upper column of Fig. 1-1) [78]. Hydrophilic inorganic particle surfaces enable the formation of single-particle films on water surfaces through expansion to the air/water interface [79]. This technique is often used in the field of organic synthesis [80] as the presence of long organic molecular chains enhances the solubility of the molecules in solvents [81]. The hydrophobic chains of the monolayer on the water surface induce particle arrangement effects by enhancing the van der Waals interaction between the hydrophobic chains [82], besides imparting amphiphilicity to the functional molecules [83].

The dispersion of inorganic fillers in organic polymers has been widely studied in the field of academia [84]. Introducing inorganic particles into organic components tends to cause phase separation [85], leading to difficulty in obtaining uniformly dispersible composite materials [86]. Although good dispersion of fillers enhances the physical properties of composite materials [87-89], it is difficult to achieve the excessive aggregation of these fillers in matrix polymers.

In the organo-modification of inorganic particle surfaces, the peripheral medium for the dispersion of particles in a solution is replaced with a solid polymer. Although solid polymers

have high melt viscosities, the use of melt-compounding techniques [90] opens up new possibilities for the dispersion of organo-modified inorganic nanoparticles. These techniques require the matrix polymer and organo-modified chain to have the same chemical compositions [91]. For example, the effective nucleator agent that can act on perfluoroalkoxy alkane (PFA), a crystalline fluorinated polymer, is polytetrafluoroethylene particles [92], indicating the importance of the affinity between fluorinated polymers with high phase separation tendency [93].

Surface modifying organic molecules with hydrocarbons and fluorocarbons of nanoclay [29], zirconia [94], zinc oxide [95], magnetic nanoparticles [96], and nanodiamonds [97] have previously been achieved by utilizing the oil/water interface [98]. This method involves reacting the modified chains in the oil phase with the surface of the inorganic nanoparticles in the aqueous phase at the oil/water interface, as if they were condensation-polymerized at the interface to synthesize polyamide/nylon [99].

As SWCNTs [100, 101] have universal water- and oil-repellent surface properties [102], such surface modification states cannot be achieved without hydrophilization via long-time acid treatment [103]. Although some polymer composite materials containing organo-modified SWCNTs have been reported to exhibit innovative functions by orientation control (middle column of Fig. 1-1) [44], there are still rare cases in which SWCNTs are uniformly dispersed in resins. When a long-chain carboxylic acid was allowed to act on the abovementioned

hydrophilized SWCNTs, the desorption behavior was confirmed at the time of solid precipitation [41]. As long-chain phosphonic acid derivatives form bidentate bonds [104], elimination can be avoided.

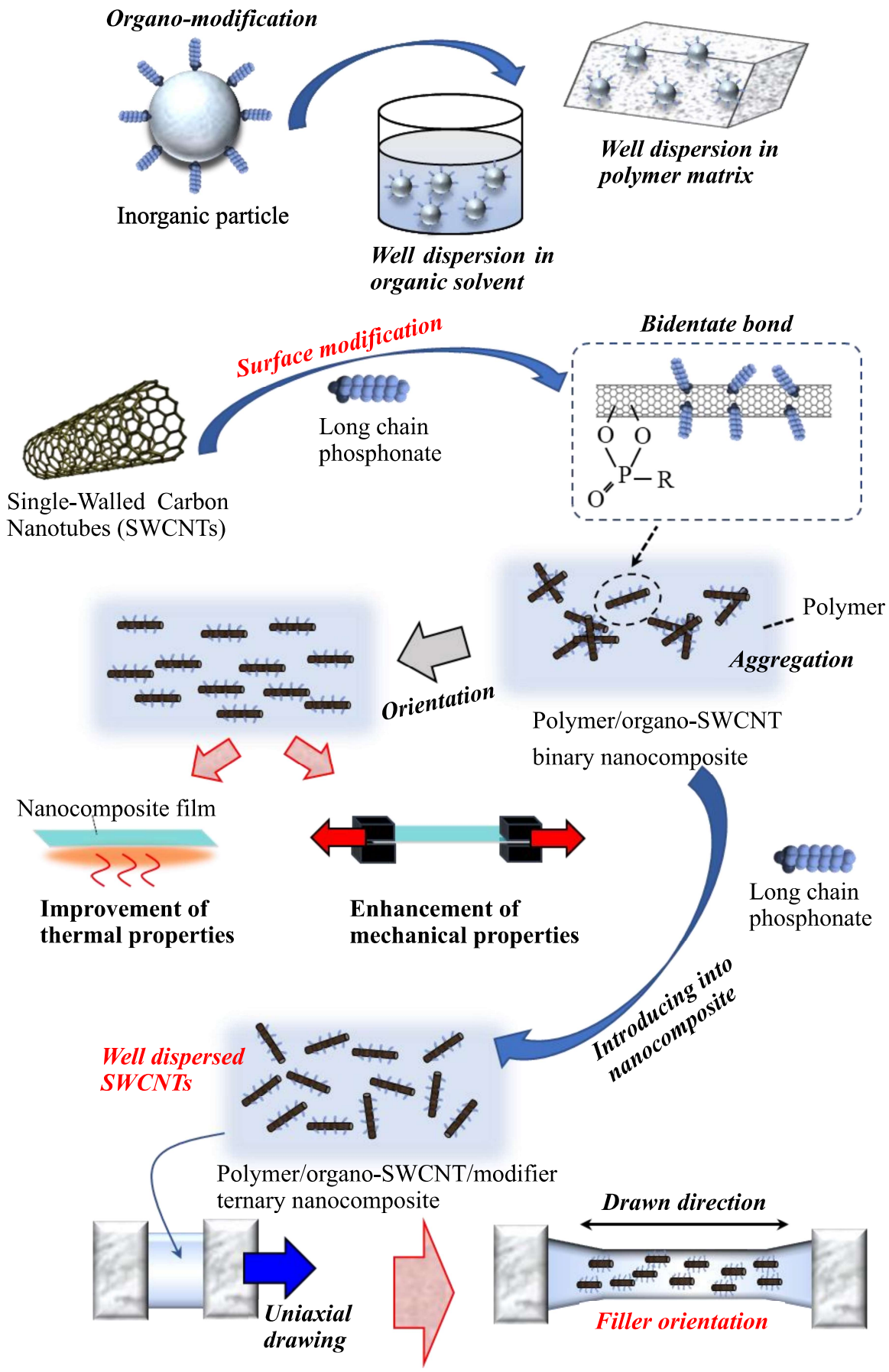

Figure 1-1. Schematic illustration of the research strategy and study background in Chapter 5.

1-4. This Study

In Chapter 3, the utilization of SWCNTs for organo-modification is an excellent way to examine the characteristics of a single layer as an extreme structure and the dispersion characteristics in a matrix as a polymer composite material. In this chapter, sgC-SWCNTs and SWCNTs obtained using the latest improved-arc discharge method (iAD-SWCNTs) (Fig. 1-2(a)) are compared with respect to Langmuir and LB films and nanocomposite preparation (Fig. 1-2(b)). It is expected that the presence of impurities centered on Fe and the distribution of tube length, which have disadvantages in the latter (improved-arc discharge method), will be eliminated during surface modification, leading to a pure physical property comparison between the two kinds of materials. This research aims to provide useful information for researchers who utilize SWCNTs.

In Chapter 4, a protease capable of cleaving the luminescent casein chain [105] is introduced into the subphase and adsorbed on organic chain-modified SWCNT monolayers. While introducing the protease, I tried precise control by forming an SWCNT monolayer film before the adsorption progressed to the air/water interface. The purpose of this chapter was to determine the consequences of immersing protease adsorbed on SWCNTs in a luminescent casein solution under harsh conditions, including temperature rise, to retain and enhance the cleaving/emitting of molecular chains (Fig. 1-3).

In Chapter 5, with low molecular weights, the sublimation/evaporation temperature of

long-chain phosphonic acid derivatives is remarkably high [106]. As such, they can be added as the third component during the melt-compounding of organo-modified SWCNTs in general-purpose polymers. When a fluorocarbon-chain-modified SWCNT was introduced into phase-separable crystalline fluorinated polymers, the addition of a fluorinated phosphonic acid derivative as the third component improved the dispersibility of the SWCNT [107]. In this chapter, I verified the effects of using a general-purpose resin and a hydrocarbon-based phosphonic acid derivative in the melt-compounding of organo-modified SWCNTs, and verified its usefulness and universality. The obtained dispersibility-enhancing three-component nanocomposite was drawn, and the improvement in the physical properties of the uniaxially oriented SWCNTs was examined (lower column of Fig. 1-1).

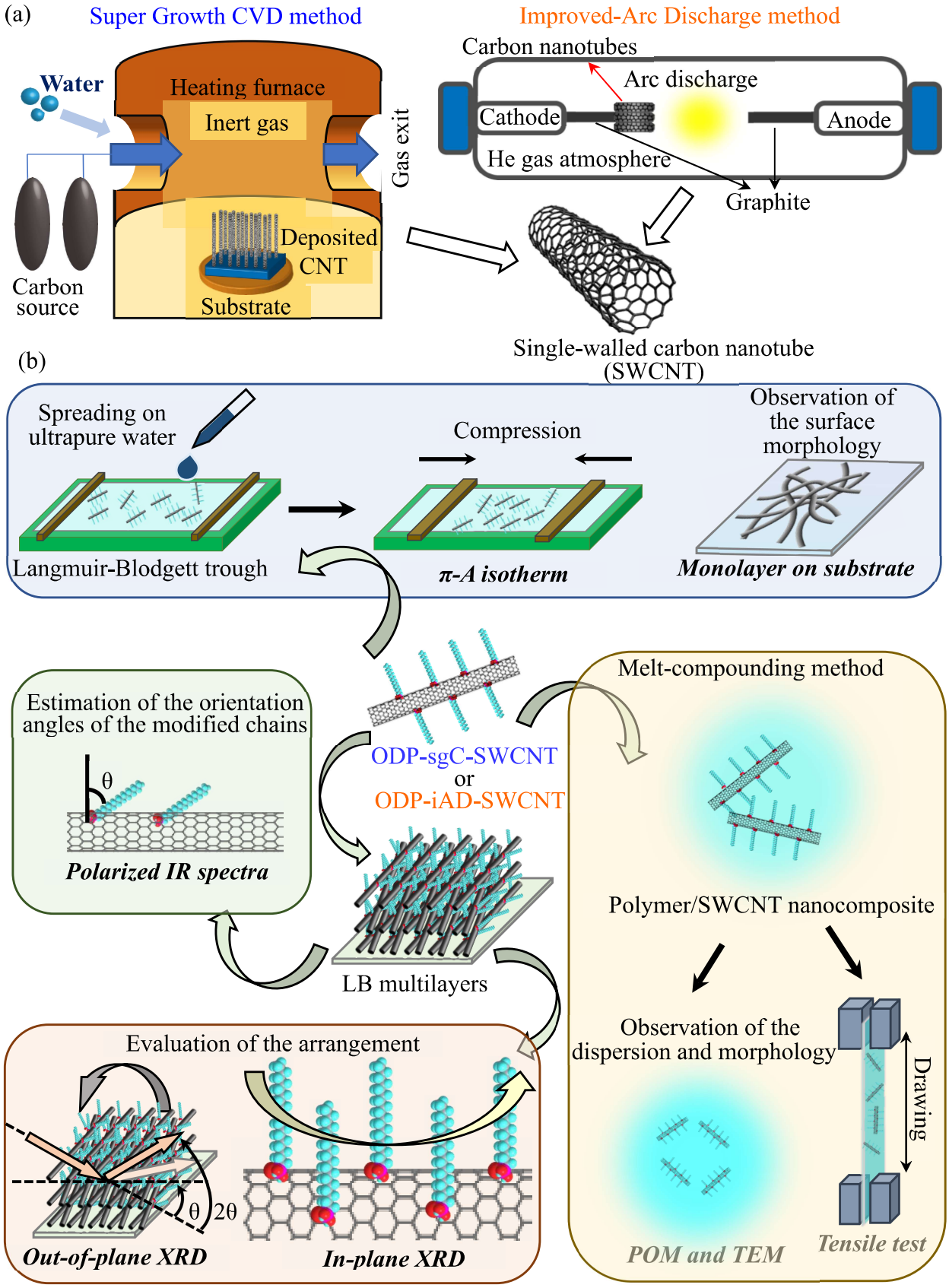

Figure 1-2. (a) Schematic illustrations of manufacturing methods of two types of SWCNTs used in this study. (b) Research strategy in this study using LB films and polymer-based nanocomposites.

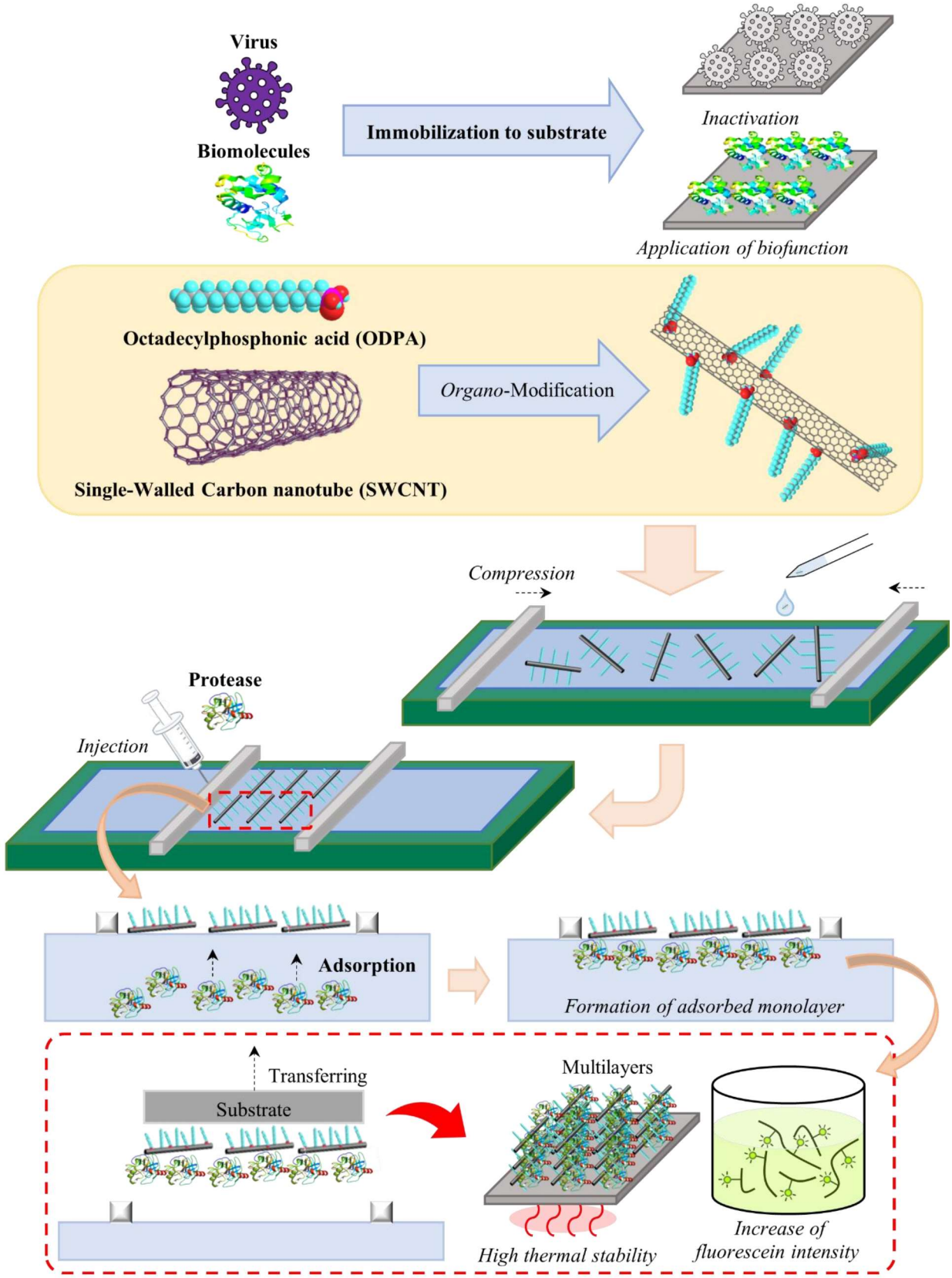

Figure 1-3. Schematic illustrations of (Upper) virus growth suppression and biomolecular function materialization by adsorption/immobilization on a solid substrate. (Middle) preparation of organo-modified SWCNTs, formation of their monolayers on the water surface, and adsorption of biomolecules from subphase to them. (Lower) immobilization of adsorbed proteases, maintenance of activity of luminescent casein chain cleavage function by them, and their materialization.

2. Materials and Methods

2-1. Sample preparation and organo-modification of SWCNTs

The SWCNTs manufactured via the super-growth CVD method used in this study were provided by ZEON Nanotechnology Co., Ltd. (ZEON NANO® SG101). In addition, the iAD-SWCNTs were provided by OCSiAl Co., Ltd. through Kusumoto Chemicals, Ltd. in Japan. Octadecyl phosphonic acid (ODPA) was used as the surface modifier, and polypropylene (PP) was used as the matrix for preparing the polymer-based nanocomposite. The modifier was purchased from Wako Pure Chemical Industries, Ltd., and the matrix polymer was a sample with an average molecular weight of Mn = 270,000 that was purchased from Prime Polymer Co., Ltd. For the organo-modification of SWCNTs at the outermost surface, according to previous reports [42–44], a mixed acid solution of sulfuric acid:nitric acid = 3:1 was sonicated [40] for 24 h and then reacted with the modifier at the oil/water interface (Fig. 2-1(a)). Since it has been reported in the past that the length of SWCNTs changes depending on the length of the period of ultrasonic treatment [41], it is expected that the universal difference derived from the manufacturing process of the two types of SWCNTs will be minimized by this type modification reaction. The two types of organo-modified SWCNTs obtained via the surface modification reaction are abbreviated as ODP-sgC-SWCNT and ODP-iAD-SWCNTs. In both cases, as shown in the schematic illustration of Fig. 2-1(b), the stearyl chain is bound to the SWCNT surface by a phosphonate bidentate bond. The proof of this bond formation is explained in the previous reports [42, 43] and its references [106]. The -OH group at the binding

site on the OH-terminated SWCNT surface protonates in solution and exists as a positively charged -OH_2^+ group. Here, electrostatic dehydration condensation occurs, and a □□□–P–O–C (SWCNT side) bond is formed. Subsequently, proton transfer occurred from the -OH of the phosphonic acid group, and from the electrostatic dehydration condensation with positively charged -OH_2^+, a bidentate chelate coordination state (μ-oxo type) formed in a self-organizing manner. For spherical particles such as nanodiamonds, the organo-modification rate was calculated based on the values for weight loss determined by thermogravimetric analysis (TG, SII TG/DTA6200 equipped with EXSTAR6000 controller) and the values for the limiting area of the organic chain determined using the surface pressure-area (π-A) isotherms [33]. However, because SWCNTs have individual tube length distributions, the comparison of modification rates was estimated by comparing the weight loss during organic chain desorption.

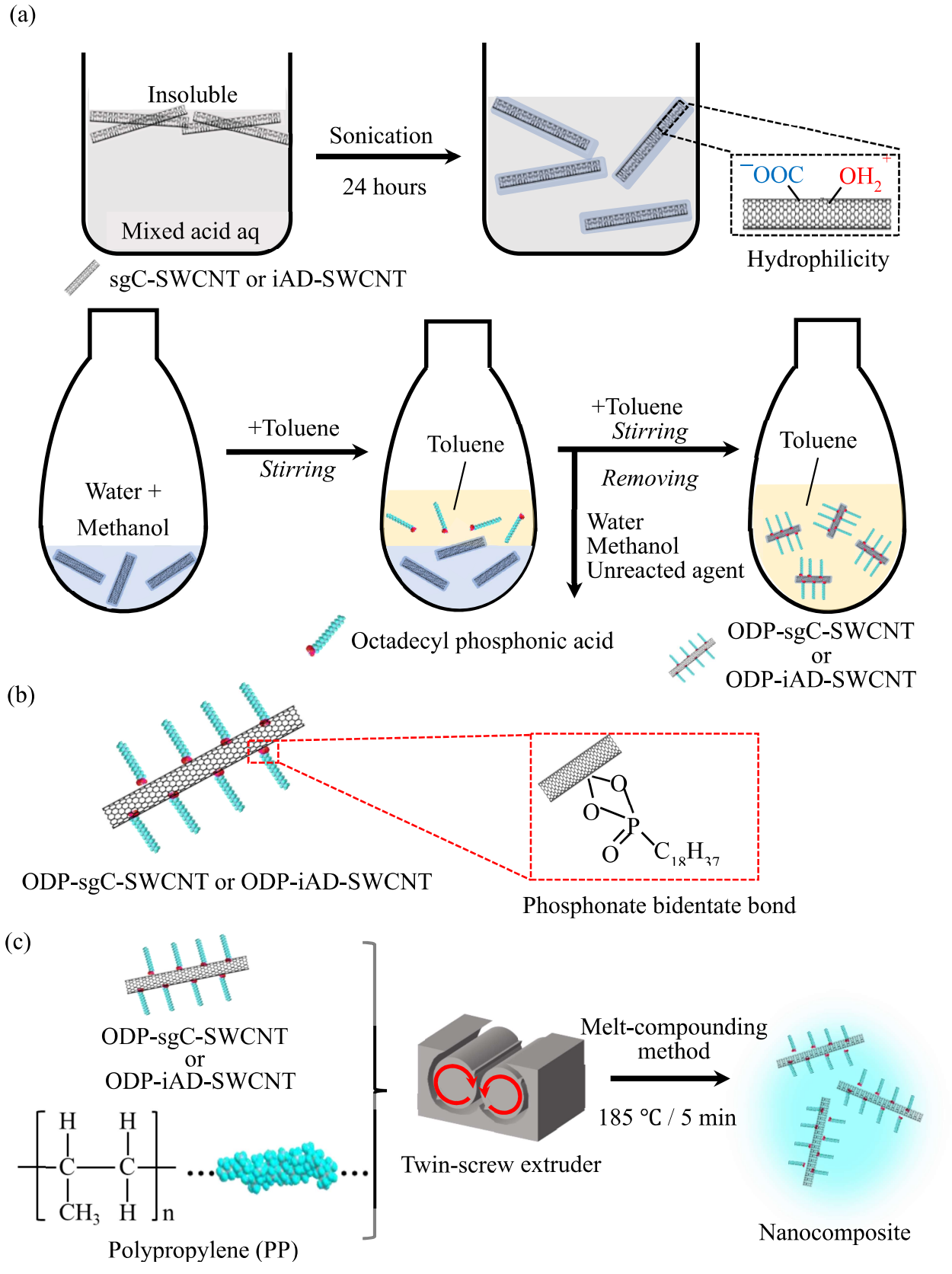

Figure 2-1. (a) Schematic illustrations of SWCNT hydrophilization process and protocol for surface modification at oil/water interface. (b) Schematic illustration of stearyl phosphonate-modified SWCNT with the formation of bidentate bond. (c) Preparation conditions for PP/organo-modified SWCNT nanocomposite and conceptual diagram of melt-compounding method.

2-2. Monolayer preparation on water surface and LB film fabrication of organo-modified SWCNTs

The behavior of the two types of organo-SWCNTs on the water surface was evaluated using the π-A isotherm (USI USI-3-22LB). Ultrapure water (Milli-Q, 18.2 MΩ·cm) was used for the subphase. Toluene was used as the spreading solvent for the organo-modified SWCNTs, and it was spread on the water surface from a diluted solution of approximately 1.5 mg/25 mL. It was set a waiting time during 30 minutes for volatilization of the toluene solvent and stabilization of the film. In this case, the compression rate of the barrier was 0.08 $mm \cdot s^{-1}$. The measurement temperatures of the π-A isotherms were changed to 10, 15, and 25 °C, and the expansion characteristics at high temperatures as derived from the mobility of the organic chains were compared. The transfer onto the solid substrate was performed by the LB method at an arbitrary surface pressure (subphase temperature 15 °C). The surface morphology was observed using an atomic force microscope (AFM, SII SPA300 with SPI 3800 probe station, silicon single-crystal cantilever, and spring constant 1.5 $N \cdot m^{-1}$) on a single-layer film on a mica substrate. The orientation of the modified chains was evaluated *via* polarized infrared (IR) spectroscopy using a wire grid polarizer to multilayers (20 layers) on a CaF_2 substrate (Bruker AXS TENSOR II spectrometer). In this case, the orientation angle was calculated using the dichroic ratio, assuming the uniaxial orientation of the modified chain. For the LB multilayers on the glass substrate, the layered period corresponding to the thickness of the single layer and

the packing mode of the modified chain were evaluated by out-of-plane and in-plane X-ray diffraction (XRD), respectively. The out-of-plane XRD profiles were obtained using a Rigaku Rint-Ultima III diffractometer (40 kV and 40 mA, Cu-Kα radiation (λ = 0.154 nm)). The in-plane XRD profiles were obtained using a custom-made device, a Bruker AXS MXP-BX (40 kV and 40 mA, Cu-Kα radiation with a multilayer mirror, incident angle of 0.6°) [108, 109]. In fact, the optical geometry of out-of-plane XRD for the LB film on the substrate is quite similar to normal powder X-ray diffraction. X-rays are incident on the sample layered on the glass substrate, and the goniometer diffracts toward the upper side of the substrate [35, 36]. On the other hand, the diffraction geometry of in-plane XRD is the oriented to the diffraction direction surrounds the sample edge. The former shows the spacing in the stacking direction of the organo-modified SWCNT multilayers, and the latter can analyze the spacing between the modified chains bonded to the SWCNT surface [29, 33].

2-3. Polymer-based nanocomposite preparation and its physical property evaluation

To evaluate the difference in the dispersion state of the two types of organo-modified SWCNTs in solid organic material and the difference in the physical properties of the resulting nanocomposite, nanohybridization with PP was performed. From a previous report [43], because the heating desorption temperature of modified chains in phosphonate-modified SWCNTs is extremely high, the nanocomposites were prepared using the melt-compounding method. Melt compounding was carried out at 185 °C for 5 min using a twin-screw extruder

(LABO kneader mill, Toshin Co., Ltd.) with 0.5 wt% organo-modified SWCNT added to the PP matrix (Fig. 2-1(c)). The particle dispersion state of the obtained nanocomposites was observed using a transmission electron microscope (TEM, JEOL JEM-1400Plus) at an accelerating voltage of 120 kV. The mechanical properties of the nanocomposites were evaluated through a tensile test (Tensilon RTG1310, A & D Co. Ltd., tensile speed of 10 mm□min^{-1} and test-piece dumbbell punching at 23 °C), and the strain-stress (S–S) curves were obtained to examine the Young's modulus and the degree of elongation.

2-4. Synthesis of organo-modified SWCNTs as a template and biomaterials as adsorbents used in this study

The template material used in this study was SWCNT (ZEON NANO® SG101) with a diameter of 5 nm using super growth chemical vapor deposition (CVD), which was kindly provided by ZEON Nanotechnology Co., Ltd. (Fig. 2-2(a)). The tube length of this SWCNT was distributed within the range 100–600 nm, and the aspect ratio was large. Octadecyl phosphonic acid was used as the surface modifier (Fig. 2-2(b)). The surface-modification procedure was as follows: First, highly water-repellent SWCNTs were sonicated for 24 h with an acid mixture of sulfuric acid: nitric acid = 3:1, and hydrophilization was then completed [41]. After this treatment, SWCNTs with hydroxyl-terminated surfaces were dispersed in the aqueous solution. Subsequently, a toluene solution containing octadecyl phosphonic acid was poured into thehydrophilized SWCNT dispersion medium to promote the organic modification

reaction at the oil/water interface. The details of this method are in a previous report [43]. As a result, a stearyl chain-modified SWCNT by phosphonate bidentate binding was obtained (Fig. 2-2(c)). This process involves a dehydration condensation reaction between a positively charged terminal hydroxyl group on the SWCNT surface and a phosphonate anion. In other words, since the water-repellent SWCNTs are dispersed in water by mixed acid treatment for 24 hours, it is considered that the surface of SWCNTs is terminated with hydrophilic functional groups. This terminal group is expected to be a hydroxyl group. After that, when forming a bond with phosphonic acid, protonation occurs from the phosphonic acid group, and then the bond is formed by dehydration between $\cdots PO^{-}$ and $\cdots OH_2^{+}$. Therefore, positively charged hydroxyl groups remain on the surface of the SWCNTs to which the modified chains are not bound and are later used for adsorption and immobilization of the protease. The stock solution of a biomolecule of 10 $mg \cdot L^{-1}$ was prepared in 1 mM phosphate buffer at pH 7.0 (potassium dihydrogen phosphate and disodium hydrogen phosphate) and stored at 4 °C. By varying the amount of each salt, a range of buffers can be prepared that buffer well between pH 5.8–8.0. Phosphates have a very high buffering capacity and are highly soluble in water. Fluorescein-modified casein and protease were purchased from Takara Bio Inc. Trypsin, which is generally known to be able to decompose serine, was used as a luminescent casein chain-degrading protease. Figure 2-2(d) shows a schematic illustration of the fluorescence-enhancing behavior of fluorescein-modified casein by the protease used in this study.

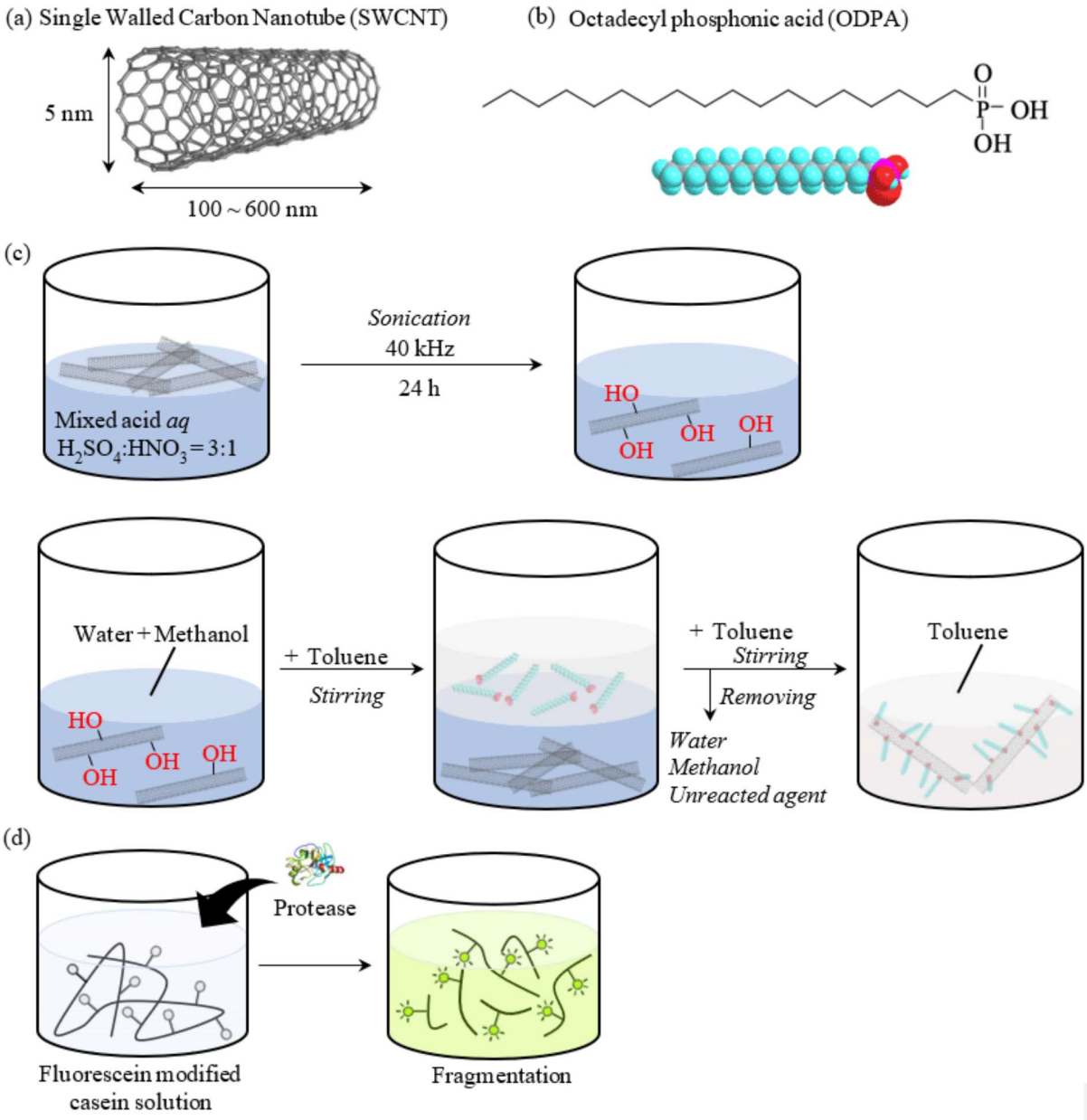

Figure 2-2. Materials and experimental methods in this study: (a) Schematic illustration of SWCNT, (b) Chemical structure of stearyl phosphonic acid as an organic modifier, (c) Scheme of organo-modification reaction of SWCNT surface, (d) Schematic illustration related to the fluorescence-enhancing behavior of fluorescein-modified casein by the action of protease.

2-5. Adsorption experiment of protease to monolayer on water surface of organo-modified SWCNTs by post-injection method

The organo-modified SWCNT obtained by the oil/water interfacial modification method was nano-dispersed in a toluene solvent, and the spreading solution of the monolayer was spread on ultrapure water (18.2 MΩ·cm) to form a monolayer on the water surface/Langmuir monolayer. The behavior of the monolayer on the water surface was evaluated by measuring the surface π–A isotherms using an LB trough surface-coated with Teflon (USI-3-22 made by USI Corp.). A subphase temperature of 15 °C was adopted as the measurement temperature. After spreading the organo-modified SWCNTs on the water surface, 30 min were for the evaporation of toluene and the stabilization of the monolayer in each case. The barrier compression rate of the LB trough was 0.08 mm·sec^{-1}. Previously, the interaction between the organo-modified SWCNT monolayer and the biomolecules was investigated by changing the subphase to a saturated buffer solution [43]. However, since water-soluble biomolecules containing both hydrophilic and hydrophobic residues can spontaneously adsorb on the air/water interface, a mixed film of organo-modified SWCNTs and biomolecules can possibly be formed using this method. Therefore, protease was injected into the lower water surface after detecting the surface pressure during the formation of the organo-modified SWCNT monolayer on ultrapure water. The resultant concentration of the aqueous solution containing protease reached 10^{-6} M, which was the same condition as previously reported using an organo-modified

magnetic nanoparticle [72]. The surface pressure–time (π–t) isotherm of the Gibbs monolayer of the protease at the air/water interface was measured with an LB trough, similar to the π–A curve.

2-6. Investigation of protease-adsorbed SWCNTs films transferred onto a solid substrate

The SWCNT monolayer on which protease was adsorbed from the subphase was transferred to the mica substrate by the horizontal lifting method (HLM) at a predetermined transferring surface pressure. This was observed by AFM. For the AFM, a SII SPA300 module equipped with a SPI3800 controller was used, and a silicon cantilever (spring constant 1.4 $N \cdot m^{-1}$) was utilized in the dynamic force mode (DFM). IR spectroscopy confirmed the amide bands of the adsorbed protease to the organo-modified SWCNT template. For IR, a Bruker AXS Tensor II spectrometer was used. For the IR measurement, a 20-layer multilayer was created on the CaF_2 substrate. Fluorescence spectra were measured using an FP-6500 fluorometer (Jasco Co., Ltd.). The excitation wavelength was 485 nm. Fluorescence measurements were performed using 4.5 mL quartz cuvettes and a bandwidth of 5 nm at excitation and emission. Raman spectra were measured using a Renishaw inVia Microscope–Laser Raman spectrophotometer.

2-7. Materials in Chapter 5

ZEON NANO® SG101 SWCNTs manufactured by ZEON Corporation (Fig. 2-3(a)) measuring 5 nm in diameter with tube lengths of 100–600 nm was used in this study. For SWCNT with a diameter larger than 3 nm, its cross-section may be oval or flat instead of round shape. Actually, in this study, the cross section of the SWCNT used this time is elliptical, with a thickness at 3 nm and a width at about 5 nm. These SWCNTs were prepared using the super-growth chemical vapor deposition method [110]. Octadecyl phosphonic acid (ODPA, melting point: 99 °C) with a purity of 98% or higher, purchased from Tokyo Chemical Industry Co., Ltd. was used as the organic modifier. Despite its low molecular weight, the ODPA had a high sublimation/evaporation temperature and a TG weight loss onset temperature of 239 °C (Fig. 2-3(b)) that was well above the melting point of polypropylene (PP). The PP, which was used as the matrix polymer, was manufactured by Prime Polymer Co., Ltd. and had a melting point of 154 °C (Fig. 2-3(c)) and a molecular weight (Mn) of 220 000–270 000.

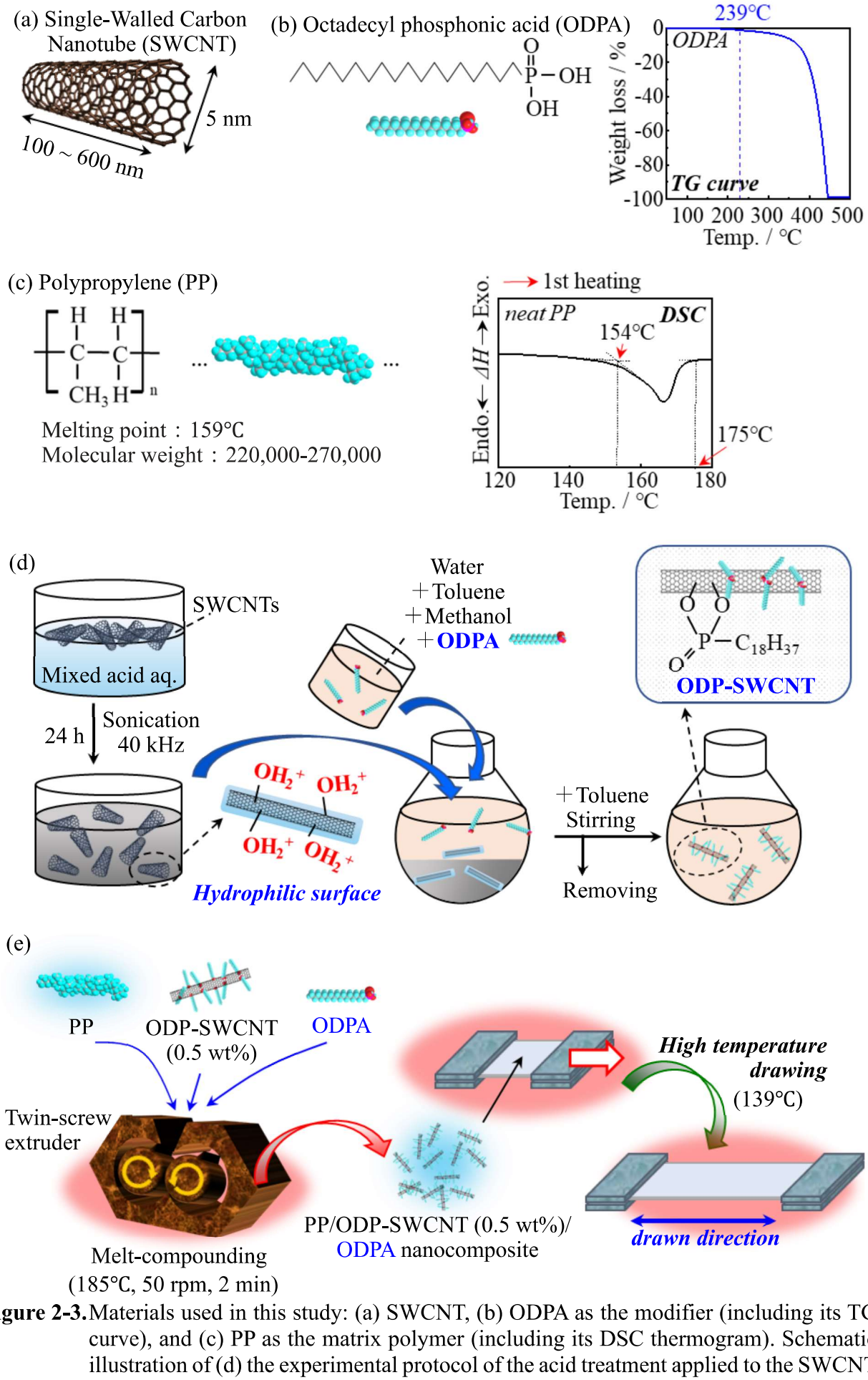

Figure 2-3. Materials used in this study: (a) SWCNT, (b) ODPA as the modifier (including its TG curve), and (c) PP as the matrix polymer (including its DSC thermogram). Schematic illustration of (d) the experimental protocol of the acid treatment applied to the SWCNT and organo-modified SWCNT surfaces, and (e) melt-compounding and uniaxial drawing used in this study.

2-8. Organo-modification procedure of Chapter 5 (Fig. 2-1(d)) [104]

Fifty milligrams of SWCNT were added to an acid solution containing 60 mL of sulfuric acid and 20 mL of nitric acid. The mixture was cooled in a water bath at room temperature for 3 h. Ultrasonic treatment was then performed for 24 h to hydrophilize the SWCNT. The ultrasonic device used in this experiment was a bus type and was using 40 kHz. The temperature was set to 25 °C, but a temperature rises at about 10 °C could be seen during 24 h. Here, in order to evaluate the oxygen content after acid treatment, the cast film was measured by X-ray photoelectron spectroscopy (Fig. 2-4). When the C1s and O1s spectra were detected, and the ratios were examined, it was found that carbon and oxygen were present in a ratio of 6:4. Therefore, it was possible that a maximum of less than 70% of the carbon surface was covered with hydrophilic functional groups. The obtained hydrophilic SWCNT was repeatedly suction-filtered for approximately four to five times until a pH of 7 was achieved. The neutralized hydrophilic SWCNT and 5 mg of the organic modifier ODPA were then added to a mixed solvent containing 10 mL of water, 20 mL of methanol, and 15 mL of toluene. The mixture was stirred for 1 week. To remove the aqueous phase, evaporation was performed using an evaporator until the bumping of water and methanol was completed. As the aqueous phase was not completely removed and the separation of the aqueous and toluene phases was confirmed during the first evaporation process, 20 mL of methanol and 15 mL of toluene were added again, and the mixture was stirred for 24 h. By repeating the "24-h stirring-evaporation-addition of

methanol and toluene" process for one week, the aqueous phase was completely removed and a black organo-modified SWCNT dispersion was obtained. The organo-modified SWCNT dispersion was vacuum-dried, and the solvent was volatilized to obtain organo-modified SWCNT powder. Characterization of the organic modifier ODP-SWCNT revealed the following: As a result of TG measurement, 0.323 mg of the modifier was eliminated from the 1.226 mg modified nanotubes. This value corresponds 26.4 wt% modification amount. Since the molecular weight of the modifier is 334.48, about 9.65×10^{-7} mol corresponds to the graft amount. The attached functional groups were found to be carboxylate anions and oxonium cations by IR measurement [44]. In addition, it was found from AFM observation that more than 80% of the tube lengths are aligned to 0.4 μm length due to the influence of ultrasonic treatment [41].

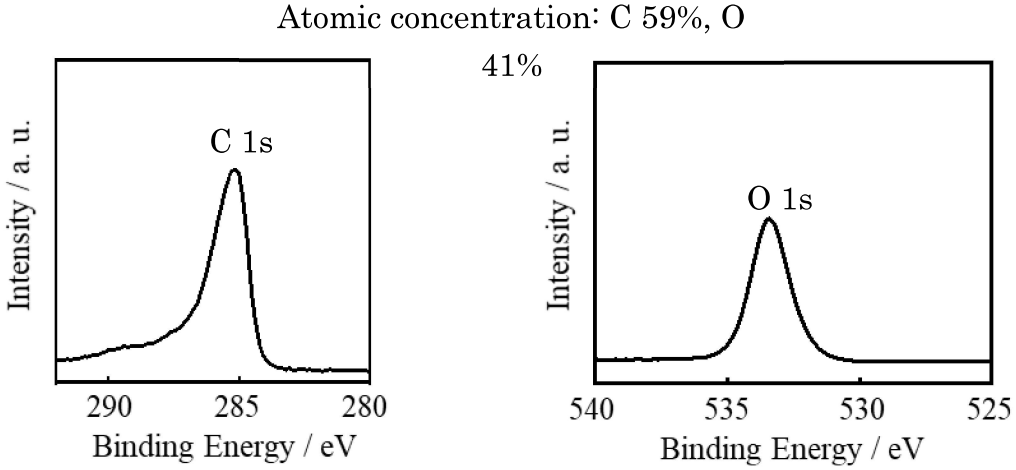

Figure 2-4. X-ray photoelectron spectra of cast film of acid-treated SWCNTs.

2-9. Preparation and drawing of polymer-based composites (Fig. 2-3(e))

As shown in Fig. 2-3(e), the PP matrix, ODPA-modified SWCNT (ODP-SWCNT, 0.5 wt%), and ODPA modifier was added to form binary and ternary composites via melt-compounding for 2 min at 185 °C. The TDR60-3M melt kneader manufactured by Toshin Co., Ltd. was used at a rotation speed of 50 rpm. In this study, the optimum compounding condition is 50 rpm for 2 min. The reason is that under severe conditions longer than this, the rupture of the molecular chain becomes induce and the mechanical properties of the polymer decrease. Prior to taking any measurements, the obtained composites were film-formed using a hot press (Mini-Test Press-10) manufactured by Toyo Seiki Co., Ltd. at a pressure of 20 MPa, molding temperature of 185 °C, and pressing time of 1 min. After pressing, the composites were rapidly cooled in water. For uniaxial drawing of the composite films, an IMC-18EB manual uniaxial drawing device manufactured by Imoto Seisakusho was used at a preheating time of 5 min, drawing temperature of 139 °C (15 °C below melting point), and drawing speed of 10 mm·min^{-1}. After drawing, the films were quenched with water. The drawing temperature was adjusted using an MO-931G jet oven manufactured by Toyama Sangyo Co., Ltd.

2-10. Characterization in Chapter 5

The mesoscopic morphologies of the obtained composite films were observed using a polarized optical microscope (POM, OLYMPUS BX-51) manufactured by Olympus Corporation. The fine structures of the composite films were evaluated using a Bruker AXS D8

ADVANCE wide-angle X-ray diffractometer (WAXD, 40 kV, 40 mA, Cu Kα radiation). WAXD was performed by the reflection method, and the scattering slit on the incident side was set to 0.1 degrees and the light receiving slit width was set to 5.1 mm. Since it is an oblique incidence measurement, the incident X-rays spread almost over the entire sample, and the average information could be fair. The melting and crystallization behaviors were evaluated using a differential scanning calorimeter (DSC, DSC-6200) attached to the EXSTAR6000 controller manufactured by SII. The thermal degradation behavior was measured using the SII TG/DTA 6200 model thermal analyzer with a similar controller. The thermal analysis using both instruments adopted a heating and cooling temperature rate of 10 °C·min^{-1}, and was performed using an Al pan in N_2 gas purge. Nitrogen purity was 99.99% or more. The tensile test was performed on a dumbbell-shaped die-cut sample using A&D MCT-2150 at a tensile speed of 10 mm·min^{-1}.

Chapter 3. Comparison of Characteristics of Single-Walled Carbon Nanotubes Obtained by Super-Growth CVD and Improved-Arc Discharge Methods Pertaining to Interfacial Film Formation and Nanohybridization with Polymers

3-1. Abstract

A comparison of SWCNTs produced by super-growth CVD and improved-arc discharge methods was performed as it pertains to the formation of their Langmuir-Blodgett films and polymer-based nanocomposite preparation. Two kinds of SWCNTs indicated amphipathic properties after surface chemical modification using long-chain phosphonic acids. The modification rates of the two types of organo-modified SWCNTs were almost the same, impurities were removed to the same extent, and the influence of the tube length distribution was considered to be low. However, it was expected that the SWCNTs made via improved-arc discharge would be superior in regularity in the two-dimensional film. Specifically, the arrangement regularity of the modified chains was high, and as a result, the layering regularity

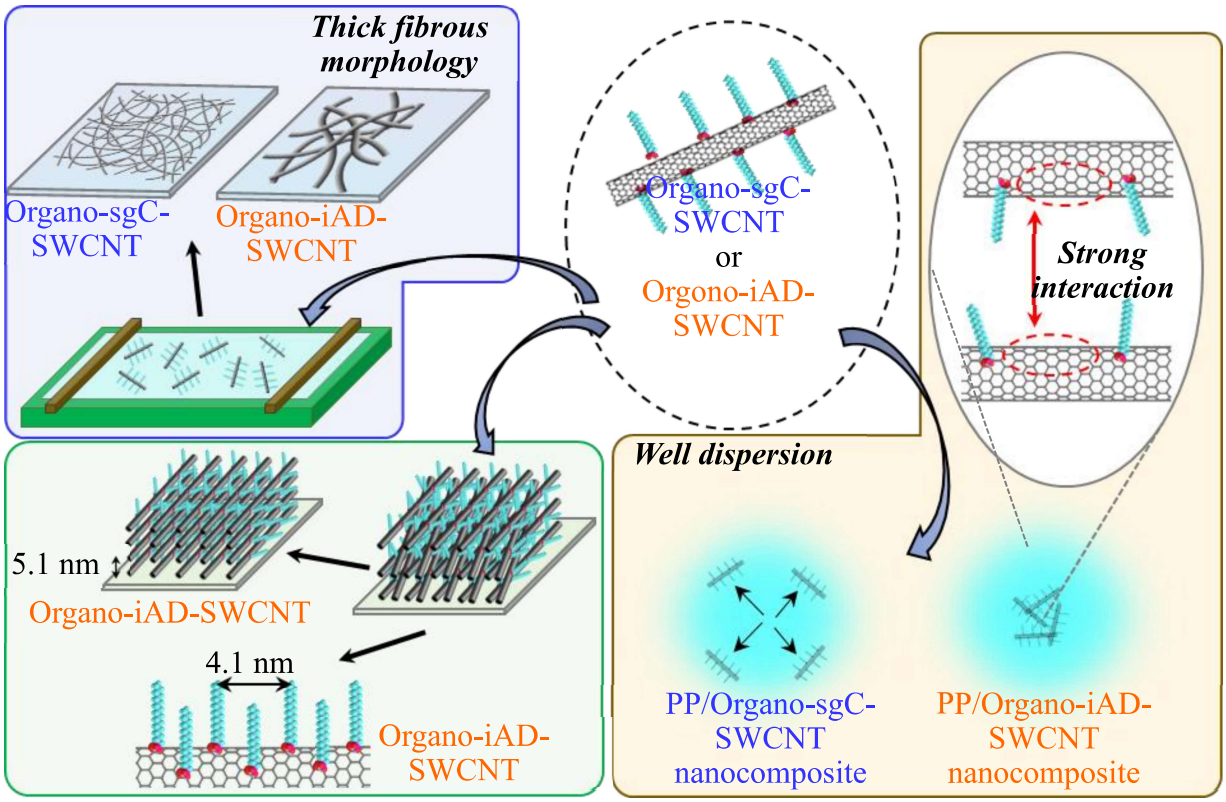

of SWCNTs itself was considered to be high. Owing to organo-modification, SWCNTs manufactured via the super-growth CVD method tended to be dispersed into finer fibers even in a monolayer. Compared to other organic polymers, this organo-modified SWCNT formed a composite material with higher dispersibility. The significant difference in the physical properties of both SWCNTs constitutes a trade-off relationship between dispersibility and two-dimensional regularity. The difference in the physical properties of the two types of SWCNTs could be related to the strength of the interaction between the exposed SWCNT-specific surfaces, even after organo-modification.

Keywords: Single-Walled Carbon Nanotube, Organo-Modification, Langmuir-Blodgett Method, Super Growth Chemical Vapor Deposition Method, Improved-Arc Discharge Method

3-2. Characterization of organo-modifications on surface of SWCNTs

Figure 3-1 shows the TG curves of the two types of organo-modified SWCNTs. Although the behavior of weight loss is slower in the sgC-SWCNT system, it appears that there is no significant difference in the amount at the weight loss start temperature starting from approximately 200 °C and the final residual amount at 500 °C for both organo-modified SWCNTs. The residue at 500 °C corresponds to the SWCNTs with the modified chains removed. Therefore, it seems that both organo-SWCNTs have almost the same modification rate. The slight weight loss before 200 °C is not the desorption of the modifier; it corresponds to the desorption of adsorbed water on the SWCNT surface [41]. Between the two SWCNTs, the iAD-SWCNT system seems to have a slightly higher modification rate. The slow desorption of the modified strands of the sgC-SWCNT system may be due to the high local modification density and strong interaction between the modified molecular chains. The effect of this tendency on the later-monolayer/LB film behavior and the dispersion behavior in the matrix polymer is very interesting.

Figure 3-2 shows the temperature dependence of the π-A isotherms of monolayers on the water surface of the two organo-modified SWCNTs and the stearyl phosphonic acid modifier alone. In this measurement, there is a distribution in the tube diameter of the monolayer materials, and the modification rate of each nanotube is not constant, so the horizontal axis notation was devised. Although the "Molecular Area [$Å^2$/molecule]" or the "Mean Area per Repeating Unit [$Å^2$]" are used in general-purpose measurements, here, the "Trough Area Reduction [%]" which means the relative reduction value of film area on the water surface, was adopted [29–33]. At a subphase temperature of 15 °C, the π-A curve of organo-modified SWCNTs, which is clearly different from that of the modifier alone, was confirmed. The fact that both modified SWCNTs can be dispersed in the toluene spreading solution and the π-A curve is drawn itself will be evidence of the formation of lipophilic organo-modified SWCNTs.

The isotherms show an expansion tendency peculiar to organic matter, indicating that the modified molecular chain contributes greatly this tendency. In the low surface pressure region, the ODP-iAD-SWCNT monolayer has a larger limiting area and indicates higher expansion characteristics. In the TG measurement, the difference in modification rate was expected to be small. In other words, the experimental fact that the weight loss rates of TG were approximately equal meant that the amounts of modified chains bound to the SWCNT surface was approximately equal. It was predicted that the behavior appearing on the π-A isothermal curve would be almost the same if the total amount of modified chains and the part of the bond position of the modified chains were equal. As a result, the behavior of the two modified SWCNT monolayers on the π-A curve was very different. As shown in Fig. 3-3 of the support information, there were almost no difference in the surface pressure-time (π-t) isotherm that the surface pressure was attained at 10 $mN \cdot m^{-1}$ in advance. Therefore, it was predicted that the distribution of the binding positions of the modified chains would be significantly different between the two types of modified SWCNTs. Hence, in ODP-iAD-SWCNTs, the modification site may be uniformly dispersed on the tube surface, the temperature dependence of the isotherms supports this hypothesis. In low temperature measurements, both materials condense equally but expand at high temperatures. This behavior also closely resembles the characteristics of organic molecules, such as long-chain fatty acids, and mainly identifies the characteristics of modified molecular chains. In a study in which the behavior single particle layer on the water surface of organo-modified nanodiamond was investigated [33], linear isotherms peculiar to inorganic monolayers were drawn. In contrast to this fact, the isotherms of the organo-modified SWCNTs monolayer obtained this time indicate a smooth curve, which is close to the characteristics of the long chain fatty acid monolayer [34]. Under these circumstances, the expansion behavior at high temperatures was also more prominently confirmed in the iAD-SWCNT system. This behavior is considered to indicate the difference

in the modified state of the organo-SWCNTs between the two systems.

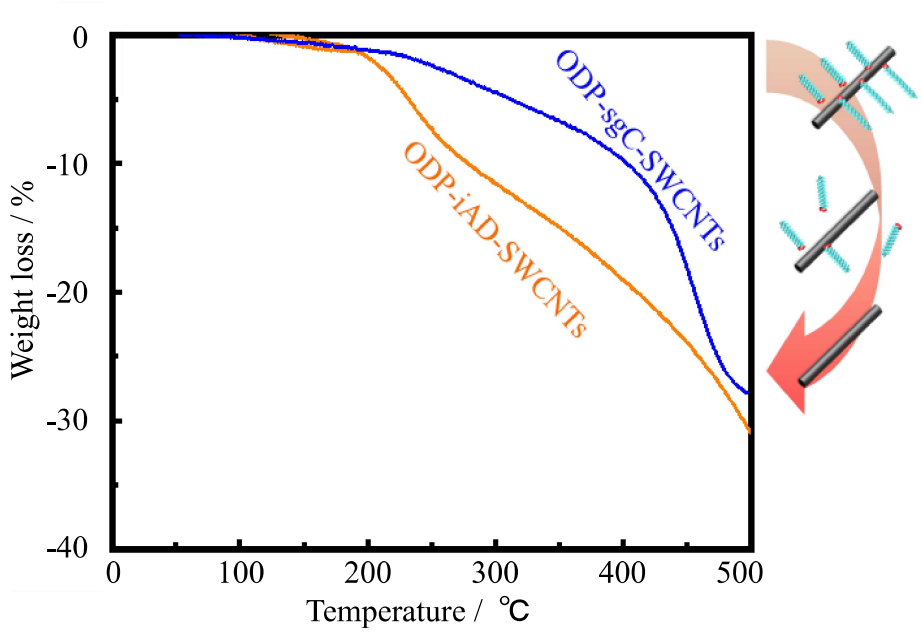

Figure 3-1. TG curves of ODP-sgC-SWCNTs and ODP P-iAD-SWCNTs (scanning rate: 10 °C·min^{-1}).

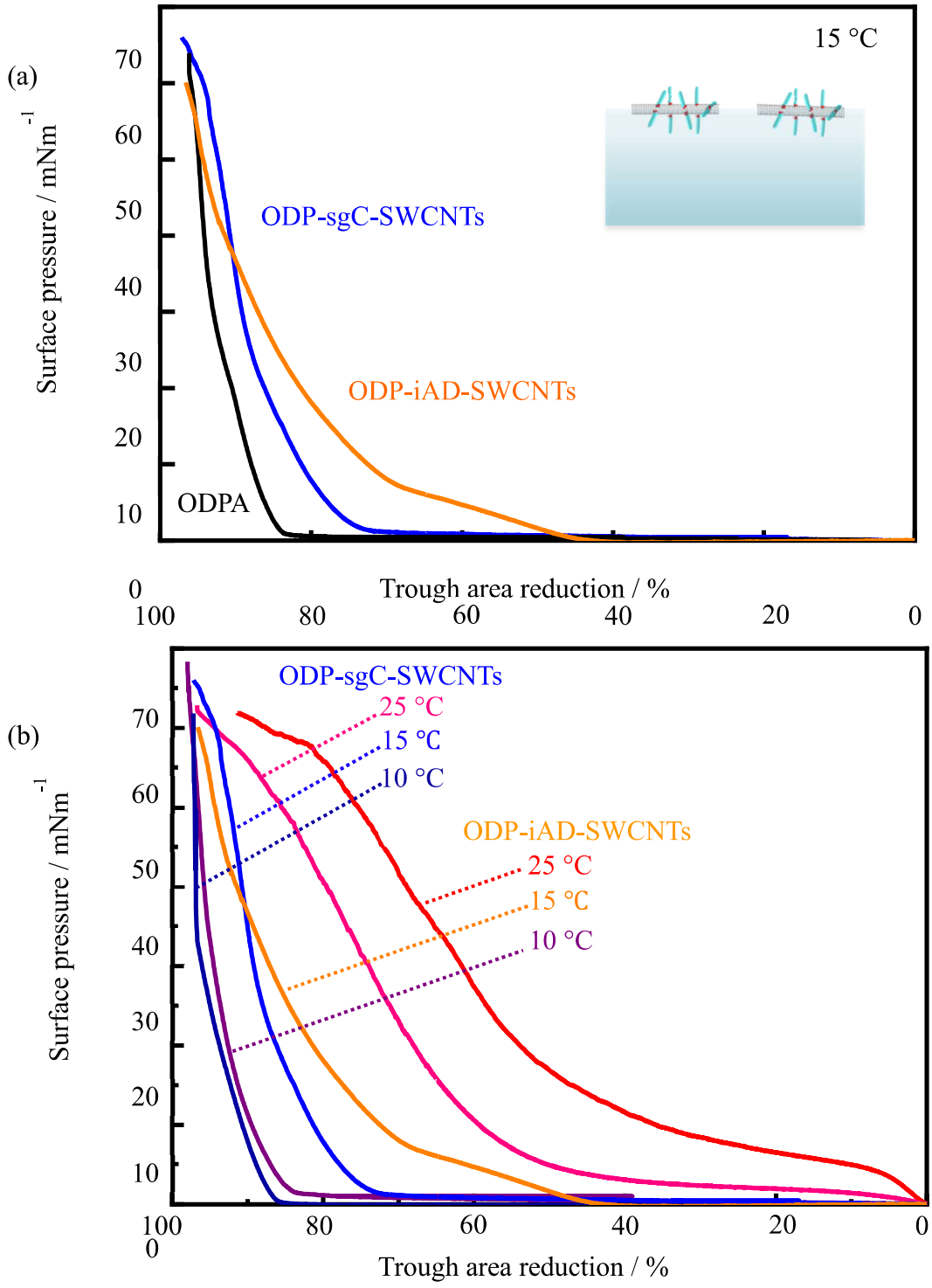

Figure 3-2. (a) π-A isotherms of monolayers of ODP-sgC-SWCNT, ODP-iAD-SWCNT and ODPA on water surface (15 °C). (b) Temperature dependence of π-A isotherms of monolayers of ODP-sgC-SWCNT and ODP-iAD-SWCNT on water surface (10, 15, and 25 °C).

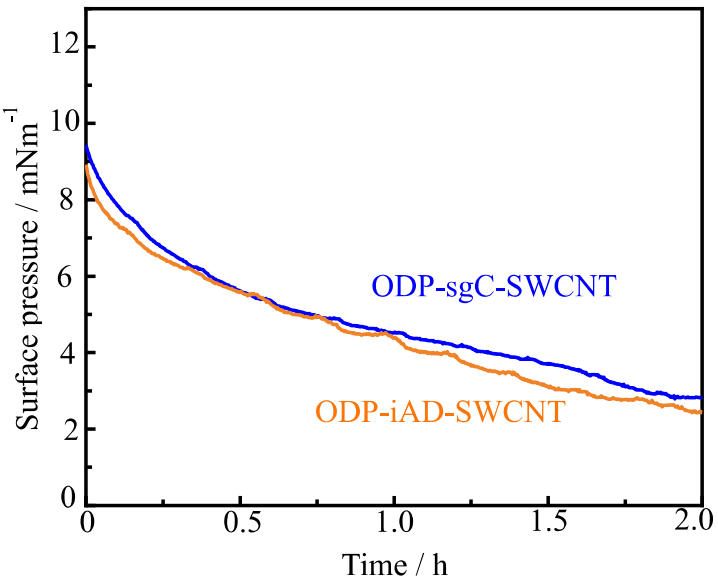

Figure 3-3. π-t isotherms of the monolayer on the water surface of two types of organo-modified SWCNTs after reaching 10 $mN \cdot m^{-1}$ by preliminary compression.

3-3. Arrangement and aggregation properties of two types of organo-modified SWCNTs transferred onto solid substrate

Even in the case of simple long-chain fatty acids, there are some structural changes that results from the rearrangement of molecules from the monolayers on the water surface to the transferred films on the solid substrate. On the water surface, there is an interaction between the hydrophilic groups and the water, and the film materials show high mobility. On a solid substrate, the mobility is reduced, and the in-plane interaction between the film constituents works independently. In SWCNTs, which are generally considered to have strong aggregation characteristics, rearrangement on a solid substrate is expected. To understand the structure and morphology of the transferred films, it is necessary to consider the above assumptions.

Figure 3-4 shows AFM images of the monolayers of two types of organo-modified SWCNTs transferred onto a mica substrate via the upstroke LB method. The transferred surface pressures were 15 $mN \cdot m^{-1}$, and the subphase temperatures were adopted at 15 °C. In this 2 μm square mesoscopic region, the morphology of both monolayers is clearly different. In other words, the ODP-iAD-SWCNT monolayer shows a very developed thick fibrous morphology, whereas the ODP-sgC-SWCNT monolayer shows an extremely fine and wide-thickness fiber aggregation morphology. This result means that even two types of SWCNTs that undergo the same surface modification reaction and indicate almost the same modification rate will show clearly different aggregation characteristics owing to the difference in the manufacturing method.

Figure 3-5 shows the estimation and comparison of the orientation angles of the modified chains via polarized IR spectroscopy of the LB multilayers of the two types of organo-modified SWCNTs. When the LB multilayers prepared under the same conditions were evaluated via XPS measurement, no substantial difference was indicated in the content of iron impurities in either nanotube type (Fig. 3-6). Although it seemed that the Fe signal was subtly larger in the

ODP-iAD-SWCNT multilayers, this result was a difference in noise level and might not be the subject of discussion. Regarding to the results for the polarized IR, it was confirmed that the two types of organo-modified SWCNT multilayers had a clear polarization dependence on the C-H stretching vibration bands appearing in the range of 2800–3000 cm^{-1}. Although the ratio of the degree of intensity was different, the band intensity/area at the time of p- and s-polarization was clearly different between the two kinds of multilayers. When the orientation angles (angle of tilt from the normal surface) of the long alkyl-modified chains were calculated based on the values obtained here, the values of the ODP-sgC-SWCNT and ODP-iAD-SWCNT multilayers were 58.1° and 56.7°, respectively. From the viewpoint of the orientation angle of the chain modified by the polarized IR, it was found that the structures of both organo-SWCNTs were significantly different.

The difference in periodicity and regularity of organo-modified SWCNTs in LB multilayers was further clarified by out-of- and in-plane XRD profiles. The out-of-plane XRD profiles shown in Fig. 3-7 show that the two types of organo-modified SWCNT multilayers indicate values of long-period between layers at approximately 5 nm. However, there is a clear difference in the clarity of the diffraction peaks, and the ODP-sgC-SWCNT LB film only provides information about the shoulder peaks. This result indicates that ODP-iAD-SWCNT multilayers have higher regularity and a larger crystallite size. This may be related to the fact that the modified chains in the ODP-sgC-SWCNT multilayers obtained from the polarized IR results are markedly tilted at 58.1°. In addition, the ODP-iAD-SWCNT multilayers showed a clear diffraction peak at 50.7 Å, indicating its high periodicity. Even for the in-plane XRD profile shown in Fig. 3-8, although the ODP-sgC-SWCNT multilayers showed only a weak amorphous halo at approximately 7.3 Å, the ODP-iAD-SWCNT multilayers showed clear crystalline peaks, indicating that the modified chains were packed as a two-dimensional orthorhombic crystalline system. The halo pattern shown in the profile of the ODP-sgC-

SWCNT multilayers does not correspond to the information related to the modified chains due to its size and is expected to be SWCNT-specific information. Therefore, the modified chains of ODP-sgC-SWCNT multilayers are not expected to have an in-plane crystalline order. In contrast, the modified chains of ODP-iAD-SWCNT multilayers are similar to the two-dimensional packing mode of stearic acid, and it is presumed that dense packing was realized.

All the measurements discussed in this section show the superiority of the regularity/ordered aggregation ability of ODP-iAD-SWCNTs. Impurities were removed to the same extent by the organic modification reaction, and modified chains were introduced into the two types of SWCNTs; however, there were differences in their periodicity and arrangement regularity. In other words, it might be said that iAD-SWCNTs are more suitable candidates for the creation of thin-film materials and crystal-like ordered materials in which only SWCNTs are integrated. Then, what kind of tendency does the difference in dispersibility in solid-state organic media will be shown? Composites with polymer materials will be discussed in the next section.

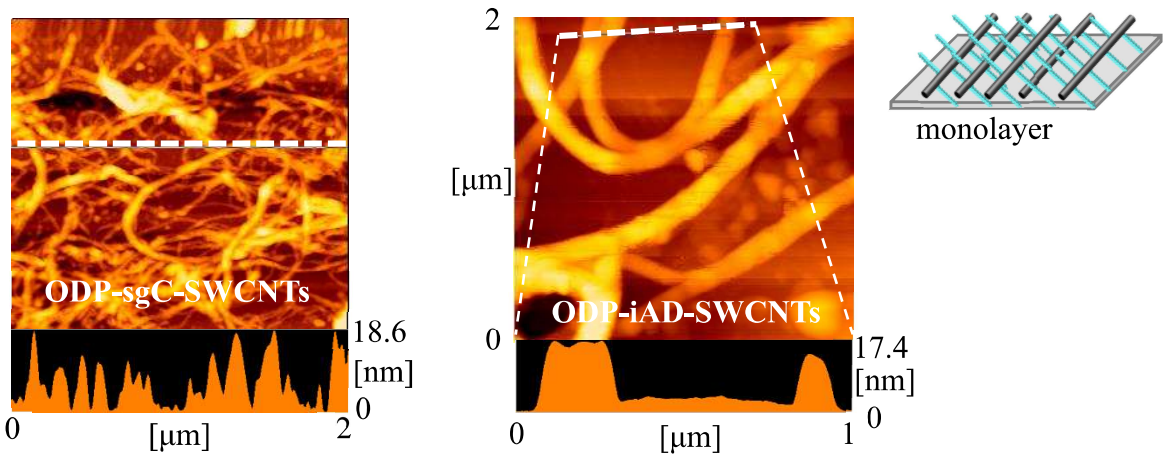

Figure 3-4. AFM images of monolayer of ODP-sgC-SWCNT and ODP-iAD-SWCNT transferred by upstroke LB method at 15 $mN \cdot m^{-1}$ on a solid (15 °C).

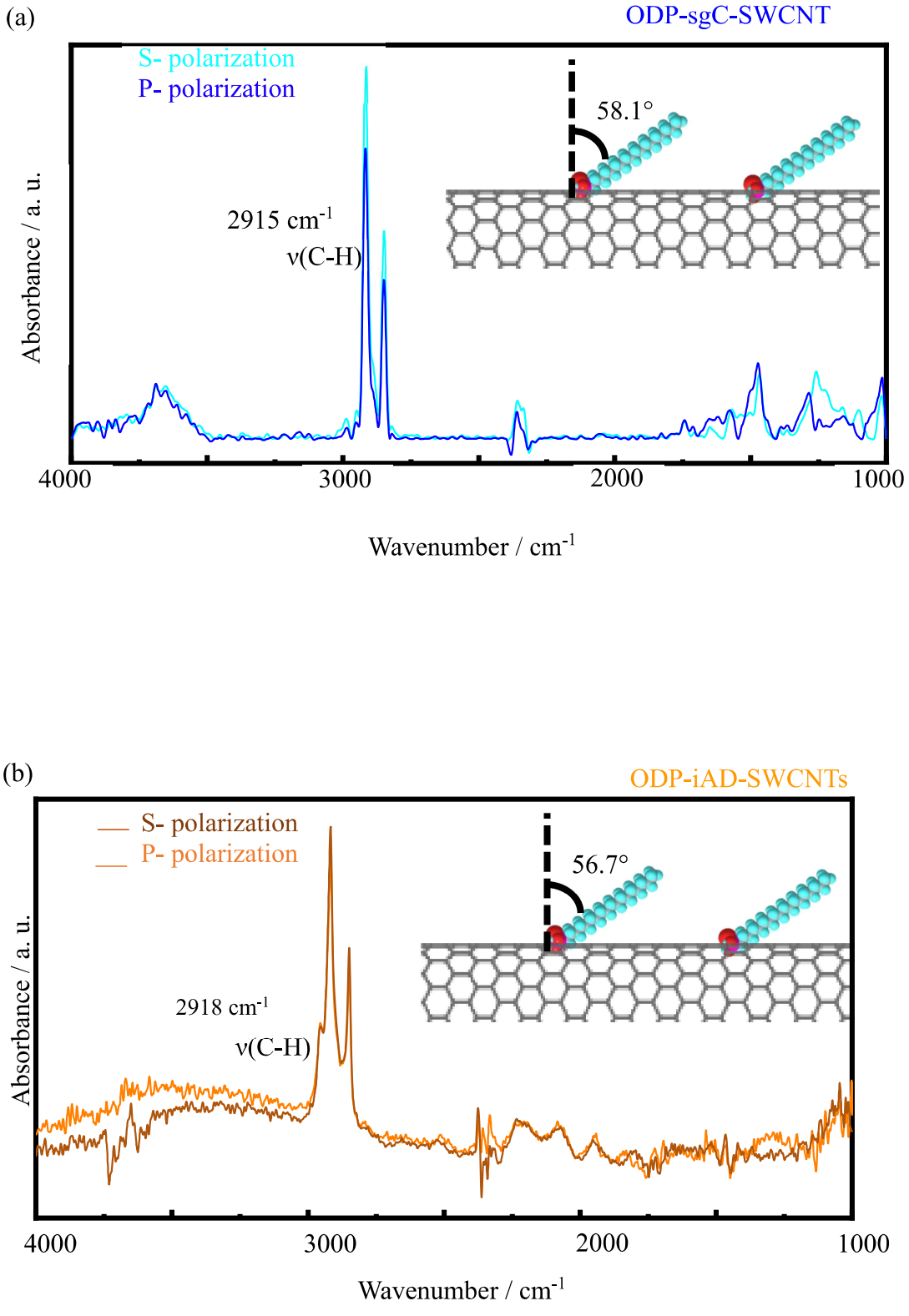

Figure 3-5. Polarized IR spectra of LB multilayers of (a) ODP-sgC-SWCNT and (b) ODP-iAD-SWCNT (15 mN·m^{-1}, 20 layers, 15 °C), and calculation of orientation angle by dichroic ratio when uniaxial orientation of modified chain is assumed.

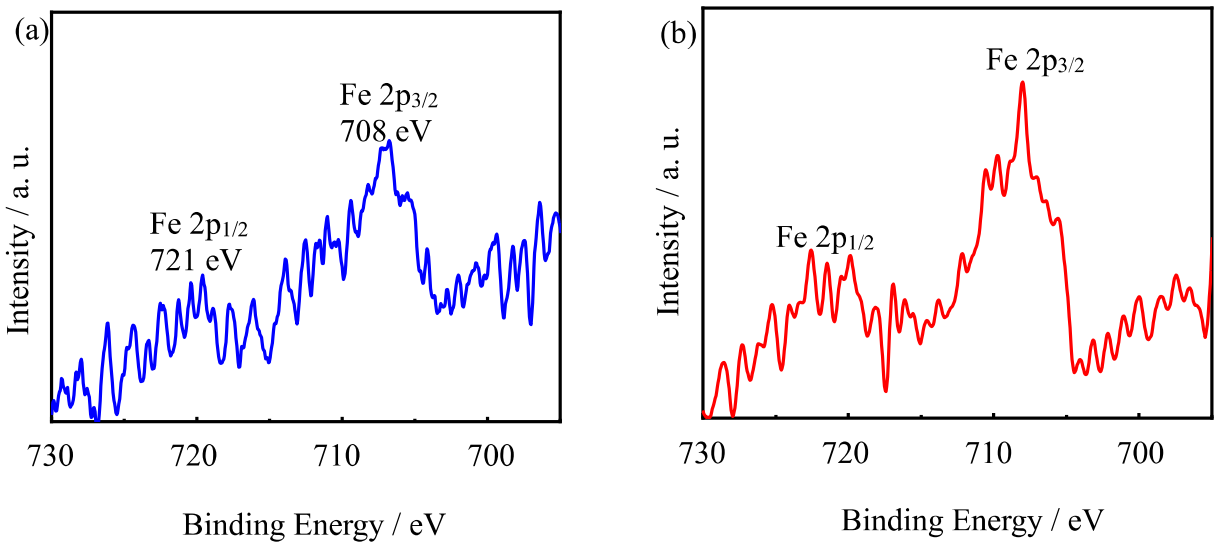

Figure 3-6. X-ray photoelectron spectra of LB films of (a) ODP-sgC-SWCNT and (b) ODP-iAD-SWCNTs.

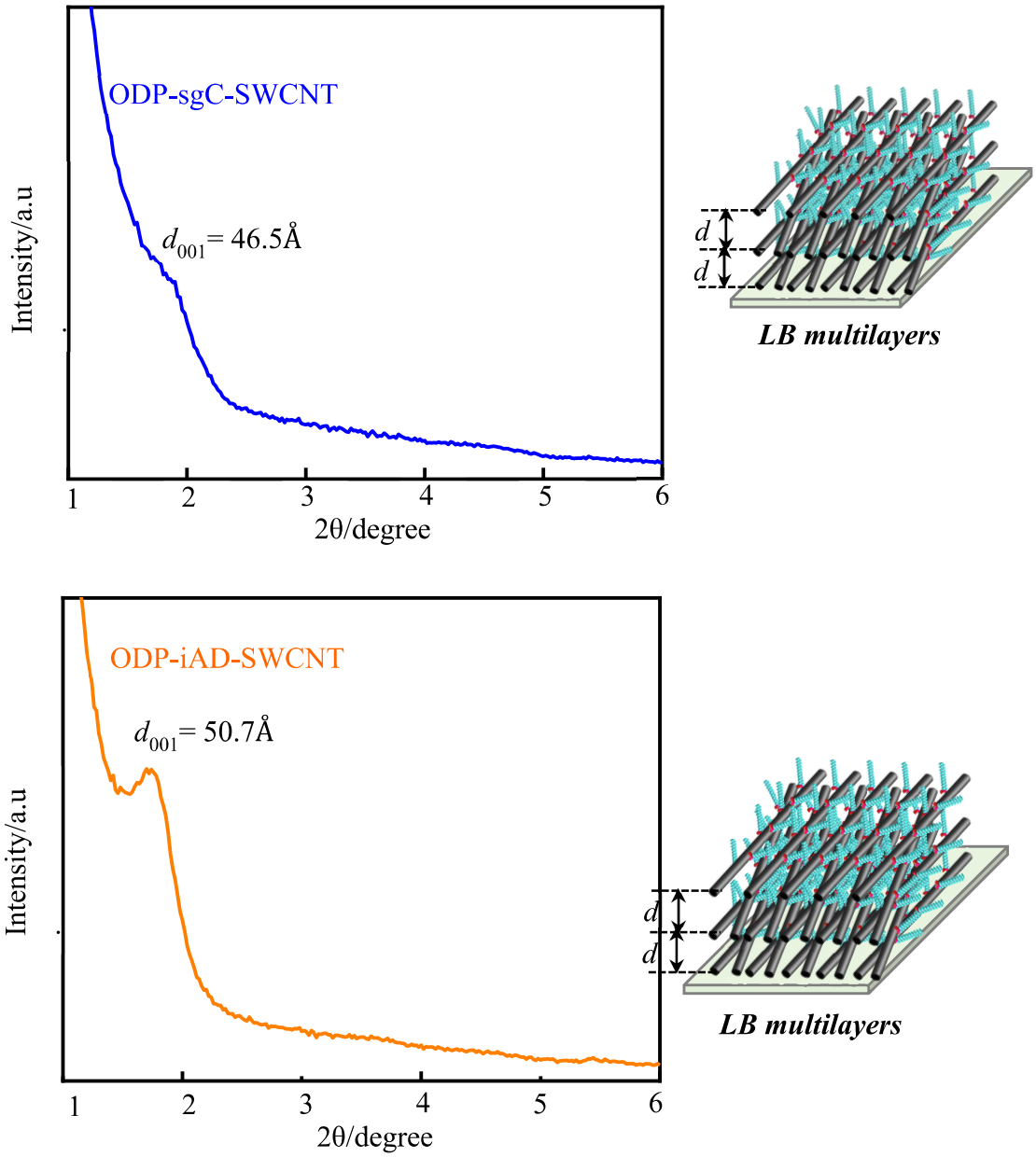

Figure 3-7. Out-of-plane XRD profiles of LB multilayers of ODP-sgC-SWCNT and ODP-iAD-SWCNT (15 $mN \cdot m^{-1}$, 20 layers, and 15 °C), and schematic illustrations of the layer structure of corresponding materials in their LB films.

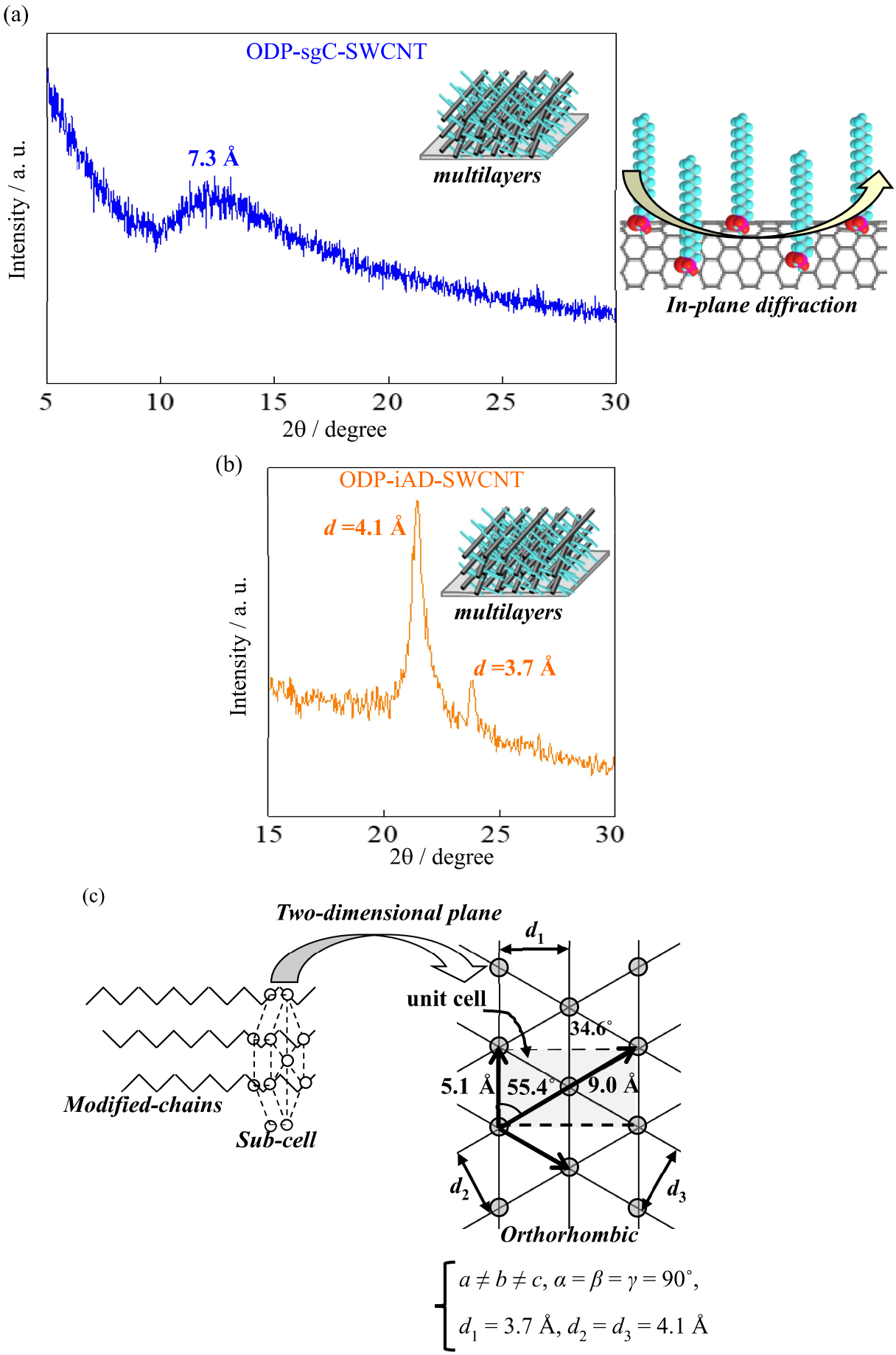

Figure 3-8. In-plane XRD profiles of LB multilayers of (a) ODP-sgC-SWCNT and (b) ODP-iAD-SWCNT (15 mN·m^{-1}, 20 layers, 15 °C). (c) Schematic illustrations of sub-cell structure of modified chains of ODP-iAD-SWCNT in its LB films.

3-4. Comparison of dispersibility and physical properties of polymer-based nanocomposite preparation containing two types of organo-modified SWCNTs as nanofillers

Figure 3-9 shows the results of nanocomposite preparation using the crystalline polymer shown in the Experimental Section and its application to two types of organo-modified SWCNTs under exactly the same conditions and addition amount. Figure 3-9(a) shows a digital camera photograph of the obtained PP-based nanocomposites. Surprisingly, the appearance of the two types of nanocomposites is quite different. The nanocomposite that was obtained by adding 0.5 wt% ODP-iAD-SWCNT to PP is a white-based material with many large black aggregates at a visible level and a heterogeneous appearance. In contrast, the nanocomposite obtained by adding 0.5 wt% ODP-sgC-SWCNT to PP is a material with a uniform black appearance that cannot be thought of as having the same amount of addition of organo-SWCNT. Comparing the two kinds of mesoscopic polarized microscopic images reveals that a fibrous black substance that seems to be SWCNTs is dispersed in the PP/ODP-sgC-SWCNT nanocomposite (Fig. 3-9(b)).

Tensile tests were performed on these two polymer/organo-nanofiller nanocomposites, and the S–S curve was drawn to obtain the result shown in Fig. 3-9(c). The S–S curves of both were similar; there was almost no difference in the Young's modulus that could be calculated from the initial gradient (a range of approximately 680–700 MPa), and both had the same extent of excellent elongation rates. However, the PP/ODP-sgC-SWCNT nanocomposite, which had excellent dispersibility, was superior in terms of yield point value and maximum stress, suggesting the superiority of sgC-SWCNTs as a filler in the composite material. Specifically, in PP/ODP-sgC-SWCNT nanocomposite, the yield point appears at 6.5% and the maximum stress strain value is 22.1 MPa. On the other hand, the yield point of PP/ODP-iAD-SWCNT nanocomposite appears at 5.4%, and the maximum stress strain value corresponds at 19.8 MPa.

Therefore, it shows that the ratio and strength of the composite material showing plastic deformation shows a higher value in ODP-sgC-SWCNT system.

When observing the SWCNTs themselves using the TEM image shown in Fig. 3-10, it can be seen that in both cases, there is a structure inside the aggregates in which several SWCNTs are assembled. Although the PP/ODP-sgC-SWCNT nanocomposite was superior to the PP/ODP-iAD-SWCNT nanocomposite in filler dispersibility, this might merely be owing to a difference in the aggregate size of the secondary particles when observed mesoscopically. If the aggregate size of the filler is smaller than the wavelength of visible light, transparency will be added to the entire material, and the mechanical properties may be improved. However, the fact that the coherent length of the aggregate size changes may indicate a difference in the lipophilicity of SWCNTs in solid organic media.

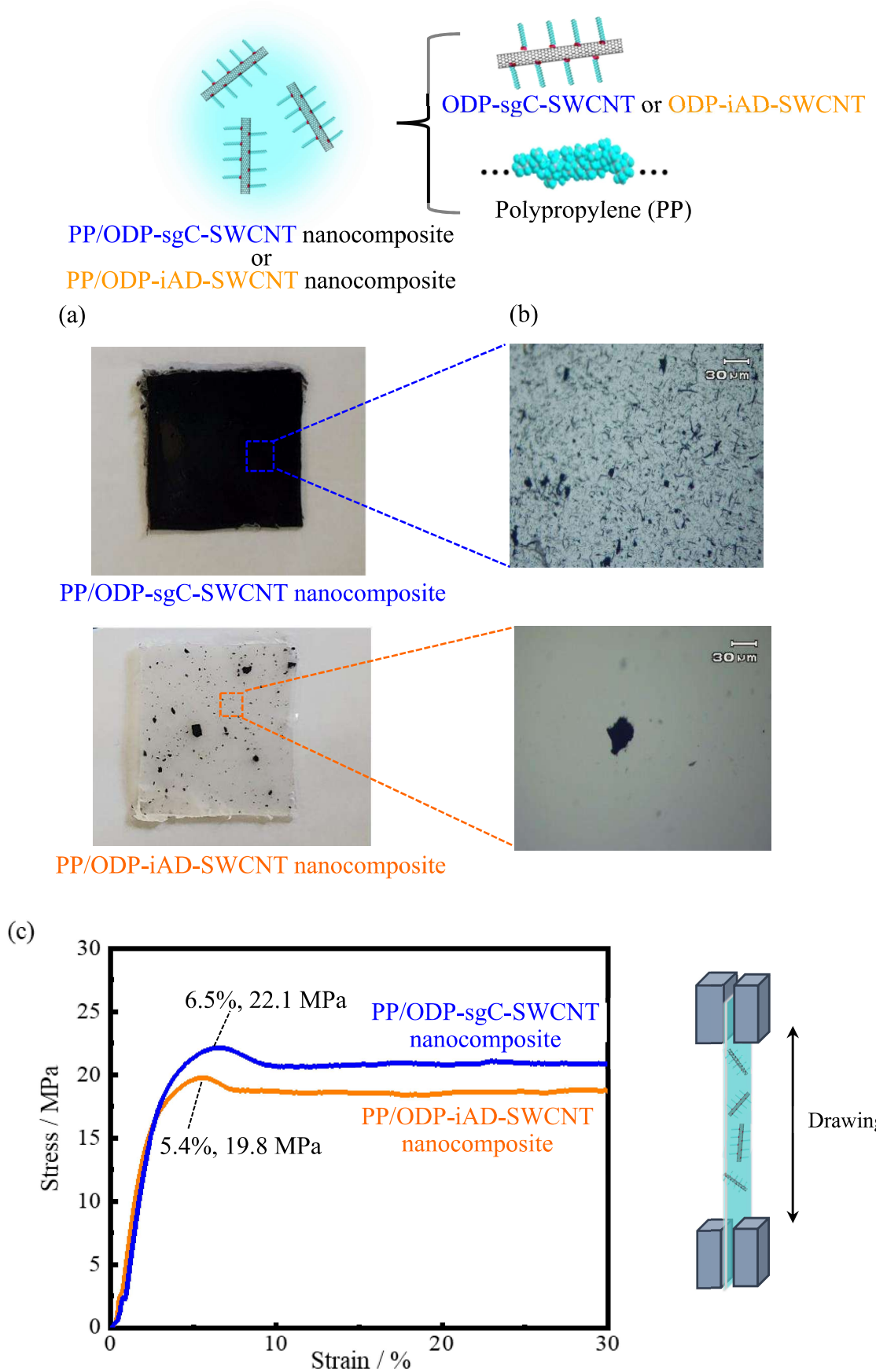

Figure 3-9. (a) Digital camera photographs, (b) polarized optical microscopic images, and (c) S-S curves of PP/ ODP-sgC-SWCNT and PP/ODP-iAD-SWCNT nanocomposites.

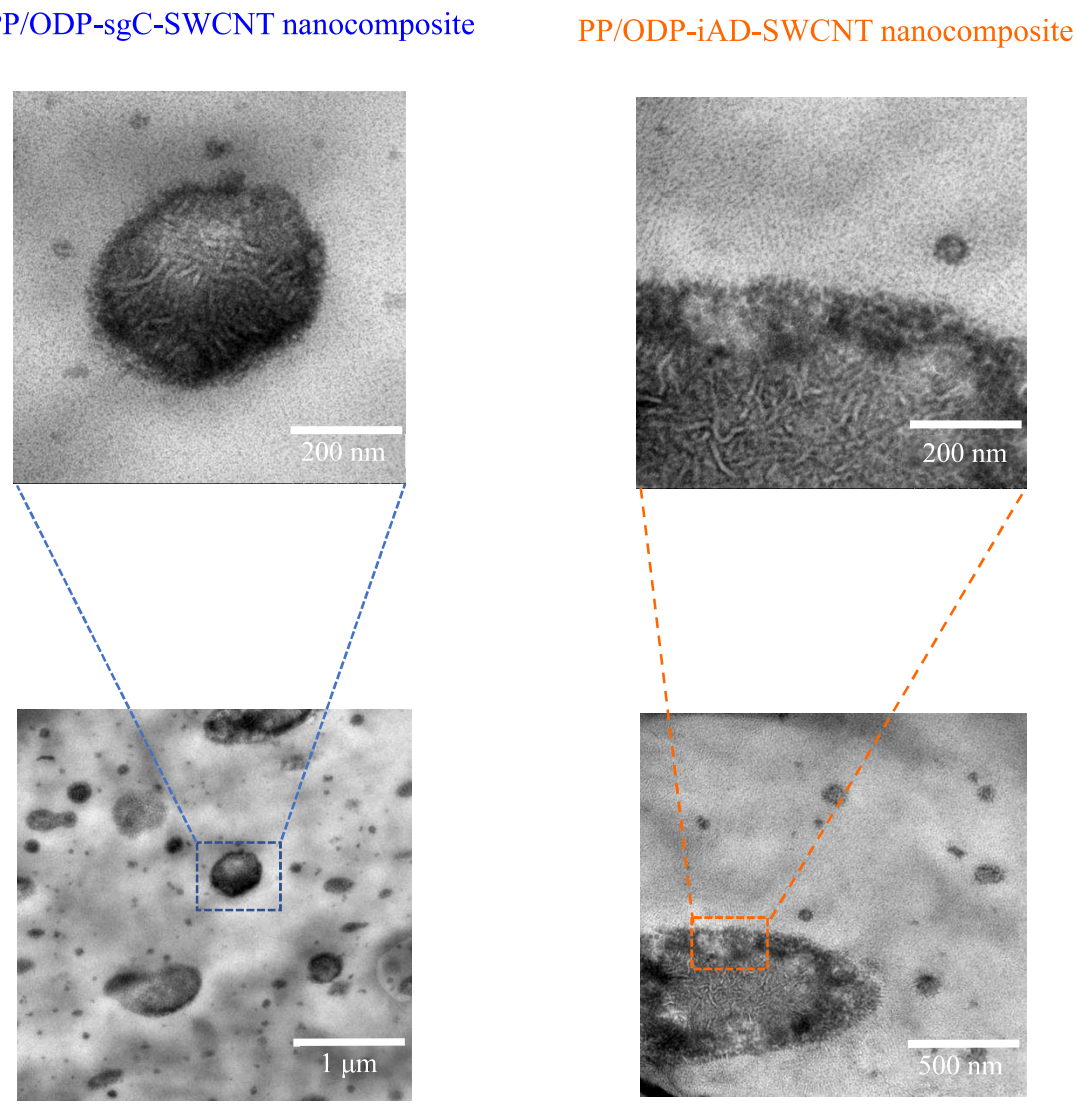

Figure 3-10. TEM images of PP/ODP-sgC-SWCNT and PP/ODP-iAD-SWCNT nanocomposites.

3-5. Conclusion

Finally, the results of this chapter are summarized in Fig. 3-11. For the SWCNTs obtained by the super-growth CVD and iAD-SWCNTs, differences in tube length distribution and impurity content are disappeared by performing phosphonate organo-modification as an operation to improve the wettability of organic media. When using the Langmuir monolayer or LB film methods, even when the organic modification rate was approximately the same, SWCNTs that were homogeneously distributed at the modification site and had an excellent crystalline arrangement were obtained via the improved-arc discharge method. Specifically, the modified chains were arranged in a relatively vertical orientation, and the in-plane crystalline packing also increased the regularity in the layering direction. In contrast, the SWCNTs obtained via the super-growth CVD method had excellent dispersibility in organic solid polymers. The mesoscopic aggregation size was reduced, and the yield point and maximum stress value of the nanocomposites containing SWCNTs were higher. It is predicted that the origin of this phenomena is the condition of the unmodified SWCNT exposed surface that prompts the difference between the two systems. The interaction between the exposed surfaces of SWCNTs is probably strong, and it is expected that iAD-SWCNTs would have excellent ordered aggregation characteristics. However, the interaction between SWCNT surfaces in the super-growth CVD method is relatively suppressed, and aggregation between nanotubes is easily disassembled. Because the organo-modification method used in this chapter underwent hydrophilic treatment in the initial stage, it is predicted that the hydroxyl group termination state will be reached. Considering the presence of positively charged hydroxyl groups that could not react with the phosphonate-modified chain, iAD-SWCNTs may have many negatively charged functional groups on their surface.

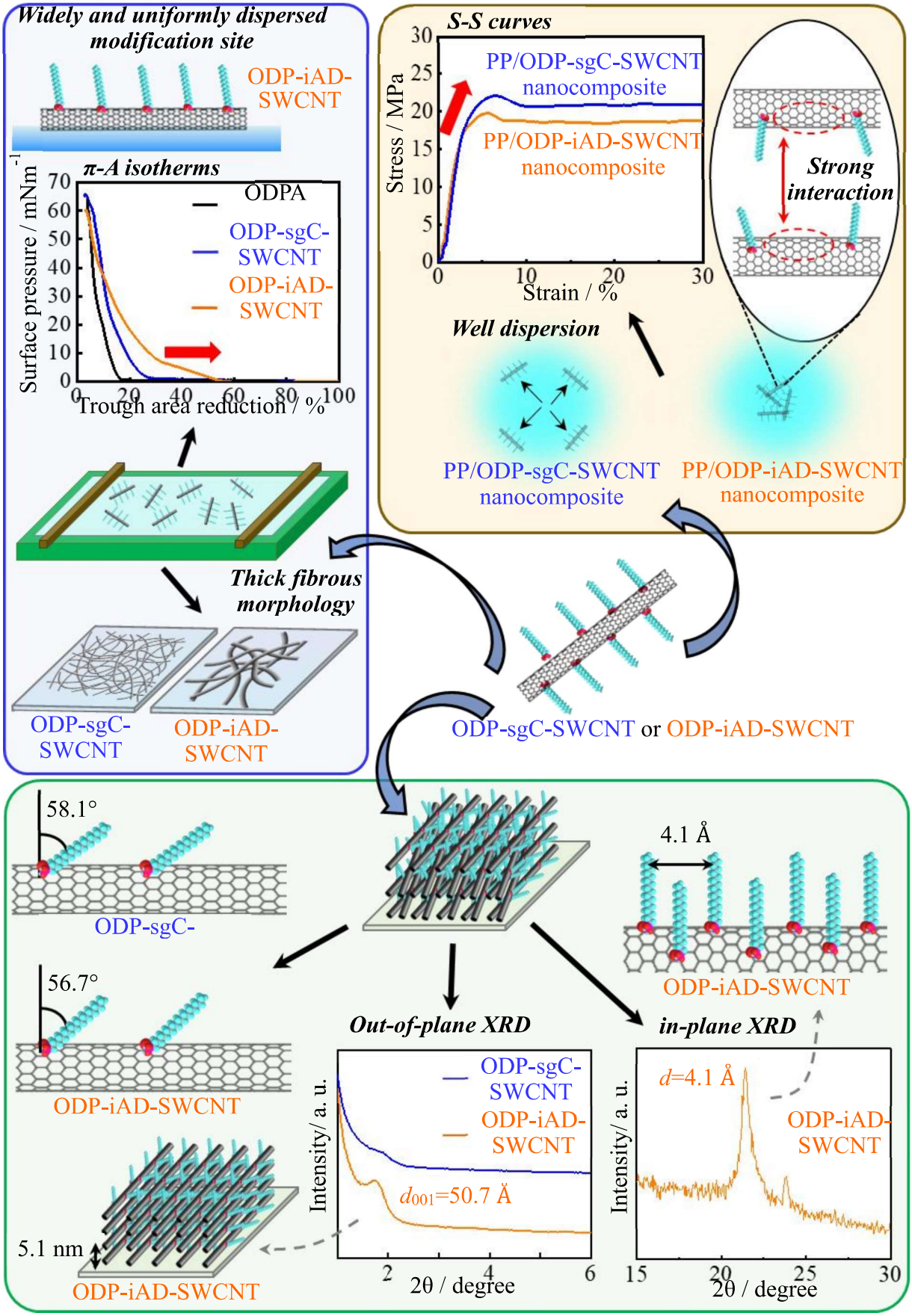

Figure 3-11. Summarized results of this chapter.

Chapter 4. Activity Maintenance Characteristics and Protease Adsorption on Langmuir Monolayer of Organo-Modified Single-Walled Carbon Nanotubes

4-1. Abstract

The activity maintenance characteristics of proteases adsorbed and immobilized on a monolayer of organo-modified SWCNTs were evaluated in this chapter. After forming a monolayer on the water surface of the organo-modified SWCNTs, protease was introduced into the subphase, and monolayer immobilization was attained by post-adsorption. The protease-adsorbed organo-SWCNT multilayers were immersed in an aqueous solution of luminescent casein, and fluorescence emission was observed. Proteases had cleaved the molecular chain of luminescent casein, which causes luminescence. Although the protease in the aqueous solution could cleave the molecular chain only up to approximately room temperature, the protease immobilized on the solid substrate could cleave the chain up to 160 °C, indicating sharp emission spectra.

Keywords: Single-Walled Carbon Nanotube, Interaction with Biomolecules, Langmuir Monolayers, Adsorption Immobilization, Organo-Modification

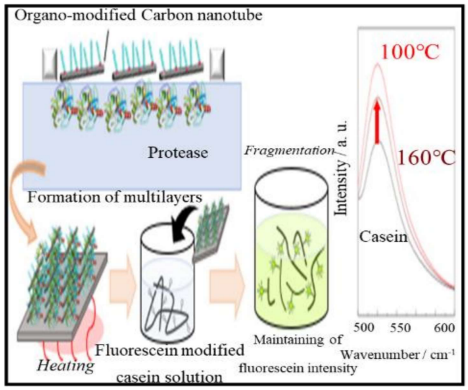

4-2. Formation behavior of the Gibbs monolayer of proteases from subphase and interaction with organo-modified SWCNT monolayer

Figure 4-1(a) displays the π–t isotherm of the Gibbs monolayer of the protease (15 °C). Generally, a monolayer formed by adsorbing a water-soluble surfactant on the air/water interface is called a Gibbs monolayer [111], wherein the surfactant forms a micelle state. This designation of terminology is used as a contrast to the insoluble Langmuir monolayer formed from a spreading solution at the air/water interface [34, 35, 37]. Biomolecules that contain both hydrophilic and hydrophobic groups, such as the protease used in this chapter, orient hydrophilic functional groups abundantly outward the aqueous solution. Conversely, when such biomolecules are adsorbed on an air/water interface to form a monolayer, they behave like a surfactant molecule in which the hydrophobic and hydrophilic functional groups are directed to the air and to the bottom of the water surface sides, respectively. Therefore, in this chapter, the monolayer of protease adsorbed on the air/water interface is called the Gibbs monolayer, and the behavior common to the surfactant molecule is emphasized. When the saturated buffer solution containing protease is allowed to stand, the surface pressure immediately increases to approximately 2 $mN \cdot m^{-1}$, and then gradually increases to approximately 12 $mN \cdot m^{-1}$ over about 6 h. After that, the increase in surface pressure was saturated, and a steep transition was observed after 12 h. This phenomenon corresponds to the behavior in which the protease begins to adsorb on the air/water interface immediately after

the aqueous solution is allowed to stand, and then gradually increases the film density. A steep increase in surface pressure is observed after 12 h, which is presumably a phase transition from the liquid film to the solid condensed film. The names of liquid films and solid condensed films are often used in the field of insoluble monolayers [34]. In this chapter, it was used because it is convenient as an expression indicating the state corresponding to the increase in film density. In the solid condensed phase, the intermolecular distance is narrowed, and the intermolecular interaction is strong; thus, there is a high possibility that the activity of the biomolecule will be lost. The aim of this chapter was to maintain the state at low surface pressure for adsorbing biomolecules on the SWCNT template and maintaining its activity even under atmospheric conditions.

Figure 4-1(b) shows the π–A isotherms of monolayers of organo-modified SWCNTs on ultrapure water and a buffer solution containing protease as the subphase (15 °C). This measurement was performed immediately after the saturated buffer solution containing protease was allowed to stand, and the starting surface pressure was corrected to zero. The fact that the behavior of the organo-modified SWCNT monolayer changes on the saturated buffer solution compared to the π-A curve on ultrapure water indicates the existence of an interaction between protease and organo-modified SWCNTs. The monolayer of organo-modified SWCNTs that interacted with proteases showed expanded behavior, and the phase transition around 40 $mN \cdot m^{-1}$ disappeared. It is predicted that such a series of behaviors

may be due to the adsorption of protease on the hydrophilic surface of SWCNTs. However, there are important concerns in this experiment. In this experiment, a protease-adsorbed monolayer at the air/water interface formed before the formation of an insoluble spreading monolayer of organo-modified SWCNTs. In other words, a mixed monolayer of the Langmuir film of the organo-modified SWCNT and the Gibbs monolayer of the protease will be formed. Proteases present in the aqueous solution at the initial stage as micelles are thought to be adsorbed on SWCNTs over time. However, proteases that quickly become Gibbs monolayers in the early stages may not be adsorbed on SWCNT surfaces. Therefore, in this chapter, a post-adsorption experiment of protease was performed after the formation of an organo-modified SWCNT monolayer. After the organo-modified SWCNT monolayer formed on ultrapure water exhibits a constant surface pressure on the π–A isotherm, protease is injected into the subphase to promote adsorption (inset illustration of Fig. 4-1). All subsequent experiments in this chapter used samples in which protease was allowed to act on organo-modified SWCNTs by post-adsorption experiments.

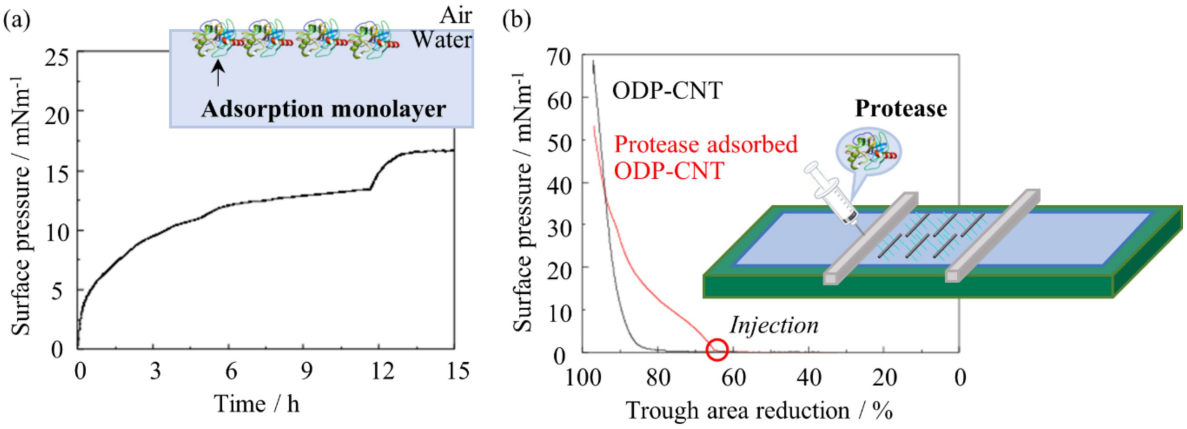

Figure 4-1. (a) π–t isotherm of Gibbs monolayer of the protease (15 ℃). (b) π–A isotherms of monolayers of organo-modified SWCNTs on ultrapure water and on buffer solution containing protease as subphase (15 ℃). (Inset illustration) Interaction induced experiment with SWCNT by post-injection of protease.

4-3. Confirmation of protease adsorption on organo-modified SWCNT monolayer and its morphology

Figure 4-2 shows AFM images of the organo-modified SWCNT monolayers. In this figure, the monolayers when the subphases corresponded to ultrapure water and the aqueous solution containing protease, respectively, were transferred onto a solid substrate by the HLM. The aqueous solution containing protease was stabilized for 30 min by post-injecting the protease solution into the subphase when the organo-modified SWCNT monolayer on ultrapure water reached a surface pressure of 10 $mN \cdot m^{-1}$. After that, an organo-modified SWCNT monolayer on an aqueous solution containing protease was transferred onto the substrate. As discussed in previous studies, the morphology of the organo-modified SWCNT monolayer itself shows a fibrous aggregated morphology [41, 43]. On the other hand, it can be confirmed that finely shaped deposits are present on the overall surface of each inorganic fiber in the organo-modified SWCNT monolayer in which protease was allowed to act from the subphase. This morphological feature is distinct from that of the organo-modified SWCNT monolayer.

Here, the distribution of SWCNT length and the length distribution of fibrous morphology are described. Although the length distribution of the SWCNTs used was 100-600 nm, it considered that the aggregated fiber length of the SWCNTs was important at the air/water interface. In the previous report, it showed a histogram of the tube length in a

monolayer of organo-modified SWCNT aggregates that were sonicated for 24 and 10 hours [41]. SWCNTs rupture during sonication in mixed acid, and the aggregated fiber lengths are fairly uniform at 400 nm, especially after 24-hour treatment. Therefore, it is considered that the influence of the distribution of SWCNT length on the adsorption of protease in this chapter is suppressed. On the other hand, if the effect of the aggregated fiber length is to be positively examined, it seems effective to change the ultrasonic treatment time to give a distribution to the aggregated fiber length.

Further, this chapter claim that protease is adsorbed in a almost monolayer on the surface of SWCNTs. However, there may be local multi-layered adsorption. On the other hand, the evidence that it is monolayer adsorption on average has been shown in resent report [112]. From the results of out-of-plane and in-plane X-ray diffraction, when multilayers were formed, the average interlayer distance was much smaller than that of bilayer adsorption, so I predicted that it would be monolayer adsorption.

By the way, the monolayer obtained by the HLM is an X-type monolayer in which the surface facing the subphase side was exposed to air. In other words, the surface on which the protease and SWCNT interacted in the aqueous solution was exposed. Regarding this point, I will further confirm the IR spectrum of the multilayers and deepen the discussion.

Figure 4-3 depicts the IR spectrum of the organo-modified SWCNT multilayers transferred onto a solid substrate with 20 layers by the HLM under the conditions of a

subphase temperature of 15 °C and a surface pressure of 10 $mN \cdot m^{-1}$. Here, I compared the spectra when the subphase was ultrapure water and when the protease was injected into the subphase. Protease-derived amide I and II bands were confirmed in the vicinity of 1550–1640 cm^{-1} in the multilayers on which the protease is acted. Furthermore, in this system, bands of N-H stretching vibration derived from the amide group of the protease with a hydrogen-bonding shift are clearly confirmed around 3300 cm^{-1}. Therefore, there is no doubt that protease is adsorbed on the organo-modified SWCNT multilayers in which protease is allowed to act from the subphase. Since the isoelectric point of trypsin (used as the protease to cleave the fluorescein-modified casein chain) is a pH of 10.5, the protease, which is also an amphoteric electrolyte, is positively charged in this experiment. At the air/water interface, it seems that organo-modified SWCNTs have surfaces with abundant organo-modified chains facing air and the surface with poorly bonded modified chains and abundant hydroxyl group termination facing the water. Therefore, the electrostatic interaction between the $-O^-$ group on the negatively charged SWCNT surface and the positive protease is considered to be the driving force of adsorption. From the above, it can be concluded that the results shown in Figs. 3 and 4 both show the morphology and spectral characteristics of the organo-modified SWCNT monolayer and multilayers before and after protease adsorption, respectively.

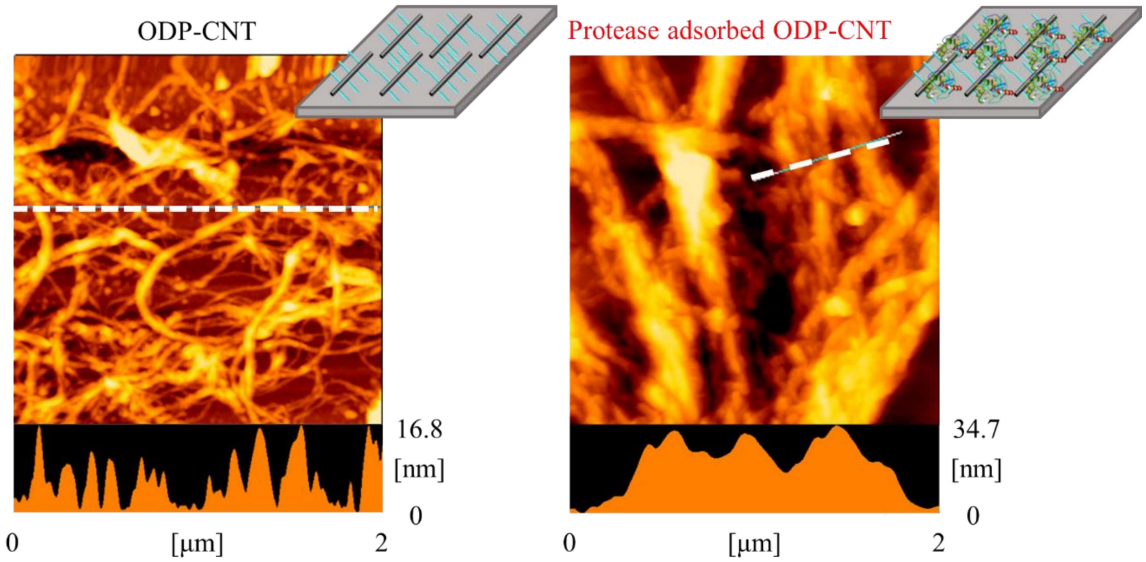

Figure 4-2. AFM images of monolayer of organo-modified SWCNTs on ultrapure water and an aqueous solution post-injected protease (15 °C, 10 $mN \cdot m^{-1}$).

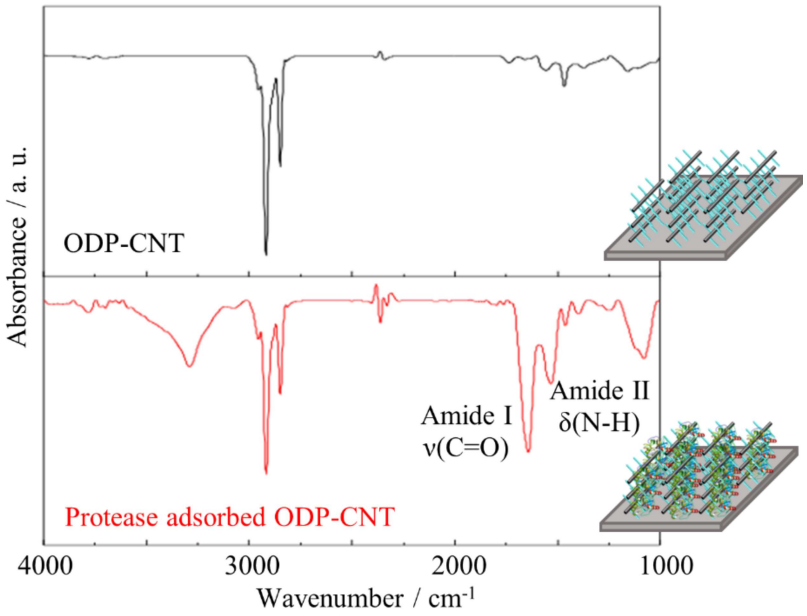

Figure 4-3. IR spectrum of X-type multilayers of organo-modified SWCNTs on ultrapure water and an aqueous solution post-injected protease (by HLM, 15 °C, 10 $mN \cdot m^{-1}$, 20 layers

4-4. Maintenance of protease activity adsorbed on organo-modified SWCNT monolayer under high-temperature conditions

Since it was found that the protease can be adsorbed and immobilized on the stearyl phosphonate-modified SWCNT monolayer, the activity maintenance characteristics are examined in this section. Figure 4-4 shows the fluorescence spectrum of fluorescein-modified casein in solution at room temperature (25 °C) with a black line. In addition, this figure shows the fluorescence spectrum after immersing the protease-adsorbed organo-modified SWCNT multilayers in a fluorescein-modified casein solution at room temperature for 5 min and removing, depicted by the red line. It can be seen that the intensity of the emission spectrum with the peak top at 520 nm clearly increased after the protease-adsorbed organo-modified SWCNT multilayers were applied. This increase in strength is because the protease adsorbed on the organo-modified SWCNT multilayers maintains its activity and induces breakage of the casein chain. The fluorescein-modified casein used in this chapter has the function of increasing its luminescence intensity by disrupting the molecular chain. Thus, protease adsorbed on an SWCNT surface maintains a three-dimensional steric structure using the SWCNT surface as a template and retains its functionality even once exposed to the atmosphere.

Figure 4-5 shows the most impressive data in this chapter. Figure 4-5(a) shows the fluorescence spectrum of the protease-adsorbed organo-modified SWCNT multilayers after

high-temperature annealing for 10 min in advance, followed by immersion in a fluorescein-modified casein solution. Surprisingly, there was no significant difference in the increase in fluorescence intensity when exposed to an environment at 100 °C. Moreover, even if the annealing temperature is further increased to 130 °C and 160 °C, the increase in fluorescence intensity itself can be confirmed. The increased value itself decreases slightly with increasing heat-treatment temperature, but the activity of the adsorbed protease is hardly lost. For comparison, Fig. 4-5(b) shows the fluorescence spectrum when the protease in the solution was subjected to the same heat treatment and allowed to act on the fluorescein-modified casein solution. In contrast to the increase in fluorescence intensity at room temperature, the value decreased significantly at 50 °C, and there was no significant increase in intensity at 90 °C. This behavior means that the steric structure of the protease in the solution completely collapses in an environment at 90 °C, and its activity is lost. On the other hand, it is suggested that the steric structure of the protease adsorbed on SWCNTs is maintained even at 100 °C, and that there may be no significant disturbances even at 160 °C.

It has similar data on adsorption to aluminosilicate / montmorillonite in past studies [71]. In this case as well, it was found that the periodic structure and secondary structure of the biomolecules adsorbed on the surface of the inorganic material were maintained under high temperature conditions. Therefore, it would be a promising proposal that the SWCNT surface, whose similar behavior can be confirmed, has the property of maintaining the

structure. However, the weakness at this point is that the difference between the two is not clear. By immobilizing biomolecules on both the aluminosilicate surface and the SWCNT surface, the structure is maintained and the activity in harsh environments is also maintained. Since SWCNT has a two-dimensionally finer periodic structure than aluminosilicate, the search for further functionality is interesting. However, at present, it is difficult to discover the unique characteristics of SWCNTs, even if they can show the superiority of immobilization on the surface of inorganic particles.

In these regards, the secondary structural changes of the protease-adsorbed organo-modified SWCNT multilayers before and after annealing at 160 and 200 °C were evaluated by Raman spectroscopy (Fig. 4-6). In the Raman spectrum, the amide I and II bands were confirmed between 1550 and 1640 cm^{-1}, as in IR. After annealing at 160 °C, the amide band intensity is slightly reduced, it becomes broad, and the secondary structure change is sensitively captured. Further, after annealing at 200 °C, the amide band intensity is further significantly reduced. Monitoring the amide band in laser Raman spectroscopy may be an indicator of the structural changes that contribute to protease inactivation.

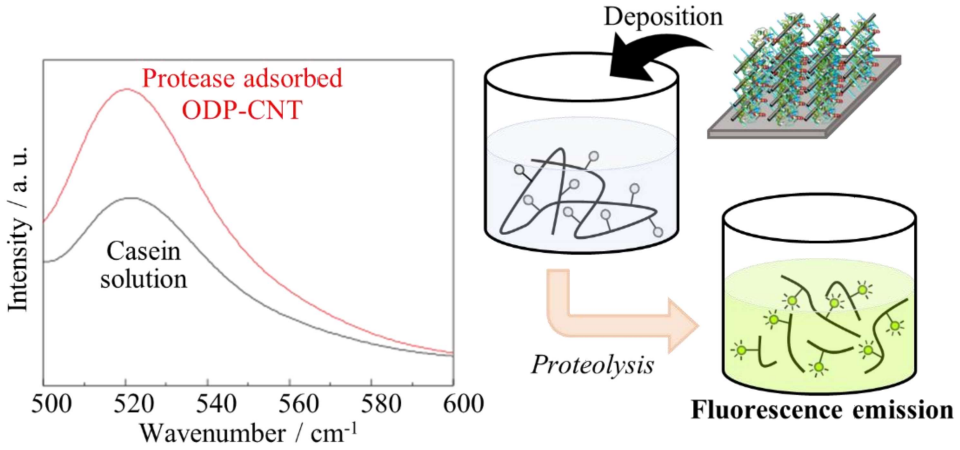

Figure 4-4. Fluorescence spectrum of fluorescein-modified luminescent casein solution. In addition, fluorescence spectrum after applying X-type multilayers of protease-adsorbed organo-modified SWCNT to the fluorescein-modified luminescent casein solution.

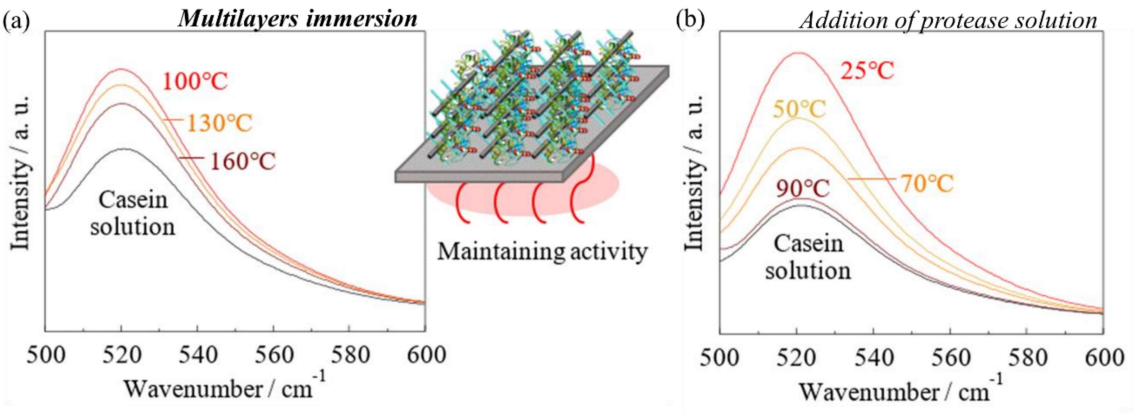

Figure 4-5. (a) Fluorescence spectrum of a fluorescein-modified luminescent casein solution in which X-type multilayers of protease-adsorbed organo-modified SWCNTs after annealing at each temperature was allowed to act. (b) Fluorescence spectrum of solution of a fluorescein-modified luminescent casein in which a protease solution exposed to each temperature was allowed to act.

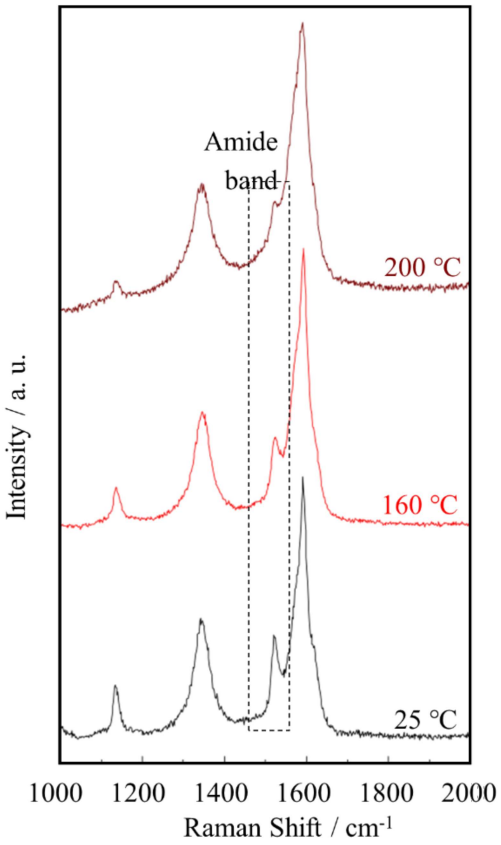

Figure 4-6. Raman spectrum of protease-adsorbed organo-modified SWCNT multilayers before and after annealing at 160 and 200 °C.

4-5. Conclusion

The above results are summarized in Fig. 4-7. The protease used in this chapter can be electrostatically adsorbed on an organo-modified SWCNT monolayer. Adsorption is achieved by post-injecting the organo-modified SWCNT monolayer into the subphase after the template exhibits a constant surface pressure and is densely packed. At this time, the protease forms a shape in which it is dispersed and adsorbed on the surface of the fibrous chain of SWCNTs. Proteases adsorbed on the SWCNT surface maintain their steric structure even when exposed to the atmosphere. Furthermore, even at a high temperature of 160 °C, its steric structure can be maintained, and its activity can occur. These data that the enzymatic reaction was confirmed even after being exposed to high temperatures were predicted to correspond that the "maintenance of steric structure" was maintained enzyme activity at high temperatures. Protease used in this chapter have the ability to cleave luminescent casein chains, and the cleaved casein emits light. The reason why the luminescence intensity does not increase at high temperature is that the activity of protease is lost, but this behavior is correlated with the disorder of the steric structure. Therefore, it can be asserted that the maintenance of the steric structure is an essential condition for confirming the enzymatic reaction. Specifically, Raman spectra are expected to show the maintenance of the steric structure of SWCNT-adsorbed protease when exposed to high temperatures. In other words, the adsorption of biomolecules on the surface of SWCNTs may contribute to the development

of biomaterials that can operate even in harsh environments.

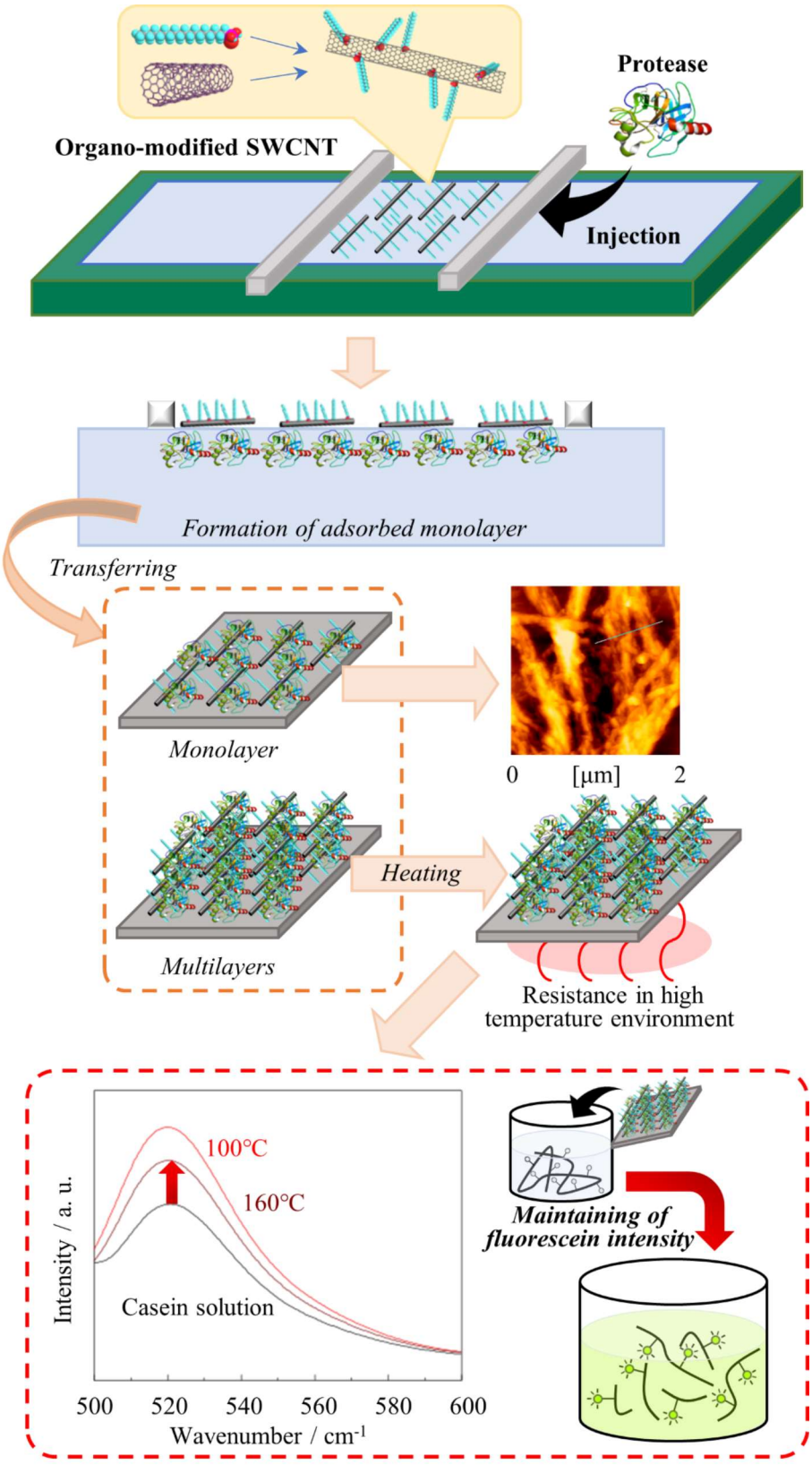

Figure 4-7. Schematic illustrations summarizing the contents of this chapter.

Chapter 5. Dispersion Characteristics of Polypropylene/Organo-Modified Single-Walled Carbon Nanotube Composites with a Long-Chain Phosphonic Acid Added as the Third Dispersant Component and Their Drawn Orientation

5-1. Abstract

A simple substance was added as the third component to a composite material comprising PP, a general-purpose resin, and long-chain phosphonate-modified SWCNTs to improve the filler dispersibility of the composite. Although SWCNTs with high aggregation characteristics could be introduced into organic polymers by modifying the organic chains on the outermost surface of the nanoparticles, their dispersibility was not sufficient. As a compound with a low molecular weight, a stearyl phosphonic acid was used as the modifier in this chapter. Due to the high sublimation temperature of this modifier, which exceeded the melting point of PP, a jet-black composite with high dispersibility was obtained when the modifier was added as the third component during melt-compounding. The jet-black three-component composite film exhibited better tensile properties than the two-component composite film. Analyzing the stretch orientation characteristics, the uniaxial stretching

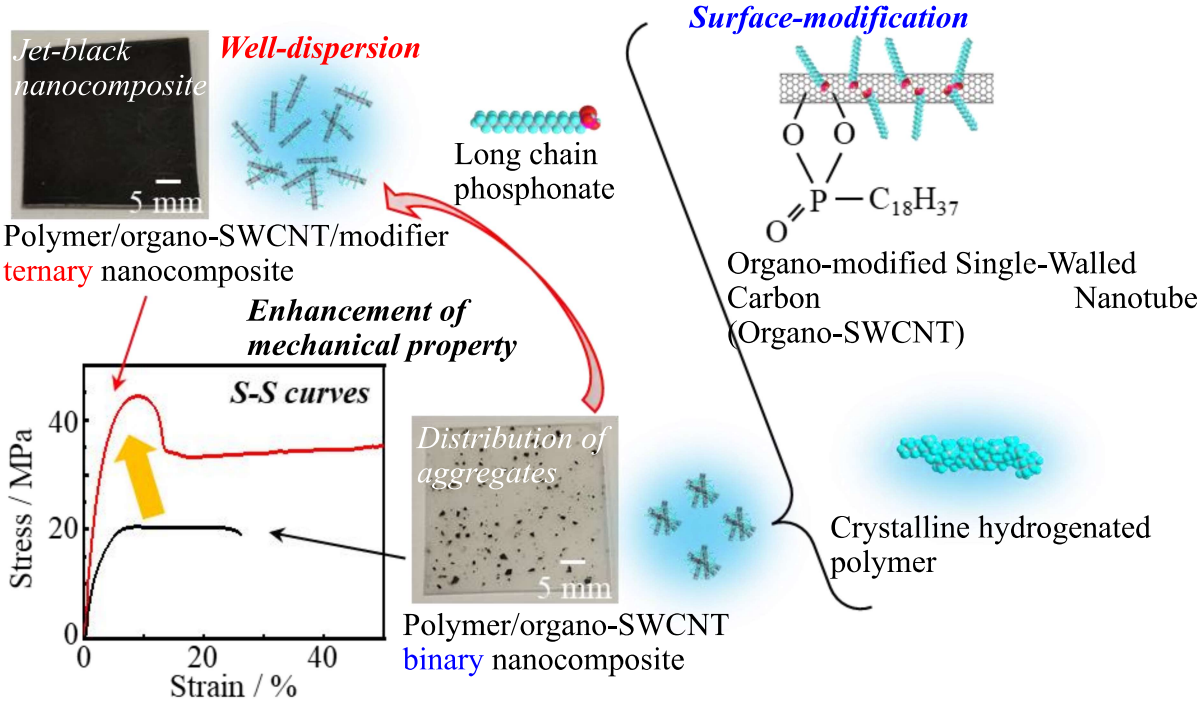

process induced deagglomeration, eliminating the difference in the initial dispersion states of the composites.

Keywords: Organo-modification; Single-walled carbon nanotube; Dispersant third component; Three-component polymer-based composite, Jet black film

5-2. Filler dispersibility and physical properties of PP/ODP-SWCNT composites containing ODPA modifier as the dispersant

Figure 5-1 shows the digital camera photographs and optical microscope images of the PP/ODP-SWCNT binary and PP/ODP-SWCNT/ODPA ternary composite films with varying amounts of the third component. In the binary composite shown in Fig. 5-1(a), macroscopic aggregation was confirmed at 0.5 wt% filler. In contrast, the ternary composite containing 0.5 wt% of dispersant exhibited a characteristic "jet-black film" (Fig. 5-1(b)). The optical microscope image of the jet-black film indicated that the fine aggregates were well-dispersed. Even though the same amount of SWCNT were added in the nanocomposites shown in Figs. 3(a) and 3(b), the difference in macroscopic color tone was significant. When the amount of ODPA added was increased to 1.0 wt% (Fig. 5-1(c)), no jet-black film was produced, and the size of the aggregates observed in the optical microscope image was not uniform. This suggested that there could be an optimum dispersant to ODP-SWCNT ratio that could maximize dispersibility. At this time, it seems extremely important to consider the intramolecular interaction between the organic modifier ODPA and the organo-modified chain portion of ODP-SWCNT. That is to say, due to the enhanced van der Waals interaction between the long-chain alkyl groups, both of chains are considered to be located close to each other in the composite. Therefore, ODPA seems to have the effect of improving the surface coverage of SWCNT in a pseudo manner. As a result, it is considered that the wettability between the hydrocarbon-based organic polymer and the matrix polymer is improved and the dispersibility is improved more than the modification rate of SWCNT.

Figure 5-2 and Table 5-1 show the crystallinity and thermal properties of the neat PP and the three composites. Fig. 5-2(a) shows the WAXD profiles of the four samples. At 2θ values of 10° to 30°, the peaks of the (110), (040), and (130) planes, as well as the combined peaks of the (111) a5-2nd (041) planes were confirmed. The absence of significant changes in any

of the peak positions indicated no change in the crystal system itself. By mathematically subtracting the amorphous curve from the intensity curve and evaluating the crystallinity based on the curve fitting, the degree of crystallinity of the neat PP, binary composite, and ternary composites with 0.5 and 1.0 wt% ODPA were 34, 39, 49, and 39%, respectively, proving that the ternary composite with 0.5 wt% ODPA showcased the highest crystallinity degree. Also, table 5-2 shows the crystallite size calculated from Scherrer formula. Here, too, a large D_{110} crystallite size of 0.5 wt% three-component composite was produced.

Figure 5-2(b) compares the thermal properties of the four samples using DSC thermograms. During the first cooling process, the crystallization peaks of the neat PP and binary composite hardly showed any difference. In contrast, the crystallization temperatures of the two ternary composites with different ODPA amounts, which were indicated by the extrapolation points of the rising curves of the baseline and peak, decreased by approximately 10 °C. As shown in the lower part of Fig. 5-2(b), this result was possibly attributed to the decrease in lamella thickness. In contrast to the WAXD analysis which suggested that the crystallinity of the composites either remained the same or was enhanced, the decreasing lamella thickness of the ternary composites indicated an increase in the crystalline region in the *ab*-plane. In the result of this study, the PP crystallization temperature decreases after adding SWCNTs and drawing. It was expecting a higher crystallization temperature if SWNTs induce the PP crystallization. However, when SWCNT was added and drawn composite, the crystallization temperature decreases, but the improvement in crystallinity was found from XRD. Since the decrease in crystallization temperature reflects the lamella thickness, the growth of lamella is suppressed. On the other hand, when SWCNT was added, many crystal nuclei were generated and the crystallinity in the ab-plane is improved. Therefore, although it does not contribute to the growth of lamella, it is thought that the degree of nucleation is improved, and the crystallinity is improved.

Figure 5-3 shows the S-S curves obtained from the tensile tests conducted on all the four composites. The changes in the mechanical properties of these samples were in good agreement with the trends observed in the optical microscope, WAXD, and DSC analysis. Compared with the neat PP represented by the broken line, the maximum stress value of the binary composite increased, but its elongation characteristics were lost, making the sample vulnerable to elongation. The yield point of the binary composite had also disappeared. In contrast, the ternary composites showcased obvious improvement in physical properties, reflecting the effect of filler dispersion. When 1.0 wt% ODPA was added, the maximum stress value was almost doubled, but the elongation characteristics were retained. For the jet-black ternary composite film in which the optimum amount of ODPA at 0.5 wt% was added, the maximum stress value was four times higher than that of the neat PP, and the elongation characteristics were maintained. Therefore, it could be concluded that the dispersion of SWCNTs on the jet-black film increased the crystallinity of the composite in the *ab*-plane, reduced the lamella thickness, and improved its mechanical properties corresponding to a fourfold increase in hardness.

In this chapter, TG analysis was also performed on all four samples: neat PP, PP/ODP-SWCNT binary composite, and PP/ODP-SWCNT/ODPA ternary composites containing 0.5 and 1.0 wt% ODPA. The TG curves shown in Fig. 5-4 accurately depicted the onset temperature at the start of thermal degradation for all samples. The jet-black PP/ODP-SWCNT/ODPA ternary composite with 0.5 wt% ODPA exhibited a thermal degradation onset temperature that was 11 °C lower than that of the PP/ODP-SWCNT/ODPA ternary composite with 1.0 wt% ODPA. However, no significance difference in behavior between the two ternary composites was observed at subsequent stages of thermal decomposition. As the thermal degradation temperature measured using TG analysis was considered to reflect the properties of the melt above the melting temperature, the two ternary

composites were expected to showcase little difference in thermal properties. Even though TG measurements could theoretically indicate the characteristics of the amorphous region of PP, which did not have a melting point, these characteristics were not reflected in the TG measurements conducted in this chapter.

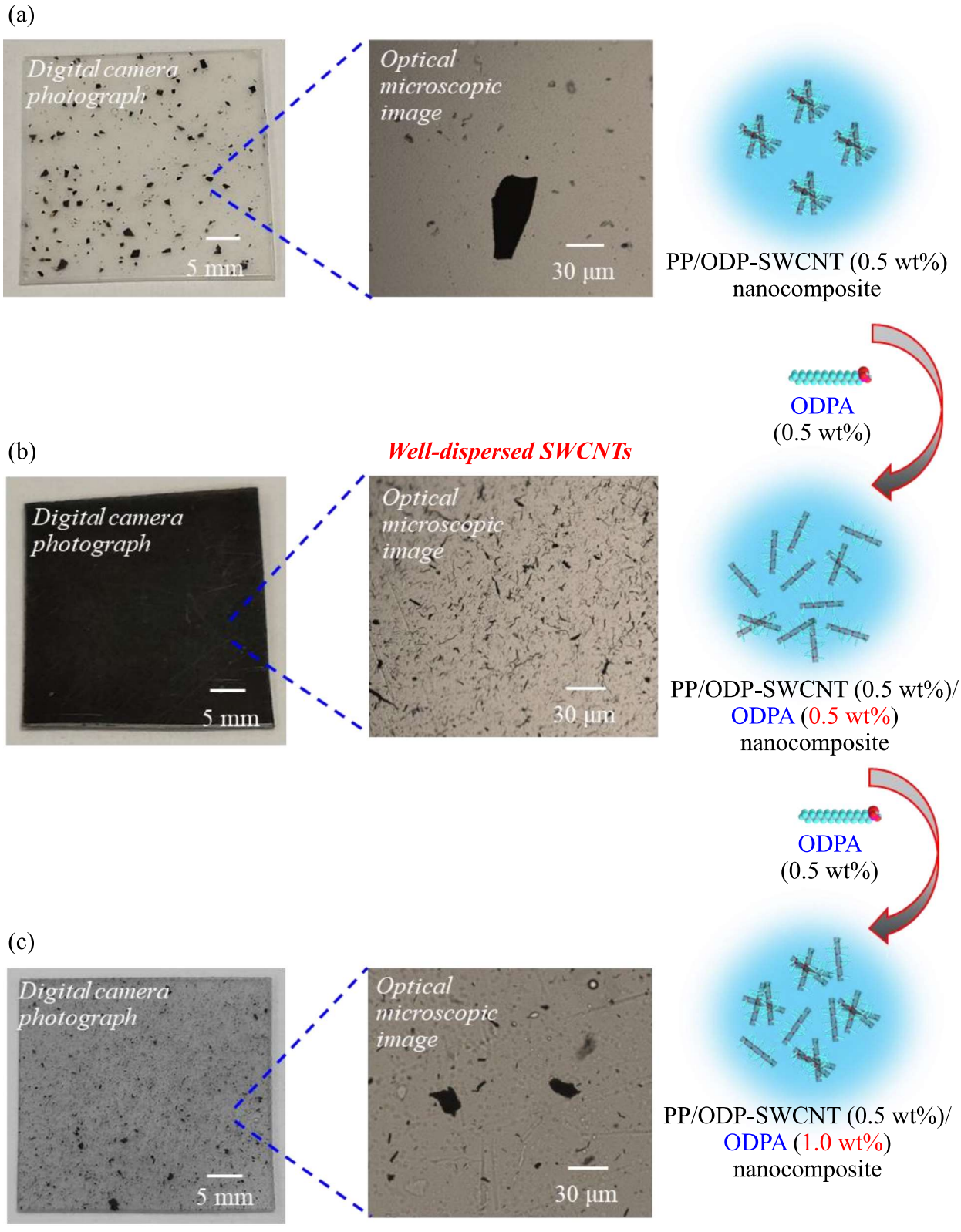

Figure 5-1. Digital camera photographs and optical microscope images of (a) the PP/ODP-SWCNT binary composite, and the PP/ODP-SWCNT/ODPA ternary composites containing (b) 0.5 and (c) 1.0 wt% ODPA modifiers.

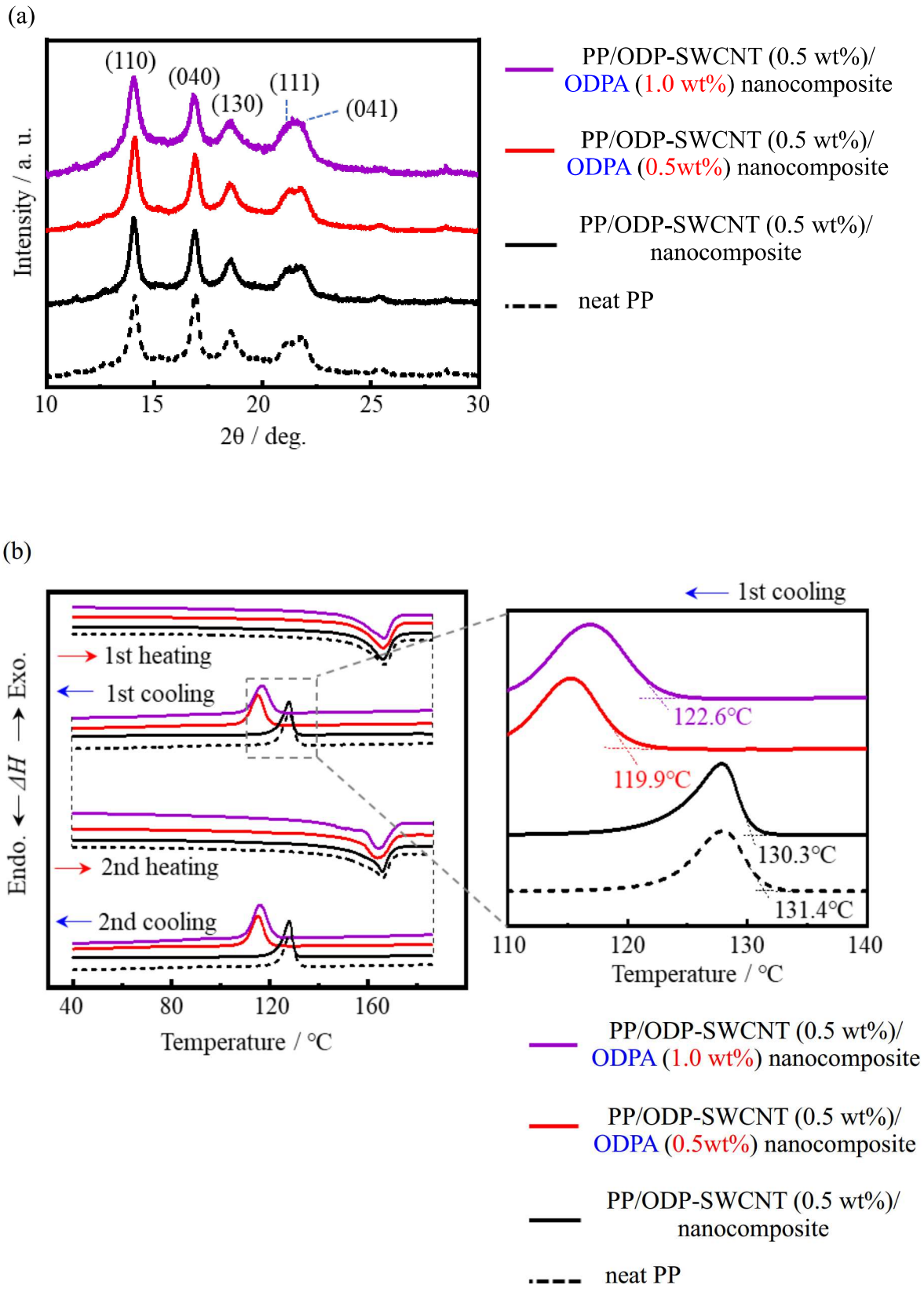

Figure 5-2. (a) Changes in WAXD profiles and (b) crystallization peaks of DSC thermograms (10 °C·min^{-1}) of the neat PP, PP/ODP-SWCNT binary composite, and PP/ODP-SWCNT/ODPA ternary composites containing 0.5 and 1.0 wt% ODPA modifiers.

Table 5-1. Crystallization degree of the neat PP, PP/ODP-SWCNT binary composite, and PP/ODP-SWCNT/ODPA ternary composites containing 0.5 and 1.0 wt% ODPA modifiers, calculated from WAXD profiles.

Samples	Crystallization degree [%]
PP/ODP-SWCNT/ODPA (1.0 wt%) nanocomposite	39
PP/ODP-SWCNT/ODPA (0.5 wt%) nanocomposite	49
PP/ODP-SWCNT nanocomposite	39
Neat PP	34

Table 5-2. Crystalline size of the neat PP, PP/ODP-SWCNT binary composite, and PP/ODP-SWCNT/ODPA ternary composites containing 0.5 and 1.0 wt% ODPA modifiers, calculated from WAXD profiles.

Samples	Crystalline size D_{110} [Å]
PP/ODP-SWCNT/ODPA (1.0 wt%) nanocomposite	227
PP/ODP-SWCNT/ODPA (0.5 wt%) nanocomposite	246
PP/ODP-SWCNT nanocomposite	225
Neat PP	214

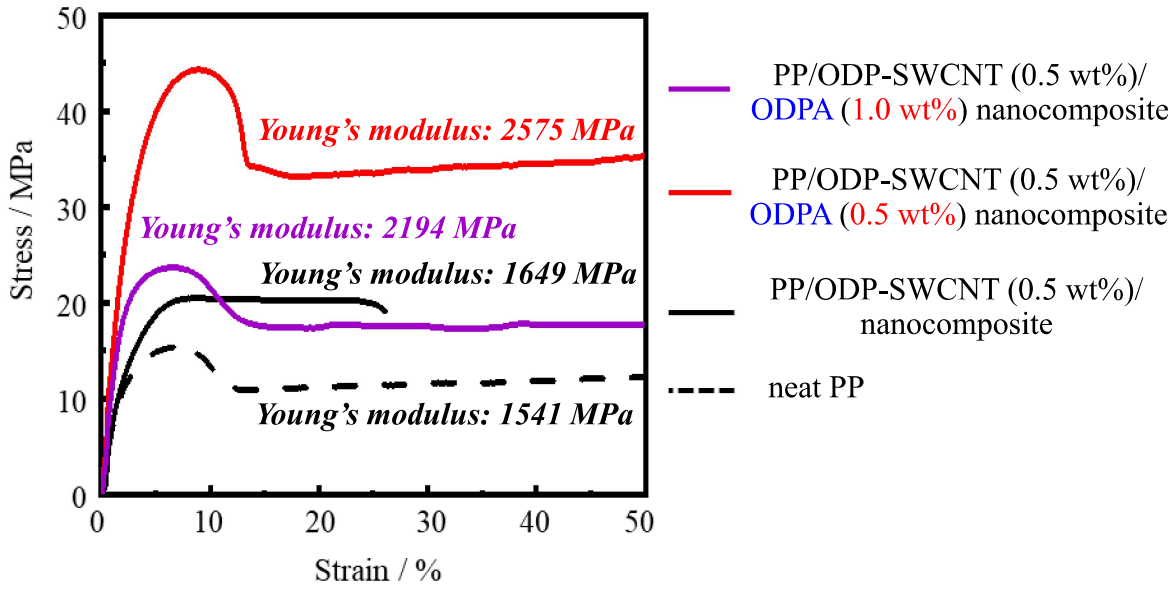

Figure 5-3. S-S curves of the neat PP, PP/ODP-SWCNT binary composite, and PP/ODP-SWCNT/ODPA ternary composites containing 0.5 and 1.0 wt% ODPA modifiers.

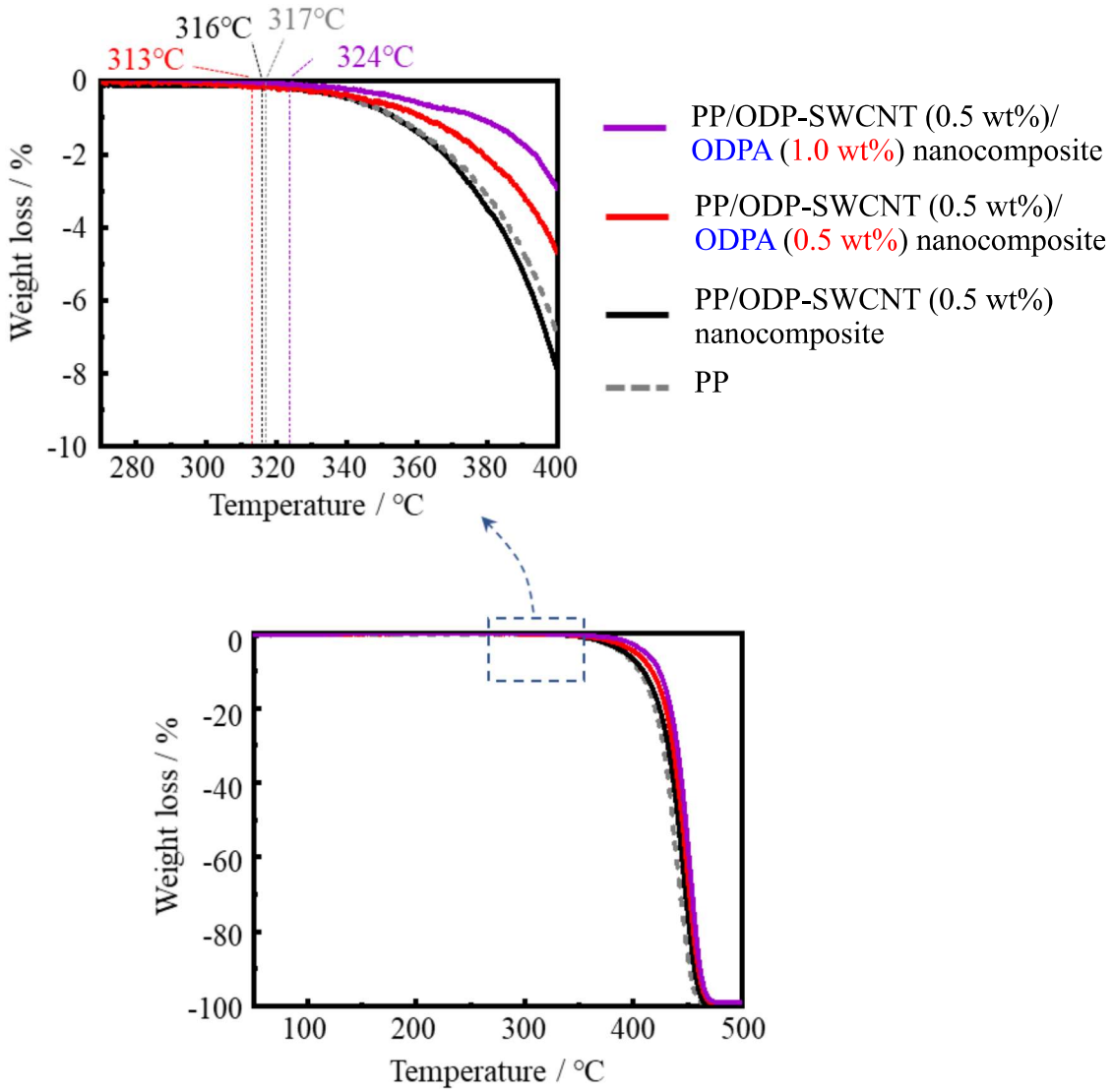

Figure 5-4. TG curves of the neat PP, PP/ODP-SWCNT binary composite, and PP/ODP-SWCNT/ODPA ternary composites containing 0.5 and 1.0 wt% ODPA modifiers (scanning rate: 10 °C·min^{-1}).

5-3. Drawn orientation characteristics of PP/ODP-SWCNT/ODPA ternary composites

Figure 5-5 illustrates the states of the binary and jet-black ternary composite films after uniaxial drawing. Fig. 5-5(a) showcases a digital camera image of the jet-black ternary composite film before and after uniaxial high-temperature drawing. As the sample was shaped like a dumbbell after drawing for the convenience of setting it in the uniaxial drawing apparatus, the effect of stretching on both ends of the sample sandwiched between the drawing apparatus was not reflected. The central part of the sample, which was elongated to five times its length by drawing, appeared lighter than the ends and was slightly transparent. When observed with a POM, as shown in Fig. 5-5(b), the SWCNT aggregates were uniaxially oriented in the drawing direction. In the binary composite with the same SWCNT content as the ternary composite (Fig. 5-5(c)), macroscopic aggregates were sparingly present. Although the density was low, the presence of uniaxially oriented SWCNT aggregates in the binary composite could be confirmed using a POM (Fig. 5-5(d)). This could be because the drawing treatment promoted deaggregation, reducing the size of the aggregates. Although the distribution was biased, the difference in initial dispersibility was suppressed.

Figure 5-6 and Table 5-3 show the WAXD curves of the binary and ternary composites with the same ODP-SWCNT content, as well as the changes in crystallinity. Almost all the crystalline peaks in the WAXD profiles of the jet-black ternary and binary composites increased in intensity at increasing draw ratios, as shown in Figs. 5-6(a) and (b), respectively. Only the combined diffraction peaks of the (111) and (041) planes in both composites were obscured by the influence of orientation. The changes in diffraction peaks of the other planes suggested the effect of orientation on crystallinity. However, quantitative calculations indicated that the crystallization degree was saturated at approximately 65% for draw ratios beyond 2 (Table 5-3). The D_{110} crystallite size shown in Table 5-4 also saturates at a draw

ratio of 2 to 3 times. This proved that the intensity of a specific diffraction peak could increase at different orientations, but its crystallinity would be saturated at draw ratios higher than 2. In addition, the difference in crystallinity between the two composites when undrawn was eliminated when the drawing process was performed, enabling the binary and ternary composites to possess similar crystallinity. In addition, in order to complement the results of WAXD analysis, representative POM images of the drawn composites are shown in (Fig. 5-7). It was found that the filler orientation was completed at between the 2 times drawing and the 3 times drawing in both the binary and the ternary system.

However, the composites exhibited different thermal behaviors (Fig. 5-8). The crystallization temperature of the jet-black ternary composite (119.9 °C) was lower than that of the neat PP. At a draw ratio of 3, the crystallization start/on set temperature (118.1 °C) decreased slightly, the crystallization peak was sharp and the distribution of lamella thickness was uniform. At a draw ratio of 5, the crystallization peak was observed at a high temperature, and the lamella thickening was considered to be due to high-magnification drawing. In contrast, the binary copolymer exhibited almost no difference in crystallization temperature from that of the neat PP when unstretched. The change in crystallization temperature was also not noticeable even after drawing and tended to shift toward the lower temperatures. Poor filler dispersibility may prevent uniaxial drawing from thickening the lamella and increasing its uniformity. However, it should be noted that the crystallization temperature of the binary copolymer was always higher than that of the ternary copolymers, and this analysis was only a relative comparison with the undrawn samples of the same composite.

Figure 5-9 compares the S-S curves obtained from the tensile tests conducted on the jet-black ternary and binary composites after uniaxial drawing. The corresponding numerical data is presented in Table 5-5. No significant difference was observed between the two types of drawn samples, possibly due to the deagglomeration of the SWCNT filler caused by the

above-mentioned drawing. At draw ratios of 3 and 5, the Young's modulus, maximum stress value, and elongation of the binary and ternary composites were almost similar. Although the physical characteristics of the ternary composite were slightly superior, there was no significant difference between the two composites, and these materials were similarly transformed into hard and brittle samples, indicating a significant increase in hardness and decrease in elongation. In other words, drawing minimized the influence of the initial dispersibility on the mechanical properties and crystallinity of the composites containing SWCNTs. Drawing also increased the Young's modulus and maximum stress at the expense of elongation.

Considering the dramatic differences on their SWNT dispersibility, the modulus and strength are close for SWNT 0.5 and SWNT0.5 ODPA 0.5. Generally, the dispersibility of nano-filler does affect the reinforcement efficiency of the nanocomposites. In this study, the improvement of mechanical characteristics is limited comparing the improvement of dispersibility. (Fig. 5-10) provides the fracture surface of ternary composite. As these reasons, it was supposed that there are two factors. One is that, judging from the cut surface, the improvement of the dispersibility inside the material is limited to the improvement of the dispersibility of the surface. The other is that the dispersibility is relatively improved, but it looks black, so the aggregate size itself is larger than the wavelength of visible light. It was supposed that the above two were the reasons why the improvement of mechanical properties is suppressed.

From the results of POM images in (Fig. 5-7), it seems about the effects of dispersity and orientation on mechanical characteristics as follows. Drawn orientation promotes de-aggregation. The difference in the initial dispersion state is noticeable in the mechanical characteristics at that time. However, after drawing, the dispersibility is improved and the difference becomes unclear. In other words, the drawing operation is a means to partially

eliminate the poor dispersibility.

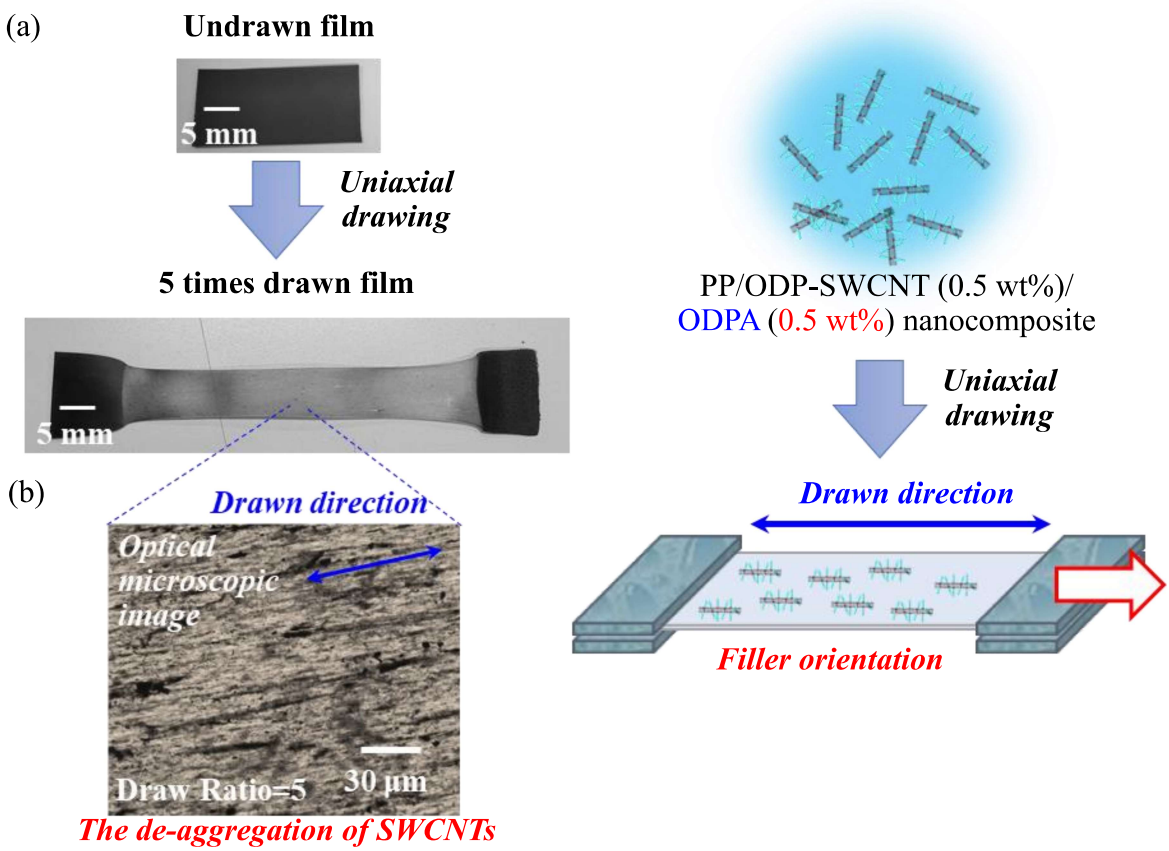

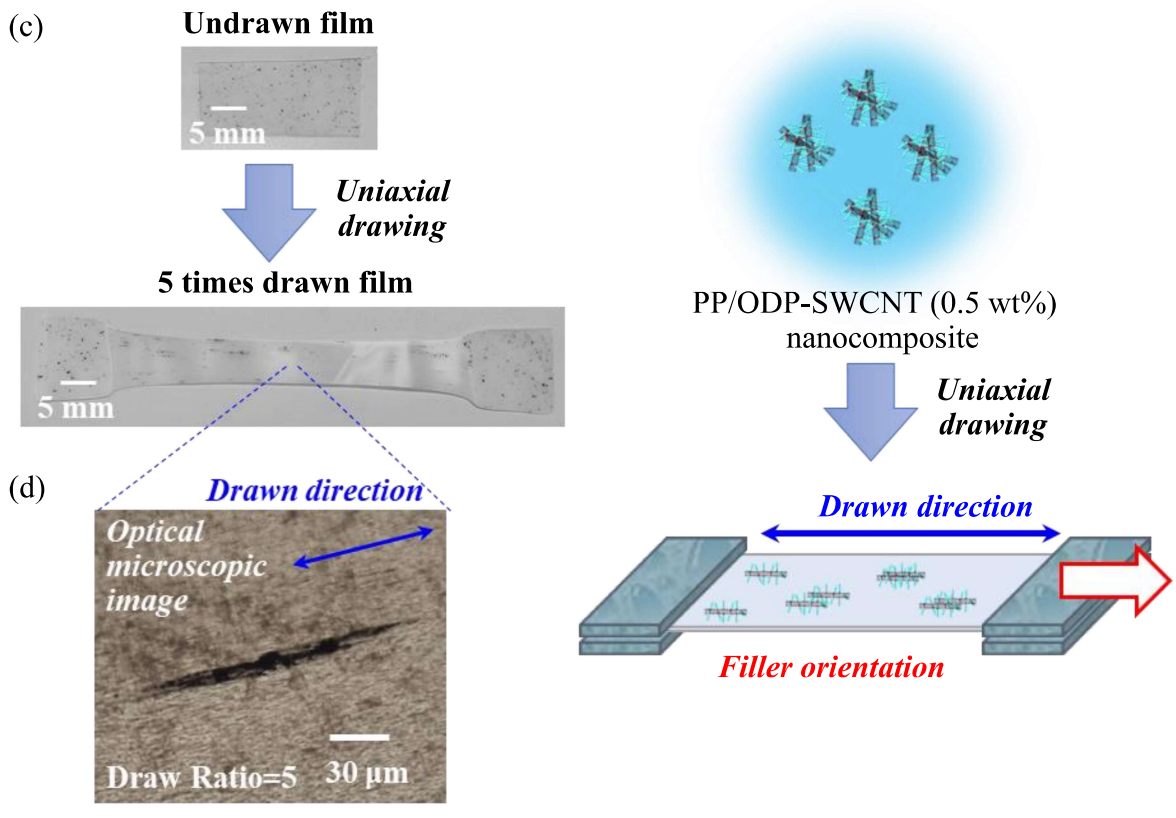

Figure 5-5. (a) Digital camera photographs and (b) optical microscope images of the PP/ODP-SWCNT/ODPA (0.5 wt%) ternary composite film before and after uniaxial drawing (draw ratio = 5). (c) Digital camera photographs and (d) optical microscope image of the PP/ODP-SWCNT binary composite film before and after uniaxial drawing (draw ratio = 5).

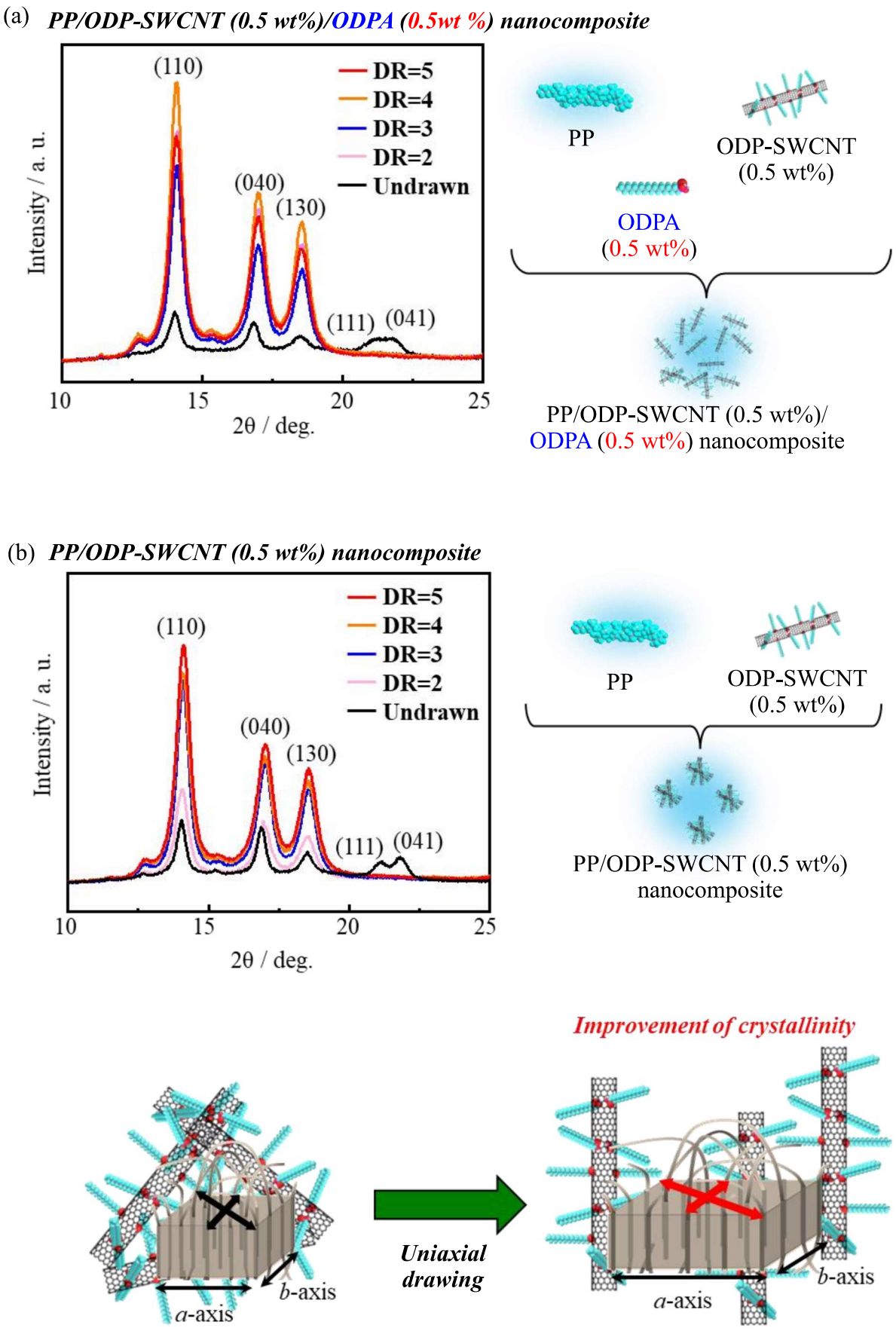

Figure 5-6. Changes in WAXD profiles of the (a) PP/ODP-SWCNT/ODPA (0.5 wt%) ternary composite and (b) PP/ODP-SWCNT binary composite depending on the draw ratio.

Table 5-3. Crystallization degree of the PP/ODP-SWCNT/ODPA (0.5 wt%) ternary composite and PP/ODP-SWCNT binary composite before and after uniaxial drawing, calculated from WAXD profiles.

Draw Ratio	Crystallization degree [%]	
	PP/ODP-SWCNT/ODPA (0.5 wt%) nanocomposite	PP/ODP-SWCNT nanocomposite
Undrawn	49	39
2	65	66
3	66	67
4	66	67
5	66	65

Table 5-4. Crystalline size of the PP/ODP-SWCNT/ODPA (0.5 wt%) ternary composite and PP/ODP-SWCNT binary composite before and after uniaxial drawing, calculated from WAXD profiles.

Draw Ratio	Crystalline size D_{110} [Å]	
	PP/ODP-SWCNT/ODPA (0.5 wt%) nanocomposite	PP/ODP-SWCNT nanocomposite
Undrawn	246	225
2	271	266
3	273	272
4	276	273
5	274	270

(a) PP/ODP-SWCNT (0.5 wt%)/ODPA (0.5 wt%) nanocomposite

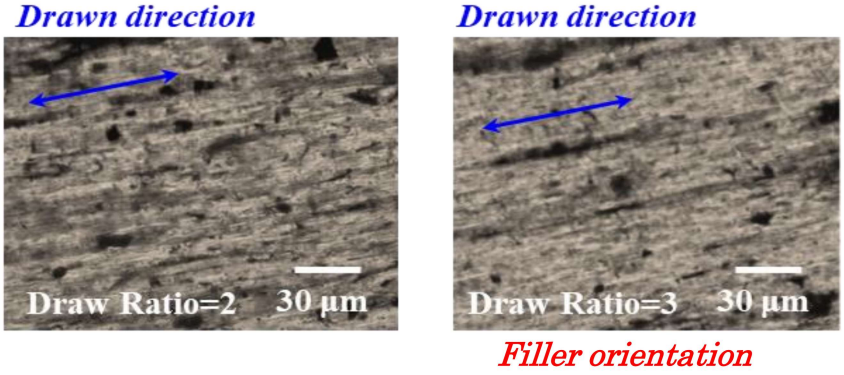

(b) PP/ODP-SWCNT (0.5 wt%) nanocomposite

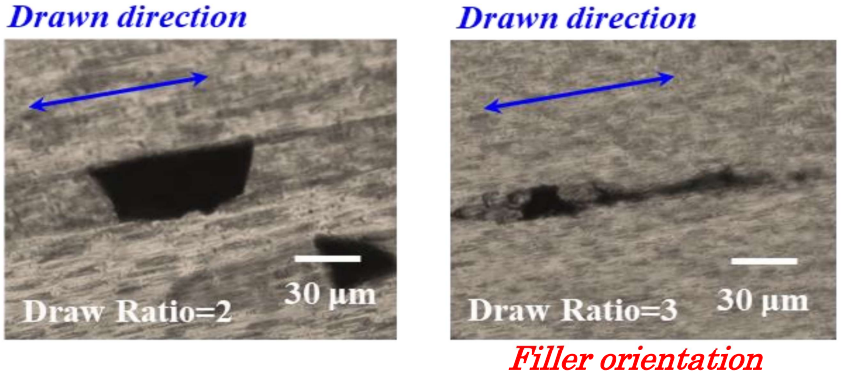

Figure 5-7. Optical microscope images of (a) the PP/ODP-SWCNT/ODPA (0.5 wt%) ternary composite film after uniaxial drawing (draw ratio = 2,3). and (b) the PP/ODP-SWCNT binary composite film after uniaxial drawing (draw ratio = 2,3).

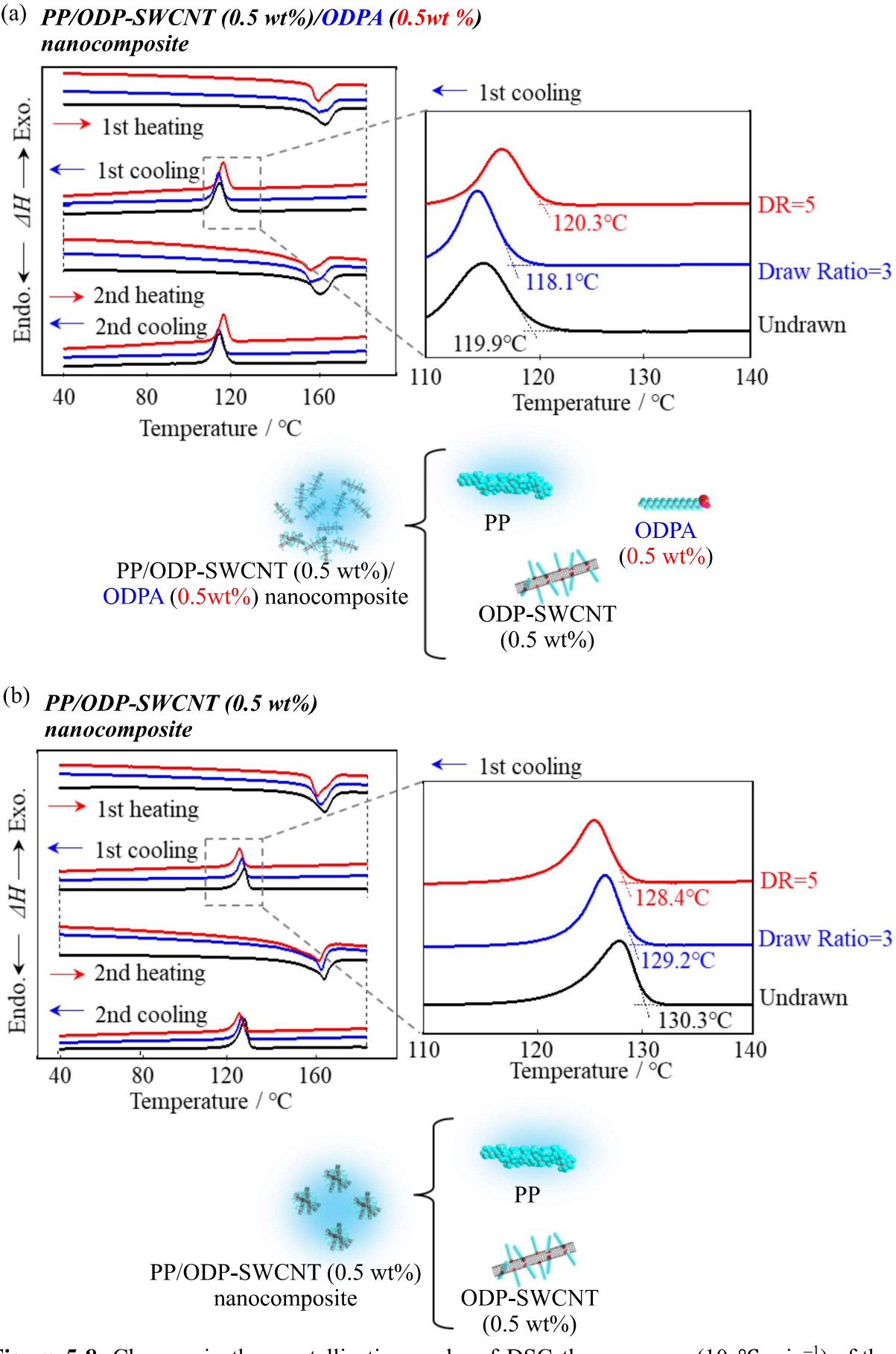

Figure 5-8. Changes in the crystallization peaks of DSC thermograms (10 ℃·min^{-1}) of the (a) PP/ODP-SWCNT/ODPA (0.5 wt%) composite and (b) PP/ODP-SWCNT composite depending on the draw ratio.

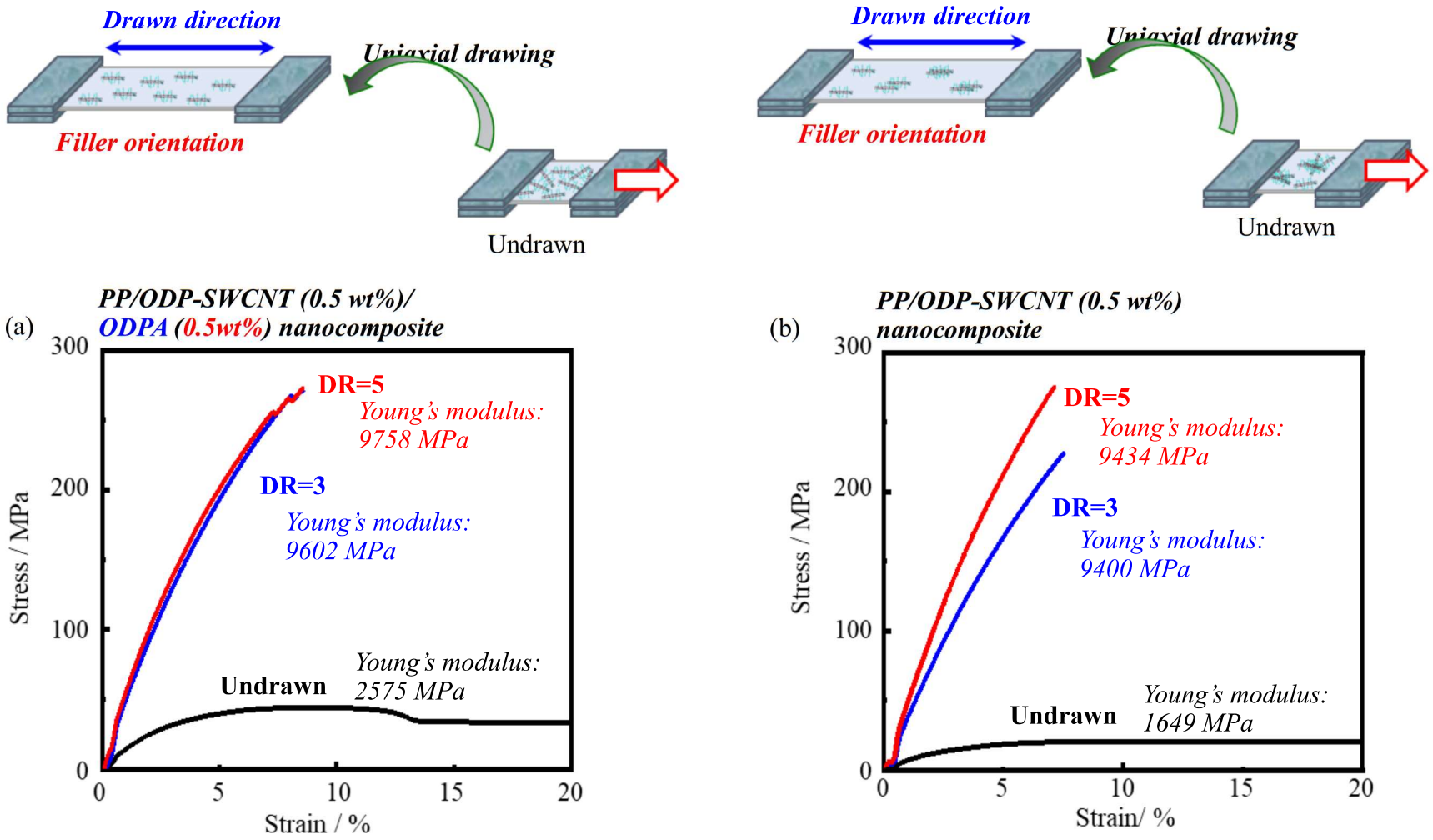

Figure 5-9. S-S curves of the (a) PP/ODP-SWCNT/ODPA (0.5 wt%) composite and (b) PP/ODP-SWCNT composite depending on the draw ratio.

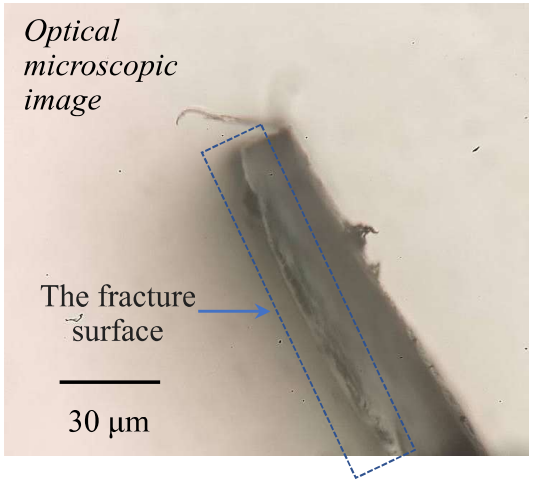

Drawn PP/ODP-SWCNT (0.5 wt%)/ODPA (0.5 wt%) nanocomposite

Figure 5-10. Optical microscope image of the fracture surface of the PP/ODP-SWCNT/ODPA (0.5 wt%) ternary composite film after uniaxial drawing (draw ratio = 5).

Table 5-5. Young's modulus, maximum stress, and maximum strain of the PP/ODP-SWCNT/ODPA (0.5 wt%) ternary and PP/ODP-SWCNT binary composites calculated from S-S curves.

Draw ratio	Young's modulus [MPa]		Maximum stress [MPa]		Maximum strain [%]	
	PP/ODP-SWCNT/ ODPA (0.5 wt%) nanocomposite	PP/ODP-SWCNT nanocomposite	PP/ODP-SWCNT/ ODPA (0.5 wt%) nanocomposite	PP/ODP-SWCNT nanocomposite	PP/ODP-SWCNT/ ODPA (0.5 wt%) nanocomposite	PP/ODP-SWCNT nanocomposite
Undrawn	2575	1649	44.31	20.42	92	28
3	9602	9400	271.1	227.2	8.6	7.5
5	9758	9434	272.8	275.0	8.6	7.0

5-4. Conclusion

The results of this chapter are summarized in Fig. 5-11. By introducing 0.5 wt% of ODPA into the PP/ODP-SWCNT composite, a characteristic jet-black composite with excellent filler dispersibility was obtained. Compared to the neat PP, the mechanical properties of this composite were significantly enhanced when not processed. However, when high-temperature uniaxial drawing was applied to the binary and ternary composites before and after introducing the ODPA dispersant, the effect of initial dispersibility was reduced. Uniaxial drawing induced deaggregation, causing the Young's modulus and maximum stress values in the ternary system to be slightly higher, but the difference was suppressed to a minimum. In this chapter, I presented a method to improve the dispersibility and minimize the difference in physical properties caused by the dispersibility effect in composite materials containing SWCNTs and general-purpose polymers. Although the ternary composite containing 0.5 wt% of dispersant exhibited a jet-black appearance, the difference in physical properties was not significant. This was because the jet-black appearance indicated the presence of SWCNT aggregates with sizes of visible light wavelengths. By reducing the sizes of these aggregate to below the wavelengths of visible light and preparing a composite that reflects the color tone of the matrix resin, further innovative improvements in physical properties of the materials could be expected.

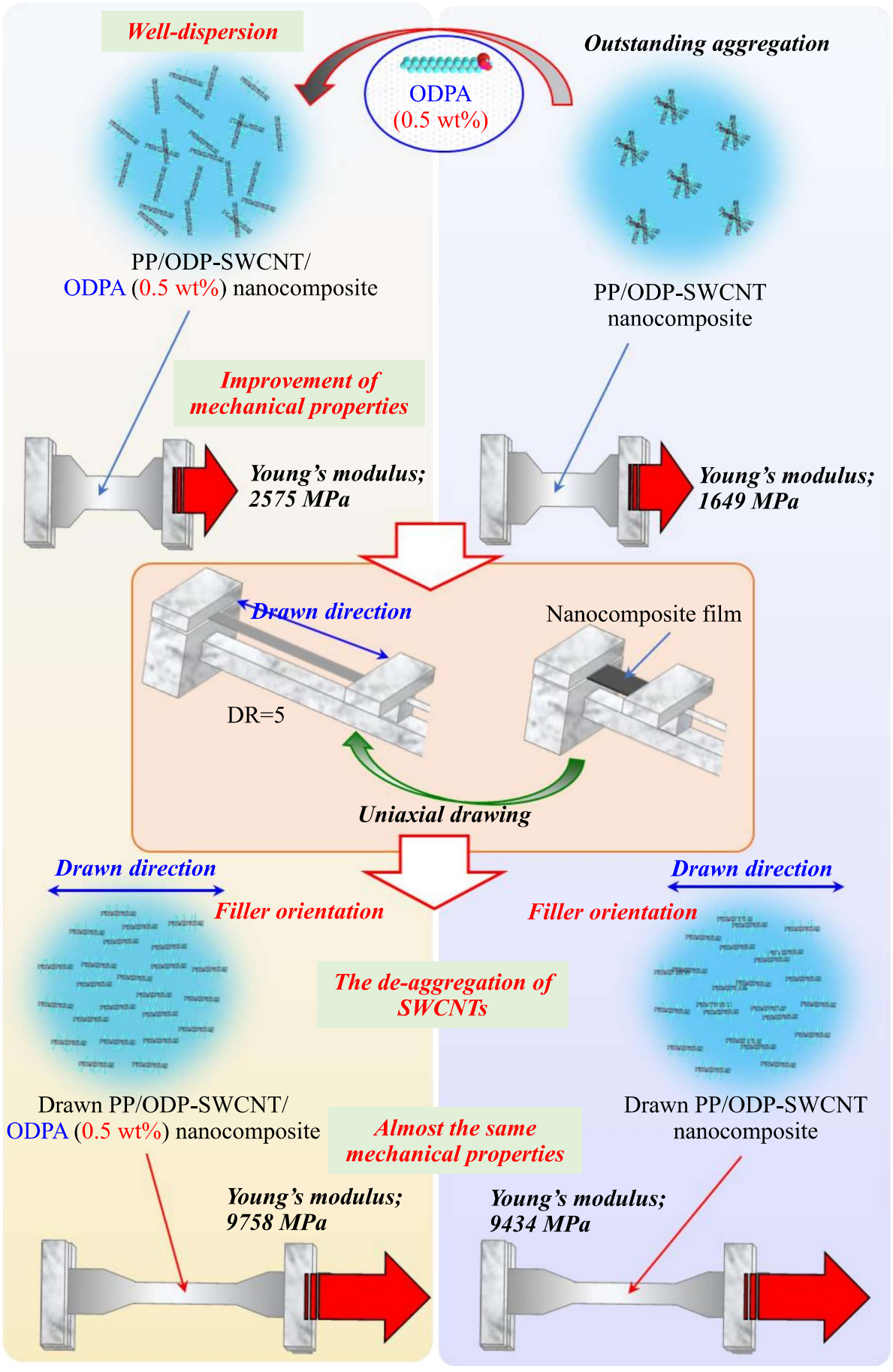

Figure 5-11. Schematic illustration of the summarized results of this chapter.

6. Concluding Remarks

The doctoral thesis has been reported the following three contents.

Chapter 3 provides information on the unique properties of materials for researchers who focus on defossilizing resources and promoting the utilization of nanocarbon materials. The physical properties of SWCNTs obtained using two different manufacturing methods were compared as it pertains to the monolayer on the water surface and the LB film after undergoing the steps of surface organo-modification. Surface organo-modification made SWCNTs lipophilic and realized nanodispersion in a toluene solvent. The organo-modified SWCNTs that were obtained by surface-modifying the SWCNTs from the improved-arc discharge method with long-chain phosphonic acid were excellent in the arrangement regularity in the in-plane and layered directions. However, the SWCNTs obtained via the super-growth CVD method with the same surface modification exhibited excellent dispersion performance in the organic polymer matrix. The difference in these properties could be derived from the original surface properties of the SWCNTs from each manufacturing method, even after surface modification. In other words, it is predicted that this difference could be nullified by making the surface organic modification rate as close to 100 % as possible. The organic modification of SWCNTs could present an effective means for promoting dispersion in solution, dispersion in organic solids, and two-dimensional integration of this material having too strong aggregation characteristics.

In Chapter 4, the activity maintenance characteristics of biomolecules using nanomaterial surfaces were investigated. SWCNTs, which are nanocarbon materials with an elaborate geometrical shape, are suitable as templates that contribute to maintaining the structure of organic molecules and biomolecules. A method was introduced that involved a monolayer on the water surface that can expose the surface of SWCNTs over a wide area. A long-alkyl chain was introduced onto the surface of SWCNTs hydrophilized by ultrasonic treatment with a mixed acid *via* a phosphonate bidentate bond. The Langmuir monolayer method, in which the alkyl group becomes a hydrophobic group and the surface rich in its bonds is exposed to air, while the unmodified SWCNT surface can be exposed below the water surface, was utilized. It was successful in adsorbing protease from the subphase on the hydrophilic surface of organo-modified SWCNTs. The morphology and presence of functional groups were confirmed by AFM and IR, respectively. The adsorption-immobilized protease retained the ability to cleave the luminescent casein chain. Its cutting function was maintained even in an environment of 100 °C and was only slightly reduced at 160 °C. Protease function in solution was significantly reduced at 50 °C and almost lost at 90 °C. From the viewpoint of the Raman band, it was confirmed that the secondary structure of the adsorbed protease was maintained after high-temperature treatment. Adsorption and immobilization on the surface of nanocarbon have been considered to be effective in maintaining the properties exhibited by biomolecules in an aqueous solution in a high-temperature environment exceeding 100 or 150 °C. In the future, the

denaturation behavior of adsorption–immobilized biomolecules due to structural transition will also arouse basic academic interest.

Further, in Chapter 5, In the sample in which ODP-SWCNT was added to PP, a general-purpose resin, the nanocomposite prepared via melt-compounding showcased excellent filler aggregation. The aggregation tendency of this composite was greater than that of the fluorocarbon-modified SWCNT in a fluorinated polymer reported in a previous study [107]. Therefore, this study presented greater improvement in the dispersibility of nanoparticles at small amounts of modifier.

When uniaxial drawing was performed, the PP/ODP-SWCNT binary composite and PP/ODP-SWCNT/ODPA ternary composite showcased equal improvement in crystallinity and hardness, even at a low magnification where the drawing ratio was 2. At a drawing ratio of 3, the maximum stress of the PP/ODP-SWCNT/ODPA ternary composite was comparable to that of the PP/ODP-SWCNT binary composite in quintuple stretching. These results were caused by the improved filler dispersibility in the undrawn state. The deaggregation behavior during drawing became more remarkable due to the homogenization of the initial dispersed state.

Both the maximum stress and maximum strain values of the PP/ODP-SWCNT/ODPA ternary composite increased. In the PP/ODP-SWCNT binary composite, the aggregation of ODP-SWCNT was remarkable; therefore, cracks were often observed around the aggregates, even in the tensile test. In other words, the improvement in SWCNT dispersibility could

suppress the occurrence of cracks during deformation. This could be proven by the strain value of the PP/ODP-SWCNT/ODPA ternary composite which were maintained even after high-magnification drawing.

By improving the dispersibility of ODP-SWCNTs through the formation of jet-black composites, the suppression of defect formation and fracture origin occurrence based on the presence of SWCNT aggregates could be expected.

References and Notes

[1] E. A. G. Schuur, A. D. McGuire, C. Schädel, G. Grosse, J. W. Harden, D. J. Hayes, G. Hugelius, C. D. Koven, P. Kuhry, D. M. Lawrence, S. M. Natali, D. Olefeldt, V. E. Romanovsky, K. Schaefer, M. R. Turetsky, C. C. Treat, J. E. Vonk, *Nature* **215**, *520*, 171–179.

[2] H. Wu, Z. Li, D. Ji, Y. Liu, L. Li, D. Yuan, Z. Zhang, J. Ren, M. Lefler, B. Wang, S. Licht, *Carbon* **2016**, *106*, 208–217.

[3] Q. Sun, M. Wang, Z. Li, A. Du, D. J. Searles, *J. Phys. Chem. C* **2014**, *118*, 2170−2177.

[4] S. Iijima, *Nature* **1991**, *354*, 56–58.

[5] S. Chowdhury, R. Balasubramanian, Holey graphene frameworks for highly selective post-combustion carbon capture, *Sci. Rep*. **2016**, *6*, 21537.

[6] C. Genovese, M. E. Schuster, E. K. Gibson, D. Gianolio, V. Posligua, R. G. Crespo, G. Cibin, P. P. Wells, D. Garai, V. Solokha, S. K. Calderon, J. J. V. Velez, C. Ampelli, S. Perathoner, G.Held, G. Centi, R. Arrigo, *Nat. Commun.* **2018**, *9*, 1–12.

[7] H. W. Kroto, J. R. Heath, S. C. O'Brien, R. F. Curl, R. E. Smalley, C60: Buckminsterfullerene, *Nature* **1985**, *318*, 162–163.

[8] A. K. Geim, K. S. Novoselov, The rise of graphene, *Nature Mater.* **2007**, *6*, 183–191.

[9] M. José-Yacamán, M. Miki-Yoshida, L. Rendón, *Appl. Phys. Lett*. **1993**, *62*, 657–659.

[10] T. W. Ebbesen, P. M. Ajayan, *Nature* **1992**, *358*, 220–222.

[11] K. Hata, D. N. Futaba, K. Mizuno, T. Namai, M. Yumura, S. Iijima, *Science* **2004**, *306*, 1362–1364.

[12] Y. Lee, K. E. Geckeler, *Adv. Mater.* **2010**, *22*, 4076–4083.

[13] H. A. Boucetta, A. Nunes, R. Sainz, M. A. Herrero, B. Tian, M. Prato, A. Bianco, K. Kostarelos, *Angew. Chem. Int. Ed.* **2013**, *52*, 2274–2278.

[14] I. A. Kinloch, J. Suhr, J. Lou, R. J. Young, P. M. Ajayan, *Science* **2018**, *362*, 547–553.

[15] J. N. Colemana, U. Khana, W. J. Blau, Y. K.Gun'kob, Carbon ***2006***, *44*, 1624–1652.

[16] A. A. Balandin, *Nat. Mater.* **2011**, *10*, 569–581.

[17] P. Wang, Y. Zheng, T. Inoue, R. Xiang, A. Shawky, M. Watanabe, A. Anisimov, E. I. Kauppinen, S. Chiashi, S. Maruyama, *ACS Nano* **2020**, *14*, 4298−4305.

[18] H. Lee, K. Watanabe, M. Kim, M. Gopiraman, K. H. Song, J. S. Lee, I. S. Kim, *Sci. Rep*. **2016**, *6*, 37590

[19] T. Premkumar, R. Mezzenga, K. E. Geckeler, *Small* **2012**, *8*, 1299–1313.

[20] C. A. C. Chazot, C. K. Jons, A. J. Hart, *Adv. Funct. Mater*. **2020**, *33*, 2005499.

[21] C. Yao, X. Yin, Y. Yu, Z. Cai, X. Wang, *Adv. Funct. Mater.* **2017**, *27*, 1700794.

[22] Z. Y. Wu, H. W. Liang, B. C. Hu, S. H. Yu, *Angew. Chem. Int. Ed.* **2018**, *57*, 15646–15662.

[23] L. Medina, Y. Nishiyama, K. Daicho, T. Saito, M. Yan, L. A. Berglund, *Macromolecules* **2019**, *52*, 3131−3140.

[24] E. Paineau, G. Monet, G. Monet, V. Peyre, C. Goldmann, S. Rouzière, P. Launois,

Langmuir **2019**, *35*, 12451−12459.

[25] W. Obitayo, T. Liu, *Carbon* **2015**, *85*, 372–382.

[26] V. J. C. Delgado, B. L. E.-Sanchez, C. A. A. Orta, F. J. M. Rodrıguez, *Polym. J.* **2012**, *44*, 952–958.

[27] L. R. MacFarlane, H. Shaikh, J. D. G. Hernandez, M. Vespa, T. Fukui, I. Manners, *Nat. Rev. Mater.* **2021**, *6*, 7–26.

[28] J. E. Millstone, D. F. J. Kavulak,, C. H. Woo, T. W. Holcombe, E. J. Westling, A. L. Briseno, M. F. Toney, J. M. J. Fréchet, *Langmuir* **2010**, *26*, 13056–13061.

[29] A. Fujimori, S. Arai, J. Kusaka, M. Kubota, K. Kurosaka, *J. Colloid Interf. Sci.*, **2013**, *392*, 256–265.

[30] A. Fujimori, N. Honda, H. Iwashita, Y. Kaneko, S. Arai, M. Sumita, S. Akasaka, *Colloids Surf. A* **2014**, *446*, 109–117.

[31] Q. Meng, N. Honda, S. Uchida, K. Hashimoto, H. Shibata, A. Fujimori, *J. Colloid Interf. Sci.* **2015**, *453*, 90–99.

[32] A. Fujimori, K. Ohmura, N. Honda, K. Kakizaki, *Langmuir* **2015**, *31*, 3254–3261.

[33] A. Fujimori, Y. Kasahara, N. Honda, S. Akasaka, *Langmuir* **2015**, *31*, 2895–2904.

[34] G. L. Gaines, Insoluble Monolayers at Liquid Gas Interfaces. Wiley: New York, **1966**.

[35] M. C. Petty, Langmuir-Blodgett Films. Cambridge Univ. Press: New York, **1996**.

[36] A. Ulman, An Introduction to Ultrathin Organic Films: from Langmuir-Blodgett to Self-

assembly. Academic Press, Boston, **1991**.

[37] K. Blodgett, *J. Am. Chem. Soc.* **1934**, *56*, 495–495.

[38] Y. Fukushima, S. Inagaki, *J. Inclus. Phenom.* **1987**, *5*, 473–482.

[39] D. K. Lee, Y. S. Kang, C. S. Lee, P. Stroeve, *J. Phys. Chem. B* **2002**, *106*, 7267–7271.

[40] J. Liu, A. G. Rinzler, H. Dai, J. H. Hafner, R. K. Bradley, P. J. Boul, A. Lu, T. Iverson, K. Shelimov, C. B. Huffman, F. R. Macias, Y. S. Shon, T. R. Lee, D. T. Colbert, R. E. Smalley, *Science* **1998**, *280*, 1253–1256.

[41] S. Hirayama, Y. Abiko, H. Machida, A. Fujimori, *Thin Solid Films*, **2019**, *685*, 168–179.

[42] Y. Abiko, T. Hayasaki, S. Hirayama, A. A. Almarasy, A. Fujimori, *Polym. Bull.* **2021**, *78*, 1585–1607.

[43] Y. Abiko, T. Hayasaki, S. Hirayama, A. A. Almarasy, Y. Kawabata, A. Fujimori, *ChemistrySelect* **2020**, *5*, 6594–6607.

[44] T. Hayasaki, Y. Abiko, A. A. Almarasy, S. Akasaka, A. Fujimori, *Polym. Bull.* **2021**, *78*, 5503–5524.

[45] C. Weiss, M. Carriere, L. Fusco, I. Capua, J. A. Regla-Nava, M. Pasquali, J. A. Scott, F. Vitale, M. A. Unal, C. Mattevi, D. Bedognetti, A. Merkoçi, E. Tasciotti, A. Yilmazer, Y. Gogotsi, F. Stellacci, L. G. Delogu, *ACS Nano* **2020**, *14*, 6383–6406.

[46] P. A. Suci, M. T. Klem, T. Douglas, M. Young, *Langmuir* **2005**, *21*, 8686–8693.

[47] C.Y. Lai, B.G. Trewyn, D.M. Jeftinija, K. Jeftinija, S. Xu, S. Jeftinija, V.S.Y. Lin, *J. Am.*

Chem. Soc. **2003**, *125*, 4451–4459.

[48] C. Richard, F. Balavoine, P. Schultz, T.W. Ebbesen, C. Mioskowski, *Science* **2003**, *300*, 775–778.

[49] R.X. Gao, X.R. Mu, Y. Hao, L.L. Zhang, J.J. Zhang, Y.H. Tang, *J. Mater. Chem. B* **2014**, *2*, 1733–1741.

[50] S.Y. Jiang, Z.Q. Cao, *Adv. Mater.* **2010**, *22*, 920–932.

[51] C. Barbe, J. Bartlett, L.G. Kong, K. Finnie, H.Q. Lin, M. Larkin, S. Calleja, A. Bush, G. Calleja, *Adv. Mater.* **2004**, *16*, 1959–1966.

[52] R. H. Baughman, A. A. Zakhidov, W. A. Heer, *Science* **2002**, *297*, 787–792.

[53] M. Freely, H.L. Worthy, R. Ahmed, B. Bowen, D. Watkins, J.E. Macdonald, M. Zheng, D.D. Jones, M. Palma, *J. Am. Chem. Soc.* **2017**, *139*, 17834–17840.

[54] D.B. Warheit, B.R. Laurence, K.L.Reed, D.H. Roach, G.A.M. Reynolds, T.R. Webb, *Toxicol. Sci.* **2004**, *77*, 117–125.

[55] L.M. Sargent, A.F. Hubbs, S.H. Young, M.L. Kashon, C.Z. Dinu, J.L. Salisbury, S.A. Benkovic, D.T. Lowry, A.R. Murray, E.R. Kisin, K.J. Siegrist, L. Battelli, J. Mastovich, J.L. Sturgeon, K.L. Bunker, A.A. Shvedova, S.H. Shvedova, *Mutat. Res., Genet. Toxicol. Environ. Mutagen.* **2012**, *745*, 28–37.

[56] E. Katz, I. Willner, *Angew. Chem., Int. Ed.* **2004**, *43*, 6042–6108.

[57] M. Couture, S.S. Zhao, J.F. Masson, *Phys. Chem. Chem. Phys.* **2013**, *15*, 11190–11216.

[58] H.N. Daghestani, B.W. Day, *Sensors* **2010**, *10*, 9630–9646.

[59] J.N. Talbert, J.M. Goddard, *Colloids Surf., B* **2012**, *93*, 8–19.

[60] S. Chakraborti, T. Chatterjee, P. Joshi, A. Podder, B. Bhattacharyya, S.P. Singh, V. Gupta, P. Chakrabarti, *Langmuir* **2010**, *26*, 3506–3513.

[61] L. Haggerty, B.A. Watson, M.A. Barteau, A.M. Lenhoff, *J. Vac. Sci. Technol.*, *B* **1991**, *9*, 1219–1222.

[62] J. Kong, N.R. Franklin, C.W. Zhou, M.G. Chapline, S. Peng, K.J. Cho, H.J. Dai, *Science* **2000**, *287*, 622–625.

[63] T.I.T. Okpalugo, P. Papakonstantinou, H. Murphy, J. McLaughlin, N.M.D. Brown, *Carbon* **2005**, *43*, 153–161.

[68] J. L. Bahr, J. Yang, D. V. Kosynkin, M. J. Bronikowski, R. E. Smalley, J. M. Tour, *J. Am. Chem. Soc.* **2001**, *123*, 6536–6542.

[69] F. Caruso, K. Niikura, D.N. Furlong, Y. Okahata, *Langmuir* **1997**, *13*, 3427–3433.

[70] A. Fujimori, M. Taguchi, S. Arai, *Colloids Surf. A* **2014**, *443*, 432–438.

[71] A. Fujimori, S. Arai, Y. Soutome, M. Hashimoto, *Colloids Surf. A* **2014**, *448*, 45–52.

[72] T. Yunoki, Y. Kimura, A. Fujimori, *Colloids Surf. B* **2019**, *173*, 759–768.

[73] T. Yunoki, Y. Kimura, A. Fujimori, *Bull. Chem. Soc. Jpn* **2019**, *92*, 1662–1671.

[74] M. Bilal, Y. Zhao, T. Rasheed, HMN. Iqbal, Int. *J. Biol. Macromol.* **2018**, *120*, 2530–2544.

[75] S. Stankovich, DA. Dikin, GHB. Dommett, KM. Kohlhaas, EJ. Zimney, EA. Stach, RD.

Piner, ST. Nguyen, RS. Ruoff, *Nature* **2006**, *442*, 282–286

[76] JR. Capadona, K. Shanmuganathan, DJ. Tyler, SJ. Rowan, C. Weder, *Science* **2008**, *319*, 1370–1374.

[77] H. Zhang, K. Dasbiswas, NB. Ludwig, G. Han, B. Lee, S. Vaikuntanathan, DV. Talapin, *Nature* 2017, 542, 328–331.

[78] P. Rittigstein, RD. Priestley, LJ. Broadbelt, JM. Torkelson, *Nat. Mater.* **2007**, *6*, 278–282.

[79] J. Zhou, XY. Qiao, BP. Binks, K. Sun, MW. Bai, YL. Li, Y. Liu, *Langmuir* **2011**, *27*, 3308–3316.

[80] YM. Zhang, S. Guo, WT. Wu, ZR. Qin, XF. Liu, *Langmuir* **2016**, *32*, 11861–11867.

[81] H. Matsuoka, S. Nakayama, T. Yamada, *Chem Lett* **2012**, *29*, 8718–8727

[82] QB. Chen, XD. Liang, SL. Wang, SH. Xu, HL. Liu, Y. Hu, *J Colloid Interf. Sci.* **2007**, *314*, 651–658.

[83] II. Perepichka, Q. Lu, A. Badia, CG. Bazuin, *Langmuir* **2013**, *29*, 4502–4519.

[84] HT. Zhu, LN. Wang, XM. Jie, DD. Liu, YM. Cao, *ACS Appl. Mater. Interfaces* 2016, 8, 22696–22704.

[85] AC. Balazs, T. Emrick, TP. Russell, *Science* **2006**, *314*, 1107–1110.

[86] XL. Pan, LH. Shen, APHJ. Schenning, CWM. Bastiaansen, *Adv. Mater.* **2019**, *31*, 1904348.

[87] MW. Akhtar, YS. Lee, CM. Yang, JS. Kim, *RSC Adv.* **2016**, *6*, 100448–100458.

[88] S. Das, S. Chattopadhyay, S. Dhanania, AK. Bhowmick, *Polym. Eng. Sci.* **2020**, *60*, 3115–

3134.

[89] O. Ersoy, *Polym Compos*. **2020**, *41*,1045–1052.

[90] BK. Goriparthi, PNE. Naveen, HR. Sankar, *Polym Compos*. **2021**, *42*, 1123–1134.

[91] JX. Zhang, JC. Ma, LQ. Zhang, CY. Zong, AH. Xu, YB. Zhang, B. Geng, SX. Zhang, *RSC Adv.* **2020**, *10*, 7065–7072.

[92] A. Khosravi, JA. King, HL. Jamieson, ML. Lind, *Langmuir* **2014**, *30*, 13994–14003.

[93] A. Bruno, *Macromolecules* **2010**, *43*, 10163–10184.

[94] O. Martin, AJ. Martin, C. Mondelli, S. Mitchell, TF. Segawa, R. Hauert, C. Drouilly, D. Curulla-Ferre, J. Perez-Ramirez, *Angew. Chem. Int. Ed.* **2016**, *55*, 6261–6265.

[95] Y. Zhou, XF. Guan, H. Zhou, K. Ramadoss, S. Adam, HJ. Liu, S. Lee, J. Shi, M. Tsuchiya, DD. Fong, S. Ramanathan, *Nature* **2016**, *534*, 231–234.

[96] K. Yang, LL. Hu, XX. Ma, SQ. Ye, L. Cheng, XZ. Shi, CH. Li, YG. Li, Z. Liu, *Adv. Mater.* **2012**, *24*, 1868–1872.

[97] D. Berman, SA. Deshmukh, SKRS. Sankaranarayanan, A. Erdemir, AV. Sumant, *Science* **2015**, *348*, 1118–1122.

[98] TY. Yang, LJ. Wei, LY. Jing, JF. Liang, XM. Zhang, M. Tang, MJ. Monteiro, Y. Chen, Y. Gu. S. Wang, DY. Zhao, HQ. Yang, J. Liu, GQM. Lu, *Angew. Chem. Int. Ed.* **2017**, *56*, 8459–8463.

[99] H. Kim, D. Kawaguchi, K. Tanaka, Y. Seo, *Langmuir* **2018**, *34*, 11027–11033.

[100] F. Yang, X. Wang, DQ. Zhang, J. Yang, D. Luo, ZW. Xu, JK. Wei, JQ. Wang, Z. Xu, F. Peng, XM. Li, RM. Li, YL. Li, MH. Li, XD. Bai, F. Ding, Y. Li, *Nature* **2014**, *510*, 522–524.

[101] JL. Blackburn, AJ. Ferguson, C. Cho, JC. Grunlan, *Adv. Mater.* **2018**, *30*, 1704386.

[102] Y. Yang, QY. Huang, LY. Niu, DR. Wang, C. Yan, YY. She, ZJ. Zheng, *Adv. Mater.* **2017**, *29*, 1606679.

[103] MMO. Thotiyl, SA. Freunberger, ZQ. Peng, PG. Bruce, *J. Am. Chem. Soc.* **2013**, *135*, 494–500.

[104] Y. Kasahara, Y. Guo, T. Tasaki, Q. Meng, MMA. Mamun, M. Iizuka, S. Akasaka, A. Fujimori, *Polym. Bull.* **2018**, *75*, 4145–4163.

[105] M. Hartmann, *Chem. Mater.* **2005**, *17*, 4577–4593.

[106] Y. Guo, K. Fukushi, S. Hirayama, H. Machida, Q. Meng, S. Akasaka, A. Fujimori, Colloids Surf. A **2018**, *556*, 227–238.

[107] T. Hayasaki, Y. Yamada, X. Kai, AA. Almarasy, S. Akasaka, A. Fujimori, *Polym Compos*. **2021**, *42*, 4845–4859.

[108] A. Fujimori, T. Araki, H. Nakahara, E. Ito, M. Hara, H. Ishii, Y. Ouchi, K. Seki, *Chem. Phys. Lett.* **2001**, *349*, 6–12.

[109] A. Fujimori, Y. Sugita, Y.; H. Nakahara, E. Ito, M.; Hara, N. Matsuie, K.; Kanai, Y. Ouchi, K. Seki, *Chem. Phys. Lett.* **2004**, *387*, 345–351.

[110] AJ. Page, S. Saha, HB. Li, S. Irle, K. Morokuma, *J. Am. Chem. Soc.* **2015**, *137*, 9281–9288.

[111] I. Mukherjee, S.P. Moulik, A.K. Rakshit, *J. Colloid Interf. Sci.* **2013**, *394*, 329–336.

[112] Y. Abiko, Y. Yamada, T. Hayasaki, Y. Kimura, AA. Almarasy, A. Fujimori, *Colloids Surf. A* **2021**, *621*, 126559-1–14.

<< Publication Lists >>

1. Original Papers (11 papers)

1) Y. Abiko, T. Hayasaki, S. Hirayama, AA. Almarasy, A. Fujimori*, "Fabrication of Organo-Modified Carbon Nanotube with Excellent Heat Resistance and Preparation of Its Polymer-Based Nanocomposite by Simple Melt Compounding.", *Polym. Bull.,* **2021**, *78*, 1585-1607. (DOI: 10.1007/s00289-020-03180-w)

2) S. Hirayama, T. Hayasaki, AA. Almarasy, H. Yabu, M. Tokita, A. Fujimori*, "Influence of Uniaxial Orientation of Fluorinated Polymer/Phosphonate-Modified Needle-Like Nanofiller Composite by Drawing.", *Polym. Compos.,* **2020**, *41*(8), 3062-3073. (DOI: 10.1002/PC.25598)

3) Y. Abiko, T. Hayasaki, S. Hirayama, AA. Almarasy, Y. Kawabata, A. Fujimori*, "Formation, Structure, and Function of Hydrogenated and Fluorinated Long-Chain Phosphonate-Modified Single-Walled Carbon Nanotubes with Bidentate Bonds.", *ChemistrySelect*, **2020**, *5*(22), 6594-6607. (DOI: 10.1002/slct.202001535)

4) T. Hayasaki, Y. Abiko, AA. Almarasy, S. Akasaka, A. Fujimori*, "Effect of the Uniaxial Orientation on the Polymer/Filler Nanocomposites Using Phosphonate-Modified Single-Walled Carbon Nanotube with Hydro- or Fluorocarbons.", *Polym. Bull.*, **2021**, *78*, 5503-5524. (DOI: 10.1007/s00289-020-03388-w)

5) AA. Almarasy, T. Hayasaki, Y. Abiko, Y. Kawabata, S. Akasaka, A. Fujimori*, "Comparison of Characteristics of Single-Walled Carbon Nanotubes Obtained by Super-Growth CVD and Improved-Arc Discharge Methods Pertaining to Interfacial Film Formation and Nanohybridization with Polymers.", *Colloids Surf. A*, **2021**, *615*, 126221–1-12. (DOI: 10.1016/j.colsurfa.2021.126221)

6) Y. Abiko, Y. Yamada, T. Hayasaki, Y. Kimura, AA. Almarasy, A. Fujimori*, "Adsorption Immobilization of Biomolecules from Subphase on Langmuir Monolayers of Organo-Modified Single-Walled Carbon Nanotube.", *Colloids Surf. A*, **2021**, *621*, 126559–1-14. (DOI: 10.1016/j.colsurfa.2021.126559)

7) AA. Almarasy, Y. Yamada, Y. Mashiyama, H. Maruyama, Y. Kimura, A. Fujimori*, "Activity Maintenance Characteristics and Protease Adsorption on Langmuir Monolayer of Organo-Modified Single-Walled Carbon Nanotubes.", *ChemistrySelect*, **2021**, *6*(21), 5329-5337. (DOI: 10.1002/slct.202100862)

8) T. Hayasaki, Y. Yamada, X. Kai, AA. Almarasy, S. Akasaka, A. Fujimori*, "Study on the Improvement of Dispersibility and Orientation Control of Fluorocarbon-Modified Single-Walled Carbon Nanotubes in a Fluorinated Polymer Matrix.", *Polym. Compose.*, **2021**, *42*(9), 4845-4859. (DOI: 10.1002/pc.26194)

9) T. Hayasaki, K. Harada, X. Kai, AA. Almarasy, A. Fujimori*, "Dispersion Characteristics of Polypropylene/Organo-Modified Single-Walled Carbon Nanotube Composites with a

Long-Chain Phosphonic Acid Added as the Third Dispersant Component and Their Drawn Orientation.", *Polym. Bull., 2022, 79*, in press (10.1007/s00289-022-04175-5).

10) X. Kai, K. Harada, A. A. Almarasy, T. Hayasaki, A. Fujimori*, "Nanofiller Dispersing, Drawn Orientation, and Mechanical Properties of Polymer-Based Composites via Organo-Modification of Two-Types of Single-Walled Carbon Nanotubes by Different Manufacturing Methods", *Polym. Compos.*, **2022**, *43*, in press (DOI: 10.1002/pc.26628).

11) Y. Yamada, K. Obuchi, N. Kikuchi, AA. Almarasy, and A. Fujimori*, "Immobilization of Trypsin from Subphase to the Langmuir Monolayer of Fluorocarbon-Modified Single-Walled Carbon Nanotube and Its Activity Maintenance", *Langmuir,* **2022**, 38, in press (DOI: la-2022-00283a).

Review Article

1. AA. Almarasy, A. Fujimori, “Attempt of uniform dispersion in polymer-based nanocomposites using surface-modified single-walled carbon nanotubes”, *Acc. Mater. Surf. Res.*, **2020**, *5*(3), 80-89.

<< Conference Presentation >>

1. ジョ カイ，Ahmed A. Almarasy，藤森 厚裕，製造法の異なる 2 種の単層カーボンナノチューブの有機修飾を介した高分子複合材調製とその構造物性，2022 年繊維学会年次大会，2022 年 6 月(オンライン口頭発表) ．
2. ジョ カイ，Ahmed A. Almarasy，藤森 厚裕，製造法が異なる 2 種の単層カー

ボンナノチューブの有機修飾を介した高分子系複合材料のナノフィラー分散化、延伸配向、および力学物性，第 71 回高分子討論会，2022 年 5 月 (オンラインポスター発表) ．

3. Ahmed A. Almarasy, 原田 亘, ジョ カイ, 藤森 厚裕, Dispersion Characteristics of Polypropylene/Organo-Modified Single-Walled Carbon Nanotube Composites with the Third Dispersant Component and Their Drawn Orientation, 第 71 回高分子討論会，2022 年 5 月 (オンライン口頭発表) ．
4. 早﨑 拓登，山田 優奈，原田 亘，ジョ カイ，Ahmed A. Almarasy，藤森 厚裕，『有機修飾カーボンナノチューブと長鎖ホスホン酸による均一分散性高分子系ナノコンポジットの創出』，第 72 回 コロイドおよび界面化学討論会，2021 年 9 月 (オンライン口頭発表) ．
5. Ahmed A. Almarasy，山田 優奈，早﨑 拓登，藤森 厚裕，『Activity Maintenance Characteristics and Protease Adsorption on Langmuir Monolayer of Organo-Modified Single-Walled Carbon Nanotubes』，第 70 回 高分子討論会，2021 年 9 月 (オンラインポスター発表) ．
6. 山田 優奈，早﨑 拓登，Ahmed A. Almarasy，藤森 厚裕，『有機修飾単層カーボンナノチューブ Langmuir 膜をテンプレートとしたバイオ分子の吸着固定化挙動』，第 70 回 高分子討論会，2021 年 9 月 (オンラインポスター発表) ．
7. 早﨑 拓登，山田 優奈，ジョ カイ，Ahmed A. Almarasy，藤森 厚裕，『第三成

分を含む結晶性高分子/有機修飾カーボンナノチューブ複合材料の分散性向上と延伸配向特性』，第 70 回 高分子討論会，2021 年 9 月 (オンライン口頭発表) ．

8. Ahmed A. Almarasy, 早﨑 拓登, 山田 優奈, 川端 庸平, 藤森 厚裕,『Comparison of Characteristics of Single-Walled Carbon Nanotubes Obtained by Super-Growth CVD and Improved-Arc Discharge Methods Pertaining to Monolayer Formation and Nanohybridization with Polymer』，第 70 回高分子討論会，2021 年 5 月 (オンラインポスター発表) ．
9. 早﨑 拓登，Ahmed A. Almarasy，藤森 厚裕，『結晶性フッ素樹脂/有機修飾単層カーボンナノチューブ複合材料調整における分散性向上技術の提案』，第 70 回高分子討論会，2021 年 5 月 (オンラインポスター発表) ．
10. 早﨑 拓登，Ahmed A. Almarasy，藤森 厚裕，『界面活性剤の導入によるフッ化炭素修飾カーボンナノチューブのフッ素樹脂中における分散効果』，第 101 日本化学会春季年会，2021 年 3 月 (オンライン口頭発表) ．
11. 早﨑 拓登，安彦 喜寛，Ahmed A. Almarasy，藤森 厚裕，『一軸高温延伸によるフッ素系ポリマー/ホスホン酸修飾単層カーボンナノチューブ複合材料に対する配向効果』，第 69 回 高分子討論会 2020 年 9 月 (オンライン口頭発表) ．
12. 安彦 喜寛，早﨑 拓登，Ahmed A. Almarasy，川端 庸平，藤森 厚裕，『炭化水素鎖，およびフッ素化炭素鎖を有するホスホン酸修飾単層カーボンナノチュー

ブの形成とその構造』，第 69 回 高分子討論会 2020 年 9 月 (オンライン口頭発表) ．

13. 早﨑 拓登，安彦 喜寛，Ahmed A. Almarasy，藤森 厚裕，『長鎖ホスホン酸修飾単層カーボンナノチューブ含むポリマー/ナノフィラーコンポジットへの一軸配向の影響』，第 71 回 コロイドおよび界面化学討論会，2020 年 9 月 (オンラインポスター発表) ．

14. 安彦 喜寛，早﨑 拓登，Ahmed A. Almarasy，川端 庸平，藤森 厚裕，『有機修飾単層カーボンナノチューブによる Langmuir 膜形成と，その累積膜の構造と機能』，第 71 回 コロイドおよび界面化学討論会，2020 年 9 月 (オンラインポスター発表) ．

15. 早﨑 拓登，安彦 喜寛，Ahmed A. Almarasy，藤森 厚裕，『両親媒性分子による有機修飾を用いた表面改質カーボンナノチューブ複合体の配向効果』, 第 100 日本化学会春季年会，2020 年 3 月 (口頭発表).

16. 安彦 喜寛，早﨑 拓登，Ahmed A. Almarasy，川端 庸平，藤森 厚裕，『有機修飾カーボンナノチューブ組織化膜の機能探求-高密度膜創出とバイオ分子との相互作用-』，第 100 日本化学会春季年会，2020 年 3 月 (口頭発表).

17. 平山 周平，Ahmed A. Almarasy，佐藤 栄一，藤森 厚裕，『高分子系における組織制御型ミルフィーユ構造の創出：延伸配向ナノコンポジットの構造/機能相関』，高分子学会第 31 回埼玉地区懇話会，2020 年 3 月 (ポスター発表) ．

Acknowledgements

I would like to express our sincere gratitude to Associate Professor Atsuhiro Fujimori for his careful guidance for three years in writing this doctoral thesis.

In addition, I would like to thank Professor Zentaro Honda, Associate Professor Kenji Kamishima, and Associate Professor Miho Suzuki for serving as vice-judgment committee members for this doctoral thesis.

I would also like to thank Mr. Mikio Yajima of Zeon Nanotechnology Co., Ltd. and Takeyoshi Kato of Zeon Corporation for providing the single-walled carbon nanotubes manufactured by the super grorth CVD method.

Also, I would like to thank Mr. Daisuke Shimizu of Kusumoto Chemicals, Ltd. for providing the single-walled carbon nanotubes derived from the improved arc discharge method manufactured by OCSiAl Co., Ltd.

We would like to thank Dr. Shuichi Akasaka of Tokyo Institute of Technology for undertaking the TEM observation.

Furthermore, I would like to appreciate Mr. Shuhei Hirayama, Mr. Yoshinori Abiko, Mr. Yusuke Kimura, Mr. Takato Ohashi, Mr. Haruka Maruyama, Mr. Takuto Hayasaki, Mr. Xu Kai, and Miss Yuna Yamada for their collaborative research on related themes.

I am exceedingly grateful to Ministry of Education, Culture, Sports, Science, and Technology (MEXT) Japan for the scholarship it offered.

I would also like to thank all the members of Fujimori Lab for spending three years together in the lab.

Finally, I would like to express my heartfelt gratitude to my parents and my brothers.

September 2022

Ahmed A. Almarasy